SHELL BIOCHEMISTRY

MAGGIE CUSACK[1], DEREK WALTON[2], and GORDON B. CURRY[1]
[1University of Glasgow; 2University of Derby, U.K.]

INTRODUCTION

GENERAL

The paired valves of the brachiopod shell are among the earliest examples of biomineralization. As with all biominerals, brachiopod valves contain organic molecules as well as the obvious inorganic components since organic material is essential for the formation of biominerals. Therefore, it is important to examine both the organic and the inorganic components of brachiopod shells with a view to understanding the formation of the valves. As well as playing an active role in the process of biomineralization, organic molecules are also potentially informative to those interested in the evolution of the brachiopods and the phylogenetic relationships between taxa. The mineral components of brachiopod valves were comprehensively identified in the 1965 *Treatise on Invertebrate Paleontology* (MOORE, 1965). Since that time, more information has become available regarding the components and the structure of the inorganic phase (see the following section of this chapter, below, and the chapter on shell structure, p. 367–320). Regarding the organic components, a wealth of information has been added to that discussed in the 1965 *Treatise.*

In brief, the valves of articulated brachiopods are composed of calcium carbonate in the form of low-magnesium calcite (JOPE, 1965) with proteins (in some instances, carotenoproteins), lipids, and carbohydrates. Inarticulated brachiopods possess valves of a carbonate fluorapatite at least crystallochemically similar to francolite (WATABE & PAN, 1984) in association with proteins, chitin, glycosaminoglycans, and, for *Lingula,* collagen (WILLIAMS, CUSACK, & MACKAY, 1994). Brachiopods with phosphatic valves contain high levels of organic material, while those with carbonate valves contain much lower levels (Table 21). The pioneering work on the analysis of proteins and amino acids of brachiopod valves was done by JOPE, who demonstrated the taxonomic value of molecular information from brachiopod shell material (JOPE, 1965, 1967a, 1967b, 1969a, 1969b, 1973, 1977, 1979, 1980, 1986).

INORGANIC COMPONENTS OF BRACHIOPOD VALVES

The division of brachiopods into articulated and inarticulated kinds is based on shell morphology and generally coincides with the nature of the inorganic component of the valves. The articulated species possess carbonate valves of stable, low-magnesium calcite (JOPE, 1965), while the inarticulated brachiopods possess phosphatic valves in the form of apatite (MCCONNELL, 1963). The exceptions to this pattern are the craniides, which, although lacking shell articulation, have carbonate shells. There is debate about whether the craniides should be classified on the basis of shell mineralogy (BASSETT & others, 1993; POPOV & others, 1993) or absence of articulation (CARLSON, 1993a).

Calcium carbonate comprises 94.6 to 98.6 percent of the inorganic material of articulated brachiopod valves and 87.8 to 88.6 percent of the craniides (JOPE, 1971). Magnesium, as a carbonate, comprises 0.4 to 1.4 percent of the articulated shells and 8.6 percent of craniid valves. Sodium is present in small amounts, and manganese and copper occur in trace amounts in *Terebratulina retusa.*

The unusual occurrence of phosphate in an exoskeleton has prompted several studies of the inorganic components of inarticulated brachiopod valves. Calcium phosphate comprises 74.7 to 93.7 percent of the inorganic component of lingulid valves and 75.2 percent in *Discinisca* (JOPE, 1971). Magnesium

TABLE 21. Quantity of organic material in brachiopod valves (new; data from Curry & Ansell, 1986; Curry & others, 1989).

Genus	mg/g	% organic by weight
Calloria	23.65	2.3
Dallina	10.00	1.0
Gryphus	4.76	0.5
Macandravia	8.13	0.8
Neocrania	44.77	4.5
Notosaria	46.60	4.6
Terebratulina	30.19	3.0
Lingula	295.73	29.6

also occurs as 0.6 to 3 percent of the inorganic components of the lingulid valves and 6.7 percent in *Discinisca.* The apatite of inarticulated brachiopod valves was described as the carbonate fluorapatite francolite (MCCONNELL, 1963; IWATA, 1981). Since those reports, the mineral of the valves of *Lingula* and *Glottidia* has been described as a carbonate containing fluorapatite similar to francolite with no other mineral phase present, i.e., no separate carbonate phase (WATABE & PAN, 1984; LEGEROS & others, 1985). Carbonate integration is analogous with other biological apatites (LEGEROS & others, 1985). The apatite of *Glottidia* and *Lingula* differs principally in the carbonate content. WATABE and PAN (1984) reported carbonate levels of 2.2 wt percent in *Lingula* and 3.6 wt percent in *Glottidia* while LEGEROS and others (1985) reported slightly lower levels for *Lingula* (1.8 wt percent). The higher carbonate level in *Glottidia* accounts for the lower crystallinity (LEGEROS & others, 1985). Integral fluorine increases crystallinity and stability of apatites, but for both *Lingula* and *Glottidia,* fluorine levels are equal. Fluorine accounts for 1.64 wt percent of whole *Glottidia* valves and about 2.58 wt percent of calcified layers (WATABE & PAN, 1984). Calcium and fluorine are localized in mineralized layers in *Lingula* and *Glottidia* valves at a constant F:Ca ratio of 0.033 ± 0.002. In 1991, IIJIMA (IIJIMA, KAMEMIZU, & others, 1991) confirmed the carbonate apatite nature of the valves of *Lingula anatina* and *Lingula shantoungensis* and reported the presence of chlorine as well as fluorine. IIJIMA and others (1991) used pyrolysis to characterize the apatite of the two species of *Lingula* and demonstrated that the structural water of *Lingula* apatite is loosely bound such that it is lost at lower temperatures than that in tooth enamel. The c-axis of apatite and the fiber axis of β-chitin are parallel and coincident with the growth direction of the *Lingula* shell (IIJIMA & MORIWAKI, 1990; IIJIMA, MORIWAKI, & KUBOKI, 1991).

PAN and WATABE (1988a) examined the uptake and transportation of calcium and phosphorus in *Glottidia pyramidata.* Calcium ions are taken up from seawater primarily by the lophophore, move through the coelomic fluid, are concentrated in the mantle, and are eventually deposited in the inner shell layer. Calcium is deposited in the shell at a rate of 12×10^{-2} μg per mg of shell weight per hour. This rate is similar to that for the bivalve *Argopecten.* Calcium uptake and deposition in *Glottidia* occurs three hundred times faster than phosphorus uptake, indicating that phosphorus is unlikely to be obtained directly from seawater and more likely to be obtained indirectly from food (PAN & WATABE, 1988a).

ORGANIC COMPONENTS OF BRACHIOPOD VALVES

A consistently high proportion of total organic mass is contained in brachiopod valves (CURRY & others, 1989). On average, 40 to 50 percent of the total organic mass of both articulated and inarticulated brachiopods is in the shell (CURRY & ANSELL, 1986; CURRY & others, 1989). Such a high percentage has implications for the predation of brachiopods, because the nutrient yield to predators varies significantly depending on whether the shell is crushed and ingested or only body tissues are consumed (CURRY & ANSELL, 1986; CURRY & others, 1989; PECK, 1993). The proportion of tissue present in the shell varies seasonally in *Liothyrella uva* from the Antarctic. This variation, from 36.3 percent in winter to 46.0 percent in summer, may result from the seasonal availability of

nutrients in the Antarctic (Curry & others, 1989). Comparable data for other brachiopods are not available, but it is reasonable to assume that the percentage of total tissue mass in the shells of other taxa will also vary seasonally in response to variations in the availability of nutrients.

The organic molecules isolated from brachiopod valves and discussed in this chapter are proteins, carotenoproteins, amino acids, lipids, carbohydrates, chitin, and glycosaminoglycans (GAGs). Proteins and nucleic acids (DNA and RNA) are the most information rich of the biopolymers. To date, there have been no reports of nucleic acids within brachiopod valves although the isolation of DNA from a range of biominerals in other phyla, both recent and fossil, suggests that brachiopod valves will also contain DNA. Analysis of any possible DNA from brachiopod valves depends on knowledge of the brachiopod genome (see section on the brachiopod genome for information, p. 189–211). Proteins are built up of long chains of amino acids, and the order of amino acids in the polypeptide chain (the primary sequence) is of great value in phylogenetic studies. Information on brachiopod shell proteins will follow in the section on proteins, and the section on amino acids in brachiopod valves discusses the use of amino acid composition *per se* as a taxonomic indicator.

INTRACRYSTALLINE ORGANIC MOLECULES

In calcitic articulated brachiopods, organic molecules are located both within the calcitic fibers (intracrystalline) and between the fibers (intercrystalline). The entombment of organic material within the secondary layer calcitic fibers protects it from contamination and even degradation. Since the calcitic fibers are essentially closed systems, any degradation occurs *in situ,* and the residues can be employed in taxonomic analyses. Thus, organic material trapped within single crystals during biomineralization offers the best hope for the study of ancient fossil molecules (Towe, 1980; Collins, Muyzer, Curry, & others, 1991; Curry, Cusack, Walton, & others, 1991). Collins (Collins, Muyzer, Curry, & others, 1991) estimated that intracrystalline organic material accounts for 0.03 percent of the weight of the articulated brachiopod valve. The phosphatic valves of inarticulated brachiopods do not contain structures analogous to the calcitic fibers of the articulated brachiopods. Although the methods for the extraction of organic molecules from inarticulated brachiopod valves are not as well established as those for the articulated valves, the same principles apply in that the organic material associated most intimately with the mineral should be the most reliable source of indigenous material and the most likely source of preserved material in fossil samples.

AMINO ACIDS IN BRACHIOPOD VALVES

GENERAL

Amino acids are ubiquitous, both as the monomeric units of proteins and in the free (uncombined) state. The use of such molecules in paleontological analysis must recognize this ubiquity to ensure that the amino acid record obtained for a sample represents the actual composition, as opposed to any diagenetic or environmental overprint. While the primary sequence of a protein provides a high level of taxonomic and evolutionary information, the amino acid composition alone may also reflect the taxonomy of the organism (Cornish-Bowden, 1983). Amino acid analysis requires much smaller amounts of shell material than protein sequencing; 10 mg is sufficient for several analyses. Such information, while not as powerful as the primary sequence, is easier to gain and is particularly important in the fossil record, where the peptide bonds that bind the amino acids are largely degraded.

Shell proteins and their associated amino acids have been studied by Jope in continuation of her research for the first edition of the *Treatise* (Jope, 1967a, 1967b, 1969b,

1973, 1979). This work examined both intra- and intercrystalline amino acids and has remained the primary source for data on amino acids of brachiopod shells. Since 1988, the focus of research has changed toward intracrystalline proteins. There are broad similarities between the nature of the inter- and intracrystalline fractions, although they differ in their composition, possibly indicating a difference in the function of the proteins.

Most of the common protein-forming amino acids are found within brachiopod valves, although in this discussion, tryptophan, methionine, and cysteine are not considered due to their variable destruction during the hydrolysis procedure (e.g., HEINRIKSON & MEREDITH, 1984). Histidine was not quantified from intracrystalline sites.

INARTICULATED BRACHIOPODS

Intercrystalline Amino Acids of Recent Brachiopods

Inarticulated brachiopods (e.g., of *Lingula* sp.) contain quantitatively more amino acid (25 percent of shell weight; JOPE, 1967a) within their shell (in the form of protein) than articulated brachiopods (0.5 percent of shell weight; JOPE, 1967a). The group is represented by shells of *Neocrania anomala* (MÜLLER), *Discina striata* (SCHUMACHER), *Lingula anatina* (LAMARCK), and *Lingula* sp., which generally contain lower relative concentrations of glycine (e.g., *L. anatina,* 15 percent; *Laqueus californicus,* 20 percent) and higher concentrations of alanine (up to four times; e.g., *L. anatina,* 20 percent; *Laqueus californicus,* 5 percent) than articulated shells (JOPE, 1967a; KOLESNIKOV & PROSOROVSKAYA, 1986). Hydroxyproline, probably indicating the presence of collagen, has been detected in the organophosphatic *L. anatina* (approximately 6 percent) and *D. striata* (approximately 14 percent; JOPE, 1967a; KOLESNIKOV & PROSOROVSKAYA, 1986). It has not been detected in any carbonate-shelled species, including the craniides. Hydroxyproline represents one-third of the amino acid residues present in collagen. Estimation of the abundance of hydroxyproline will therefore give an indication of the amount of collagen present within the shell.

The anomalous taxonomic position of the craniides is reinforced through amino acid taxonomy (JOPE, 1967a). The shells of this group have relatively high glycine and low alanine, indicating similarity with the articulated brachiopods, but they also contain the amino sugar glucosamine, indicating allegiance with other inarticulated species. The craniid shell has characteristically high aspartic acid and serine, in contrast with all the other brachiopods, confirming the anomalous position of the group.

Paracrystalline Amino Acids of Recent Brachiopods

Organic material is extracted for paracrystalline material as it is for intracrystalline material of articulated brachiopods (CUSACK & others, 1992). The term paracrystalline or mineral-associated material is more accurate for inarticulated brachiopods since they lack the protein-containing mineral fibers of the articulated brachiopods. In *Discinisca tenuis* the most abundant peptide-bound paracrystalline amino acids are glycine, alanine, aspartic acid, and glutamic acid, all at about 13 percent. In *Glottidia pyramidata,* aspartic acid is the most abundant amino acid at 15 percent, followed by glycine at 14 percent, and arginine at 11 percent.

Intercrystalline Amino Acids of Fossil Brachiopods

JOPE (1969b) published the only study of the amino acid composition of fossil inarticulated brachiopods, studying *Petrocrania scabiosa* (HALL), *Orbiculoidea forbesi* (DAVIDSON), and *Lingula* sp. Amino acids recovered from the proteinaceous compounds remaining after demineralization differed proportionally from those of the nearest living relatives. Comparisons cannot be directly made, as figures are given as relative rather than actual abundance. Any de-

composition of amino acids over time will alter the relative abundance of the molecules and therefore minimize the level of the signal recovered.

Paracrystalline Amino Acids of Fossil Brachiopods

There is no published information on the amino acid composition of this fraction from fossil inarticulated species.

ARTICULATED BRACHIOPODS

Intercrystalline Amino Acids of Recent Brachiopods

Examination of the intercrystalline fraction has proceeded with amino acid taxonomy in mind, concentrating on the proteins recovered after demineralization in the form of the intercrystalline protein web. Articulated brachiopods are represented by *Neothyris* sp., *Laqueus californicus* (Koch), *Terebratella* sp., *Terebratalia transversa* (Sowerby), *Macandrevia cranium* (Müller), *Terebratulina* sp., *Hemithiris psittacea* (Gmelin), and *Notosaria nigricans* (Sowerby) (Jope, 1967a); and *Neothyris lenticularis* (Deshayes), *Terebratulina* sp., and *Hemithiris psittacea* (Gmelin) (Kolesnikov & Prosorovskaya, 1986).

Glycine (up to 40 percent) is the most abundant of the amino acids present in the intercrystalline fraction, followed by alanine (up to 14 percent). The acidic amino acids, aspartic and glutamic acid, which are abundant within the shells of molluscs (Weiner, 1983), are of generally low relative abundance in brachiopods (up to 12 percent and 8 percent respectively), possibly indicating a difference in function of the proteins from the two phyla. No hydroxyproline was detected, indicating that no collagen is present.

Taxonomy based on amino acid composition within articulated shells shows an ordinal level of separation, with the Terebratulida having lower acidic to basic ratios than the Rhynchonellida (1.3 to 1.9 as opposed to 2.3 to 2.5; Jope, 1967a). Familial separation may also be possible through differences in the relative abundance of amino acids (e.g., higher alanine in the Terebratellidae), although there are as yet insufficient analyses to test the separation of groups below this level. Initial conclusions tend to reinforce the morphological classification of these groups, although much further work will be required before a full assessment of the usefulness of this technique in taxonomy is possible.

Intracrystalline Amino Acids of Recent Brachiopods

Recent brachiopod shells contain appreciable amounts of intracrystalline amino acid, ranging between 70 and 800 ng/mg, most (generally >90 percent) of which is contained within proteins while the organism is living. Detailed analyses of the abundance of intracrystalline amino acids are available only for a limited but increasing number of samples of the orders Rhynchonellida and Terebratulida (Curry, Cusack, Endo, & others, 1991; Curry, Cusack, Walton, & others, 1991; Al-Rikabi, 1992; Walton, Cusack, & Curry, 1993), outlined below.

The intracrystalline amino acid compositions so far reported account for between 30 and 40 percent of the total amino acid present throughout the shell, excluding body tissue, and comprise 0.007 to 0.08 percent of the total mass of the shell. The absolute and relative abundance of intracrystalline amino acids varies taxonomically, reflecting variation in the number of types or sizes of the proteins present within the shell (Walton, Cusack, & Curry, 1993).

Rhynchonellide brachiopods are represented by *Notosaria nigricans* (Sowerby) and contain the highest concentrations of intracrystalline amino acid so far recorded. These shells are especially rich in the acidic molecule aspartic acid (214.52 mg/g; 36.94 mol percent) and in glycine (218.20 mg/g; 37.57 mol percent). Rhynchonellides also have a somewhat different organic matrix, and shell biomolecules are more resistant to the effects of oxidation by sodium hypochlorite. This may be related to the hard and soft

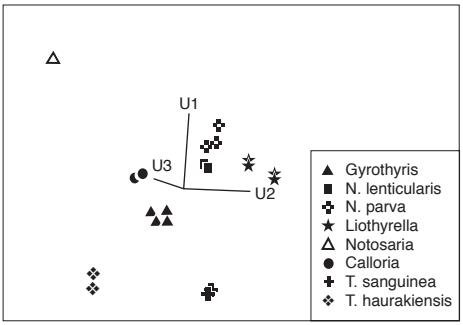

FIG. 204. Graph of the first three principal components of the relative proportion data for amino acids from recent brachiopods (complete organic extract). Note close groupings of the related species (e.g., members of the *Neothyris* genus) and the distance of more distantly related species (e.g., *Notosaria*) (new).

protein layers discussed by JOPE (1967a) for intercrystalline molecules.

Terebratulide brachiopods (represented by *Neothyris lenticularis* (DESHAYES), *Neothyris parva* (COOPER), *Calloria inconspicua* (SOWERBY), *Terebratella sanguinea* (LEACH), *Terebratella haurakiensis* (ALLAN), *Liothyrella neozelanica* (THOMSON), and *Gyrothyris mawsoni* (THOMSON) are all generally characterized by high concentrations of glycine (up to 55 percent), proline (up to 9 percent), and alanine (up to 8 percent). High concentrations of glycine and proline may reflect the conformation of the included protein; such amino acids are common in tightly folded proteins.

The information derived from the amino acids for taxonomic purposes is difficult to assimilate objectively from the raw data alone: the information is contained within up to 17 variables. Several investigations have used factor and principal component analysis (PCA) to differentiate between species (DEGENS, SPENCER, & PARKER, 1967; KING & HARE, 1972; HAUGEN, SEJRUP, & VOGT, 1989), although as yet this has only once been applied to brachiopods (Fig. 204; WALTON, CUSACK, & CURRY, 1993). Scatter plots and three-axis plots allow the variation summarized in the principal components to be observed directly. Brachiopods that are closely related should have fewer differences in the abundance of amino acids and therefore should have less variation. This may be observed in Figure 204, where rhynchonellide brachiopods plot at a distance from terebratulides. Within the terebratulide genus *Neothyris,* two species investigated plot closely together. This contrasts with the situation in *Terebratella* where two species studied are widely separated on the basis of their amino acid compositions. Further research is necessary to explore the taxonomic value of such results.

Intercrystalline Amino Acids of Fossil Brachiopods

Amino acids have been extracted from intercrystalline sites in brachiopod shells as old as Silurian and have been compared with those in recent brachiopods from similar sites in a number of studies (JOPE, 1977, 1980; KOLESNIKOV & PROSOROVSKAYA, 1986). Comparisons of the amino acid composition allowed some phylogenetic interpretation (to the class level), which generally confirm the morphological discrimination. Amino acid compositions from fossil articulated brachiopods show marked differences from their nearest living relatives, probably resulting from the diagenetic alteration of the proteins, although this has not been quantified.

Articulated brachiopods are represented by *Camarotechia* sp., *Epithyris oxonica* (ARKELL), *Globirhynchia subobsoleta* (DAVIDSON), *Loboidothyris kakardinensis* (MOISSEEV), and *Gusarella gusarensis* (MOISSEEV). All samples released amino acids only on hydrolysis, indicating the presence of acid labile bonds. In all instances the soluble proteins analyzed for recent shells had been lost through the action of migrating fluids, and thus two different sets of proteins have been sampled, probably accounting for the marked differences in the amino acid compositions of the two fractions. In addition, all free amino acids (those formed through the degradation of peptide bonds) have been lost. Intercrystalline amino acids from fossil samples appear not to contain much phylogenetic information.

The composition of each of the five samples is markedly different from that of their nearest recent relatives. Of particular note in the work of both JOPE (1967b) and KOLESNIKOV and PROSOROVSKAYA (1986) are the raised levels of serine and glutamic acid in the fossil samples, which contrast strongly with the data from the intracrystalline sites (see below). Serine is a common, natural contaminant, and thus the raised levels of this amino acid might indicate some contamination of the sample from extraneous sources (e.g., ORÓ & SKEWES, 1965; WALTON & CURRY, 1991). Intercrystalline amino acids from fossil samples appear not to contain significant amounts of phylogenetic information.

Intracrystalline Amino Acids of Fossil Shells

Amino acids and paleoproteins have been sampled from several genera of brachiopods ranging in age from 0.12 to 2.6 Ma (WALTON, 1992). Compared to those of recent samples, both the relative and absolute abundances of the molecules are altered, sometimes dramatically. Although such differences in amino acid composition could be due to either genetic or diagenetic change, the most notable effect is likely to be the degradation during diagenesis of the structure of the proteins and amino acids that were originally present within the shell. The peptide bond (linking the amino acids) is the most unstable part of the protein structure, and the cleavage of this bond, by hydrolysis, is the first step in the degradation of the protein (HARE & MITTERER, 1969; VAN KLEEF, DE JONG, & HOENDERS, 1975). In the intracrystalline proteins of brachiopods, this process is extremely rapid. By the time the valve is 0.12 Ma old, more than 60 percent of the total amino acid that remains is present in the free state (WALTON, 1992). Such observations indicate that perfect protein preservation within the shell is not likely; peptide bonds are degraded, and only the free amino acids survive, which remain trapped within the biocrystal. In intercrystalline sites, it is possible that these will be lost through leaching from the shell matrix. The degradation products of the proteins may be directly sampled from intracrystalline sites.

Individual amino acids vary in their stability toward oxygen and water (Fig. 205). Once free from the relative protection of the protein structure, amino acids will themselves degrade at a rate dependent on their stability and ambient temperatures and the time they are exposed to these conditions. The molecules present within the shell form a complex mixture of preserved short chains of paleoprotein-peptide, released (free) amino acids, and the variously degraded remains of amino acids.

The most common amino acids found in fossils are glycine, alanine, aspartic acid and glutamic acid. They are present in absolute abundances that generally reflect their original proportions; for example, glycine remains the most abundant amino acid but decreases in concentration from 76 ng/mg to

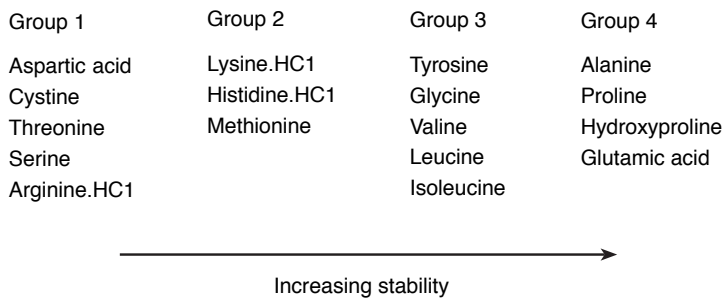

FIG. 205. Relative stability of the amino acids determined by pyrolysis experiments (new; data from Vallentyne, 1964).

31 ng/mg over a 2.2 Ma time interval (WALTON, 1992). The exception is alanine, which increases greatly in concentration in young fossil samples. This increase is due to the diagenetic production of alanine during the decomposition of serine (BADA & others, 1978) and possibly of phenylalanine and tyrosine (WALTON, 1992).

Glutamic acid is preserved in the fossil record by conversion of the released biomolecule to its lactam pyroglutamic acid (WILSON & CANNON, 1937). In fossil samples this has a dramatic effect. First, lactam may only form after natural hydrolysis has taken place so that its formation is evidence of cleavage of the peptide bond on either side of a particular glutamic acid residue. Second, the formation of the lactam releases a molecule of water, allowing further degradation of the protein. Third, this is a method whereby much of the original amino acid may be preserved: the lactam reverts to glutamic acid on hydrolysis and thus a large proportion of the original amino acid is preserved.

Further protein diagenesis accelerates degradation of the molecules with individual amino acids undergoing irreversible degradation. Such degradation rapidly reduces the level of taxonomic information, which may be revealed through the amino acid record. For example, a well-documented degradation pathway is the degradation of the hydroxy amino acids serine and threonine (BADA & others, 1978), whereby a number of products may be derived from the amino acid parent molecules, including other proteinaceous amino acids.

Such amino acids that are readily degraded as arginine, threonine, and serine quickly become unavailable for taxonomic differentiation. In Calloria inconspicua for example, serine drops from 7 ng/mg to 0.8 ng/mg, arginine from 6.7 ng/mg to 0, and threonine from 3.7 ng/mg to 0 over 2.2 Ma (WALTON, 1992). It is likely that reduction in the specificity of the PCA calculations is due to this information loss. In any local sedimentary succession, however, it is likely that samples have been subjected to a similar thermal history, and the level of organic degradation is likely to be the same for different fossil species. Coeval species from different localities cannot accurately be compared using PCA unless corrections can be made to diagenetic effects on the proportions of the amino acids.

Shells of terebratulides and rhynchonellides from the Plio-Pleistocene South Wanganui basin of New Zealand have been analyzed using PCA by WALTON (1992), and a trend has been observed in the information recovered by this technique. In the youngest fossil samples, there is good separation between the species, with out-groups of molluscs included to demonstrate that the amino acid signal had not homogenized. Progressively older samples move closer together within the dimensions defined by the principal components (Fig. 206–207). This indicates how decomposition of susceptible amino acids at various sites within an organism might preclude discrimination. A basic taxonomic distinction can still be derived to the ordinal level although how much this discrimination is affected by diagenesis is not yet known. Such analyses may provide some preliminary evidence for the use of amino acids as taxonomic indicators in the fossil record.

PROTEINS

GENERAL

Proteins are highly information-rich molecules since the order of amino acids in the polypeptide chain, the primary sequence, relates to the order of nucleotide bases within the genome. By characterizing the proteins, it should be possible to comment on the relationships between brachiopod species at a molecular level. Attempts to obtain phylogenetic information from shell proteins have led to a range of approaches being employed. Some studies (CURRY, CUSACK, ENDO, & others, 1991; CURRY, CUSACK, WALTON, & others, 1991; CUSACK & others, 1992) extract only intracrystalline material, while others extract all of the soluble protein from within the valves (JOPE, 1965, 1967a, 1967b,

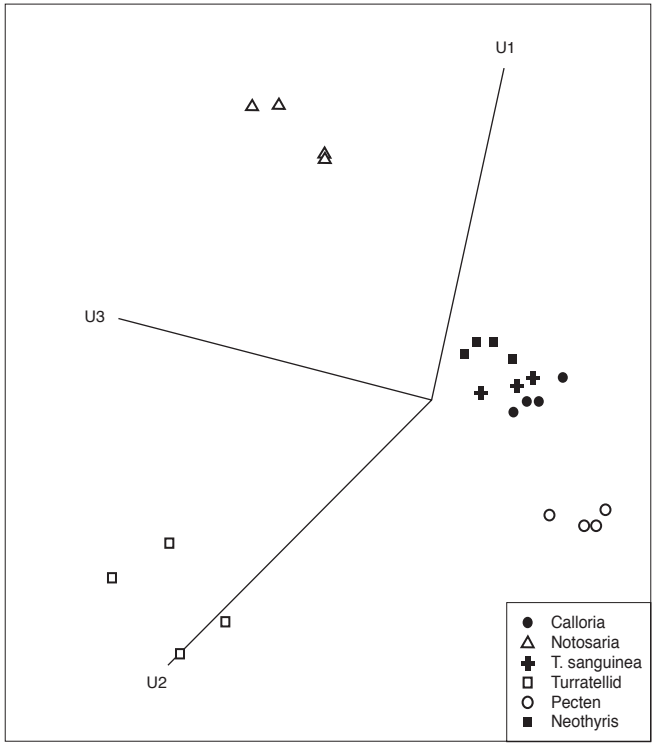

FIG. 206. Graph of the three principal components calculated for the reactive proportions of amino acids from the Tainui shell bed. Separation of the species is at the subordinal level; although the *Terebratulida* plot close together, they may still be separated (new).

1969b, 1973, 1979). In addition, in some instances, proteins are extracted and then purified to homogeneity to allow characterization of individual protein species (JOPE, 1969a, 1969b) and determination of primary sequences (CURRY, CUSACK, ENDO, & others, 1991; CURRY, CUSACK, WALTON, & others, 1991; CUSACK & others, 1992); other studies have analyzed the total protein fraction (JOPE, 1965, 1967a, 1967b).

PROTEINS OF ARTICULATED BRACHIOPODS

Proteins are extracted from the mineral of the articulated brachiopods by chelating the calcium of the calcite with ethane diamine tetra acetic acid (EDTA) (CUSACK & others, 1992). Dissolution of the mineral is effected after the intercrystalline proteinaceous material has been destroyed by oxidation with sodium hypochlorite, ensuring that only proteins within the mineral are isolated. EDTA is removed and the sample concentrated using the Minitan tangential-flow filtration system fitted with filters of 10 kDa molecular weight cutoff. This cutoff depends on the conformation of the protein, and, therefore, some molecules smaller than 10 kDa will be retained.

Typically, a final volume of 2 ml concentrated extract is obtained from 100 g of shell. The proteins extracted from the valves are then separated by sodium dodecyl sulphate polyacrylamide gel electrophoresis (SDS PAGE). The separated proteins are revealed by staining with Coomassie Brilliant Blue R250, and the molecular weight of each protein is estimated. Samples for SDS PAGE are generally 10 µl from the 2 ml extract, approximately equivalent to the extract from 0.5 g of shell material. Proteins can be either fixed and stained in the gel using Coomassie

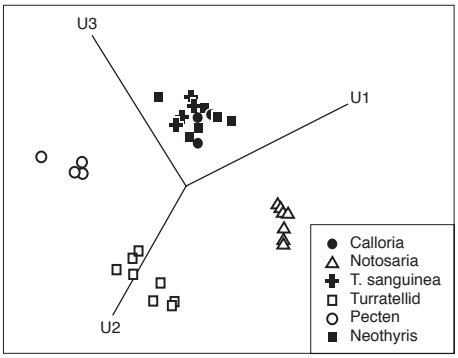

FIG. 207. Graph of the three principal components calculated for the relative proportions of amino acids from the Kupe Formation. Separation of the species is at the ordinal level with *Notosaria* samples plotting away from the rest of the samples, although the *Terebratulida* plot close together (new).

or electroblotted onto ProBlott™ membrane and revealed on the membrane, again with Coomassie. Immobilizing the protein mixture on the membrane provides a stable record of the protein samples, and the amino acid composition and N-terminal sequence can be determined from the immobilized proteins. The articulated brachiopods included in this study and their collection localities are listed in Table 22.

SDS PAGE analyses of the intracrystalline proteins of the above articulated brachiopods are presented in Figures 208 to 213, and a summary of the number and size of intracrystalline proteins is presented in Table 23.

T. retusa appears to contain three intracrystalline proteins (Fig. 208). The major protein, of molecular weight 44 kDa, may be further fractionated to two protein bands on extended electrophoresis (Julie LAING, personal communication, 1995). In addition, highly concentrated extracts obtained using filters with 5 kDa cutoff indicate that other protein species, in addition to those of 18 and 79 kDa, are also present (Julie LAING, personal communication, 1995). *C. inconspicua* contains three proteins of molecular weights 6.5, 16, and 49 kDa (Fig. 209). In Figure 210 the four proteins of *N. lenticularis* are evident. These proteins are of the same molecular weight as those from C. inconspicua with an additional 20 kDa protein. The mixture of intracrystalline proteins from *T. sanguinea* comprises two major proteins of 6.5 and 49 kDa molecular weight as well as three minor proteins of 10, 16, and 20 kDa (Fig. 211). The three proteins of *T. coreanica* are of similar molecular weight (Fig. 212) to those of *C. inconspicua* (Fig. 209). *L. rubellus* contains three major proteins of 6.5, 10, and 50 kDa molecular weight as well as a minor protein of 47 kDa (Fig. 213).

Carotenoproteins

CUSACK and others (1992) demonstrated the presence of carotenoprotein in three species of terebratulid brachiopods. These pigmented brachiopods are *Neothyris lenticularis, Calloria inconspicua,* and *Terebratella sanguinea.* The pigmentation in all three species results from a carotenoid bound to the 6.5 kDa protein. The N-terminal sequence of this 6.5 kDa protein has been determined from these three New Zealand brachiopods with red valves (Fig. 214).

The low level of carotenoprotein (27.22, 41.11, and 47.58 ng/g shell in *N. lenticularis, C. inconspicua,* and *T. sanguinea* respectively) precluded the extraction of the carotenoid directly from purified carotenoprotein for identification, and so carotenoid was extracted from whole valves. The pig-

TABLE 22. Species and localities used in SDS PAGE analysis of intracrystalline proteins of valves of articulated brachiopods (new).

Brachiopod	Locality
Terebratulina retusa (LEACH)	Kerrera Sound, Scotland
Calloria inconspicua (SOWERBY)	Portobello Caves, New Zealand
Neothyris lenticularis (DESHAYES)	Paterson Inlet, Stewart Island, New Zealand
Terebratella sanguinea (LEACH)	Paterson Inlet, Stewart Island, New Zealand
Terebratalia coreanica (ADAMS & REEVE)	Oki Island, Shimane, Japan
Laqueus rubellus (SOWERBY)	Jogashima, Sagami Bay, Japan

ment could not be extracted from finely powdered shells using cold or warm organic solvents such as methanol, ethanol, acetone, or dichloromethane (CLEGG, 1993). Demineralization of the shell with EDTA resulted in the release of the pigment indicating an intimate association between the carotenoprotein and the mineral. The red pigment was extracted using the acetone-diethyl ether method of POWLS and BRITTON (1976). Two carotenoids are present in the valves, canthaxanthin, and the tentatively identified mono-acetylenic analogue of astaxanthin, according to the standard color test of DUNNING (1963), solubility in organic solvents, co-chromatography with pure carotenoid standards, β-carotene and canthaxanthin, and mass spectroscopy. The total amount of carotenoid in the valves is 0.76 μg, 1 μg, and 0.81 μg/g shell for *N. lenticularis, C. inconspicua,* and *T. sanguinea,* respectively (CLEGG, 1993). It is not known which of the two carotenoids is attached to the 6.5 kDa protein.

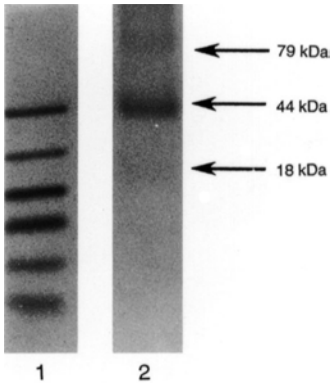

FIG. 208. Separation of intracrystalline proteins of *Terebratulina retusa* by SDS PAGE in a 15 percent polyacrylamide gel according to the method of SCHÄGGER and VON JAGOW, 1987. Proteins were fixed and revealed using Coomassie Brilliant Blue R250 stain. Lane 1 contains protein standards of the following molecular weight: 45 kDa, 29 kDa, 18 kDa, 15 kDa, 6 kDa, and 3 kDa. Lane 2 contains the intracrystalline protein extract (new).

PROTEINS OF INARTICULATED BRACHIOPODS

The inarticulated brachiopods (and localities) included in this study are presented in Table 24. A summary of the number and size of mineral-associated proteins in the inarticulated brachiopod valves is given in Table 25.

The molecular components of *Lingula anatina* (LAMARCK) have been studied more extensively than any other species of inarticulated brachiopod. JOPE (1973) extracted three proteins from the valves of *Lingula anatina.* TUROSS and FISHER (1989) used guanidine to extract nonmineral-associated protein, which they described as analogous to those extracted by JOPE in 1973. TUROSS and FISHER (1989) also used EDTA to extract mineral-associated proteins from *Lingula anatina* valves; and the extract was dominated by a 43 kDa protein, which they suggested may play a role in the control of the formation of the mineral phase. TUROSS and HARE (1990) reestimated the molecular weight of this protein as 40 kDa and, using a polyclonal antibody generated against the protein, demonstrated that the protein can

TABLE 23. Estimated molecular weight of intracrystalline proteins of articulated brachiopod valves as determined by SDS PAGE (see Fig. 208–213; see Fig. 214 for N-terminal sequence) (new).

Brachiopod	Protein Number	Molecular weight (kDa) Major	Minor
Terebratulina retusa (LEACH)	3	44,	79, 18
Calloria inconspicua (SOWERBY)	3	6.5*, 16, 49	
Neothyris lenticularis (DESHAYES)	4	6.5*, 16, 20, 49	
Terebratella sanguinea (LEACH)	5	6.5*, 49	10, 16, 20
Terebratalia coreanica (ADAMS & REEVE)	3	6.5, 16, 49	
Laqueus rubellus (SOWERBY)	4	6.5, 10, 50	47

*carotenoprotein.

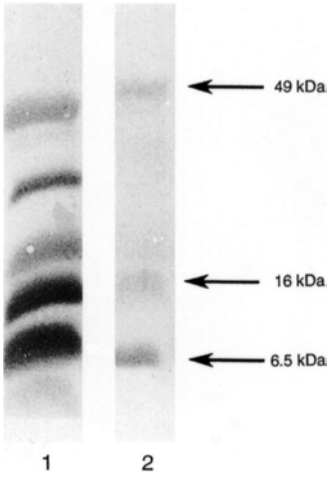

FIG. 209. Separation of intracrystalline proteins of *Calloria inconspicua* by SDS PAGE as described in the caption of Figure 208. Following SDS PAGE, the proteins were electroblotted onto ProBlott™ membrane and revealed using Coomassie Blue staining (new).

be detected in fossil *Lingula*. WILLIAMS, CUSACK, and MACKAY (1994) extracted all of the soluble protein from *Lingula anatina* valves; at least ten proteins were identified in the 6 to 50 kDa molecular weight range (Fig. 215) with the major protein of molecular weight 36 kDa likely to be that described by TUROSS and FISHER (1989) as 43 kDa and as 40 kDa by TUROSS and HARE (1990). In each case the molecular weight of the protein was assessed by SDS PAGE, which provides only an estimate of molecular weight.

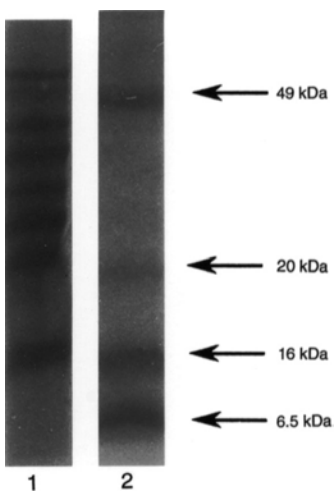

FIG. 210. Separation of intracrystalline proteins of *Neothyris lenticularis* by SDS PAGE as described in the caption of Figure 208. The molecular weights of the standard protein in Lane 1 are 66 kDa, 45 kDa, 36 kDa, 29 kDa, 24 kDa, 20 kDa, and 14.2 kDa (new).

Clean, powdered valves of *Glottidia pyramidata* were incubated with an aqueous solution of sodium hypochlorite to destroy the exposed organic material. Following removal of the sodium hypochlorite, the mineral phase was dissolved using EDTA to release the organic material more intimately associated with the mineral. *G. pyramidata* valves contain five, mineral-associated proteins of estimated molecular weights 28, 35, 52, 62, and 144 kDa (Fig. 216). In addition to these distinct bands, there are two diffuse bands in the 8 and 17 kDa molecular weight range, which may be glycosylated proteins.

Powdered valves of *Discinisca tenuis* were demineralized after incubation with hypochlorite or phosphate buffer. The proteins extracted after treatment with hypochlorite are those more closely associated with the mineral. Three mineral-associated proteins of molecular weight 6, 9, and 14 kDa are evident (Fig. 217). Bleach treatment removes the large range of higher molecular weight proteins found in unbleached samples. In addition, the 6 kDa protein is present in higher levels in the extract that has not been bleached, indicating that the bleach treatment may also destroy some of the mineral-associated protein.

Although *Neocrania anomala* lacks articulation, the valves are calcitic, and the proteins were extracted from the valves as for the articulated, calcitic brachiopods (CUSACK & others, 1992). One major protein, of molecular weight 40 kDa, is evident; there appears to be a minor protein of molecular weight 44 kDa as well as a protein of 8 kDa (Fig. 218).

Collagen

JOPE (1967a) detected the modified amino acid hydroxyproline in the shell of the phosphatic, inarticulated brachiopods *Lingula anatina* and *Discinisca striata,* while it was

absent from the nine species of carbonate brachiopods in her survey, including the inarticulated carbonate brachiopod *Neocrania anomala.* Although hydroxyproline is considered indicative of collagen, JOPE did not present direct evidence of the presence of collagen in the phosphatic valves other than to mention the unpublished work of OWEN, who detected fibrous, collagen-like structures in the valves of *Discina striata.* These fibers, however, lacked the characteristic banding pattern of collagen fibers. JOPE (1967a, 1973) also reported insufficient levels of glycine, since glycine makes up one-third of the total amino acids in collagen. TUROSS and FISHER (1989) confirmed the presence of hydroxyproline in *Lingula anatina,* although no collagen was extracted. WILLIAMS, CUSACK, and MACKAY (1994) clearly demonstrated the presence of fibrillar collagen with a banding periodicity of 45 nm in the body platform of *Lingula anatina* valves.

Biological systems generally employ one of the three, major molecular systems in skeletal support: the cellulose system so widely present in plants, the collagenous system common in animals, and the chitinous system. Chitin often occurs in fungal cell walls, replacing cellulose, but chitin is best known for its occurrence in the cuticle of arthropods (RUDALL, 1969). It is intriguing that *Lingula* valves should possess collagen as well as chitin (see section on chitin, p. 260, for more information). The presence of collagen in a phosphatic, biomineralized system, the *Lingula* valve, is analogous with the composition of vertebrate bone.

LIPIDS IN BRACHIOPOD VALVES

GENERAL

The presence of lipids in brachiopod valves was first described by JOPE (1965) from recent brachiopod valves. Within shells generally, the organic matter is predominantly proteinaceous, but small amounts of lipids, pigments, and polysaccharides also occur (HARE, 1962). Analysis of the organic components of brachiopod valves has tended to concentrate on proteins and amino acids since such molecules yield taxonomic information. Lipids, however, have a greater preservation potential than proteins due to their low solubility in water (EGLINTON & LOGAN,

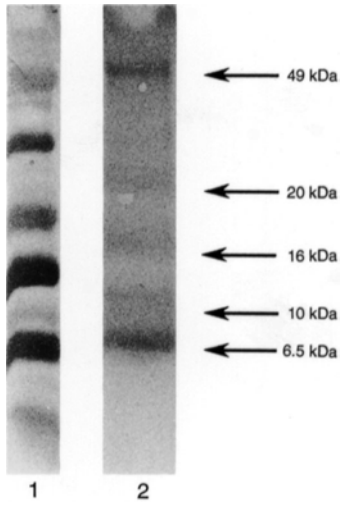

FIG. 211. Separation of intracrystalline proteins of *Terebratella sanguinea* by SDS PAGE as described in the caption of Figure 208. Following SDS PAGE, the proteins were electroblotted onto ProBlott™ membrane and revealed using Coomassie Blue staining (new).

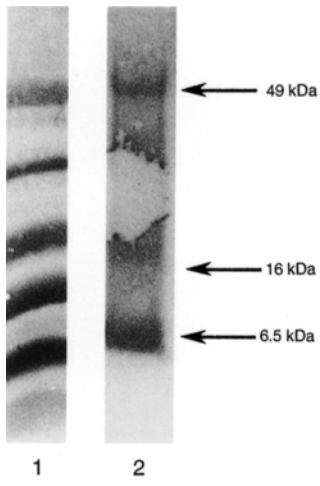

FIG. 212. Separation of intracrystalline proteins of *Terebratalia coreanica* by SDS PAGE as described in the caption of Figure 208. Following SDS PAGE, the proteins were electroblotted onto ProBlott™ membrane and revealed using Coomassie Blue staining (new).

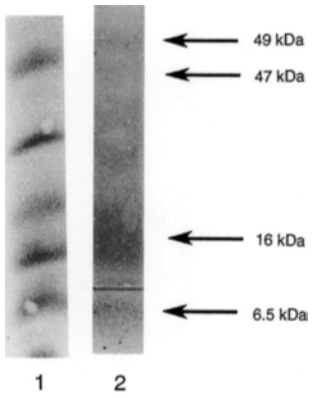

FIG. 213. Separation of intracrystalline proteins of *Laqueus rubellus* by SDS PAGE as described in the caption of Figure 208. Following SDS PAGE, the proteins were electroblotted onto ProBlott™ membrane and revealed using Coomassie Blue staining (new).

1991). Although diagenesis may alter the lipids especially by the hydrogenation of double bonds, aromatization of rings, or loss of such functional groups as hydroxyl groups, the carbon skeleton is retained such that an unequivocal link can be made with a known biological molecule (EGLINTON & LOGAN, 1991).

Lipids in Living Brachiopods

JOPE (1971) estimated that lipids comprise 5 percent of the total organic material in the valves of the rhynchonellides *Notosaria* and *Hemithiris,* 40 percent of which are neutral lipids, chiefly cholesterol or its ester and 60 percent polar lipids. The polar lipids contain a high proportion of phosphatidylethanolamine, phosphatidylserine, and small amounts of phosphatidylcholine, phosphoinositide, and sphingomyelin. In the terebratulides, the proportion is 30 percent neutral and 70 percent polar lipids.

	10			20
N. lenticularis	**GWEQL**	**PYATM**	**ISKTS**	**NA_KP**
C. inconspicua	**GWEQL**	**PYATM**	**ISKTS**	**QAKNP**
T. sanguinea	**GWEYL**	**PYASM**	**ISKTS**	**QADNP**

FIG. 214. N-terminal amino acid sequence of the 6.5 kDa protein from *N. lenticularis, C. inconspicua,* and *T. sanguinea.* The sequence is presented using the one-letter code for amino acids. Those amino acid residues that are identical in all three proteins are presented in bold to highlight the high degree of sequence similarity (new).

CLEGG (1993) isolated three fractions of lipids from the brachiopod valve: intercrystalline free lipids (IFL), intracrystalline free lipids (FIL), and bound intracrystalline lipids (BIL), that is, lipids bound to crystals. The lipids were isolated and characterized using GC-MS from the valves of living *Neothyris lenticularis* (DESHAYES), *Calloria inconspicua* (SOWERBY), and *Terebratella sanguinea* (LEACH). The identity and quantity of intercrystalline free lipids (IFL) from shells of living *N. lenticularis, C. inconspicua,* and *T. sanguinea* are presented in Table 26.

C. inconspicua contains a higher concentration of sterols (19.86 μg/g) than *N. lenticularis* (10.16 μg/g) and *T. sanguinea* (17.18 μg/g). Cholest-5-en-3β-ol was the dominant sterol for all three species but particularly for *C. inconspicua,* representing more than 50 percent of the sterol composition. *C. inconspicua* contains the highest percentage of C_{27} sterols, 59.3 percent, compared with 54.3 percent and 50 percent for *N. lenticularis* and *T. sanguinea,* respectively. C_{28} sterols, however, constituted 39.6 percent of the total sterols in *T. sanguinea* compared with 33.2 percent and 29 percent in *N. lenticularis* and *C. inconspicua*. *n*-C_{28} alcohol was found in *N. lenticularis* and *C. inconspicua.*

The identity and quantity of intracrystalline free lipids (FIL) from shells of living *N. lenticularis* and *T. sanguinea* are presented in Table 27.

T. sanguinea contains the highest concentration of fatty acids in the FIL fraction (1.73 μg/g) compared with 1.54 μg/g for *N. lenticularis.* $C_{16:0}$ is the dominant fatty acid in both species. $C_{12:0}$ and $C_{18:0}$ are the second most abundant fatty acids of *T. sanguinea* and *N. lenticularis,* respectively. In both species there is a dominance of even-numbered fatty acids. The identity and quantity of intracrystalline, crystal-bound fatty acids and *n*-alcohols from shells of living *N. lenticularis, C. inconspicua,* and *T. sanguinea* are presented in Table 28.

C. inconspicua contains the highest concentration of fatty acids and *n*-alcohols (23.62 μg/g) in the BIL fraction, while *N. lenticularis* contains 9.82 μg/g and *T. sanguinea* contains 18.77 μg/g. There is a dominance of even-numbered fatty acids in the three species. The BIL fraction contains the highest concentration of lipids compared with the FIL and IFL fractions of the three species studied. $C_{16:0}$ fatty acid is the dominant compound in the BIL fraction. *T. sanguinea* contains the highest concentration of unsaturated fatty acids in the BIL fraction (6.06 μg/g) in comparison with *C. inconspicua* (3.21 μg/g) and *N. lenticularis* (2.85 μg/g).

Lipids in Recent Brachiopods

CLEGG (1993) examined the lipids in the shells of recent *N. lenticularis* dredged from Otago Head Peninsula, South Island, New Zealand, and *C. inconspicua* and *Notosaria nigricans* (SOWERBY) that were washed up on the seashore. No estimate of age of the shells was available. No lipids could be extracted from the IFL fraction of recent *N. lenticularis, C. inconspicua,* and *N. nigricans.* Lipids could not be extracted from the FIL fraction of *N. nigricans.* The quantities of fatty acids in the FIL fraction of *C. inconspicua* and *N. lenticularis* are presented in Table 29.

Recent *N. lenticularis* contains a greater concentration of fatty acids in the FIL fraction (0.41 μg/g) than *C. inconspicua* (0.06 μg/g). Polyunsaturated fatty acid $C_{20:2}$ and monounsaturated fatty acid $C_{20:1}$ do not occur in recent *N. lenticularis* but do occur in the FIL fraction of living *N. lenticularis.* Odd-numbered fatty acids did not occur in the FIL fraction of *C. inconspicua.* Recent *N. lenticularis* has decreased saturated fatty acids but not unsaturated fatty acids.

The lipids of the BIL fraction of *N. nigricans* are nonvolatile and not amenable to GC analysis. Recent *N. lenticularis* contains a higher concentration of lipids (3.65 μg/g) in the BIL fraction than recent *C. inconspicua* (2.11 μg/g). This is the reverse of the situation in living shells, where *C. inconspicua* contains more than twice the amount of lipids in the BIL fraction than *N. lenticularis.* All of the fatty acids in the BIL fraction decreased in concentration from living to dead recent shells, especially for *C. inconspicua.* Saturated fatty acids decrease more rapidly in the FIL fraction than in the BIL fraction of *N. lenticularis.*

TABLE 24. Species and localities used in SDS PAGE analysis of mineral-associated proteins of valves of inarticulated brachiopods (new).

Brachiopod	Locality
Lingula anatina (LAMARCK)	Ariake Bay, Japan
Glottidia pyramidata (STIMPSON)	Panacea, Florida
Discinisca tenuis (SOWERBY)	Swapokmund, Namibia
Neocrania anomala (MÜLLER)	Kerrera Sound, Scotland

Lipids in Fossil Brachiopods

Lipids from fossil brachiopods have been analyzed by THOMPSON and CREATH (1966), IVANOV and STOYANOVA (1972), IVANOV, STOYANOVA, and DASKALOV (1975), and STOYANOVA (1984). THOMPSON and CREATH (1966) examined the lipids in the atrypidine brachiopods *Atrypa spinosa* (Devonian) and the orthidine *Platystrophia* sp. (Ordovician), which contained 6.8 μg/g and 7.5 μg/g respectively of C_1 to C_5, low-molecular-weight

TABLE 25. Estimated molecular weight of mineral-associated proteins of inarticulated brachiopod valves as determined by SDS PAGE (see Fig. 215–218). Values in parentheses represent diffuse bands that may be glycosylated (new).

Brachiopod	Protein Number	Protein Molecular weight (kDa)
Lingula anatina (LAMARCK)	10	6–50
Glottidia pyramidata (STIMPSON)	7	28, 35, 52, 62, 144 (8, 17)
Discinisca tenuis (SOWERBY)	3	6, 9, 14
Neocrania anomala (MÜLLER)	3	8, 40, 44

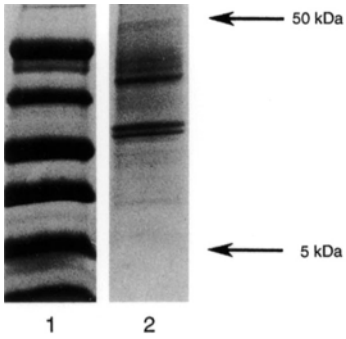

FIG. 215. Separation of paracrystalline proteins from *Lingula anatina* valves by SDS PAGE as described in the caption of Figure 208 (new).

hydrocarbons. IVANOV and STOYANOVA (1972) analyzed an unspecified brachiopod species (Devonian) that contained a homologous series of normal alkanes from *n*-C_{14} to *n*-C_{35}. They also reported branched (unspecified) and normal fatty acids from C_{14} to C_{26} from an unknown brachiopod species of Devonian age. $C_{16:0}$ and $C_{18:0}$ were present in the highest proportions. STOYANOVA (1984) studied in detail the normal alkanes and normal fatty acids in *Atrypa reticularis* (Upper Silurian), *Sieberella sieberi* (Lower Devonian), *Spirifer elegans* (Middle Devonian), *Marginifera* sp. (Upper Permian), and *Productus horides* (Upper Permian). The survey revealed a trend of increasing amounts of alkanes and decreasing levels of fatty acids with increasing age of the fossil.

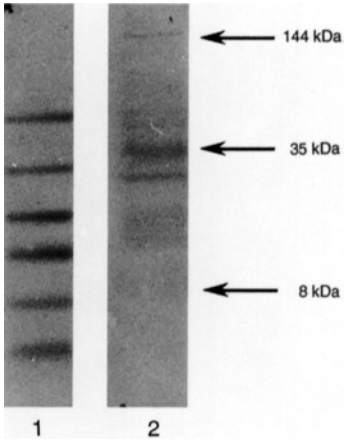

FIG. 216. Separation of paracrystalline proteins from *Glottidia pyramidata* valves by SDS PAGE as described in the caption of Figure 208 (new).

These studies did not distinguish between intercrystalline and intracrystalline lipids. CLEGG (1993) analyzed fossil brachiopod shells to compare the lipids of the shells of living brachiopods with those from the corresponding fossil ancestors. The fossil samples included in the survey are presented in Table 30.

Fossil terebratulides were analyzed as well as a specimen of chonetidine *Daviesiella llangollensis* (Carboniferous) from northern Wales to assess the long-term survival of lipids. Alcohols *n*-$C_{22\text{-}30}$ are an important component of the IFL fraction of the fossil samples, particularly *n*-C_{22} and *n*-C_{28} alcohols. Identification of the compounds in the FIL fraction of the fossil samples was not possible due to the very low level of purified compounds. Only the tentative identification of the fatty acids in the FIL fraction of the *Neothyris* sp. was possible (Table 31). Samples of *Neothyris* sp. analyzed were from the Kupe shell bed (0.45 Ma), Waipuru shell bed (1.49 Ma), and the Wairarapa Formation (1.47 to 1.7 Ma).

All three samples contained very low levels of fatty acids. $C_{16:0}$ is the dominant fatty acid in the FIL fraction of *Neothyris* from the Kupe shell bed, while samples from Waipuru and Wairarapa contained $C_{14:0}$ and $C_{16:0}$ as the most abundant fatty acids. The quantities of lipid components from the BIL fraction of fossil brachiopods are presented in Table 32. The dominant class of lipids in the BIL fraction of all the fossils examined are the fatty acids. *Neothyris* sp. (Rapanui Formation, 0.12 Ma and Waipipi, 2.65 Ma) and *C. inconspicua* (Kupe shell bed, 0.45 Ma) do not contain unsaturated fatty acids. Analysis of the lipids in the BIL fraction of three different genera from the Kupe shell bed, *Neothyris* sp., *T. sanguinea,* and *C. inconspicua,* revealed differences in the lipid composition that are likely to be important at the generic

level since the samples are all from the same locality. *C. inconspicua* contains the greatest range of lipids. The concentration of $C_{16:0}$ fatty acid in *C. inconspicua* was more than twice that of *T. sanguinea. C. inconspicua* contains no unsaturated fatty acids in the BIL fraction. *Neothyris* sp. contains the highest amount of $C_{14:0}$ and $C_{18:0}$ fatty acids. The BIL fraction of *Neothyris* sp. also contains C_{21}, C_{24}, C_{26} α-hydroxy fatty acids and C_{22} ω-hydroxy fatty acids, which are not present in the BIL fraction of *C. inconspicua* and *T. sanguinea. C. inconspicua* contains $C_{19:0}$ and $C_{30:0}$ fatty acids that are not present in *Neothyris* sp. and *T. sanguinea.* C_{14} β-hydroxy fatty acid present in *T. sanguinea* is not present in the BIL fraction of *Neothyris* sp. or *C. inconspicua.* The major similarity between the three species is the dominance of saturated fatty acids.

The dominant constituent of the BIL fraction from *Neothyris* sp. and *T. sanguinea* from Waipipi (2.5 Ma) are saturated fatty acids. *T. sanguinea* contains a higher concentration of $C_{14:0}$, $C_{15:0}$, $C_{16:0}$, $C_{17:0}$, $C_{18:0}$, $C_{19:0}$, $C_{22:0}$, and $C_{23:0}$, while *Neothyris* sp. contains a higher concentration of $C_{24:0}$, $C_{26:0}$, and $C_{28:0}$ fatty acids. *T. sanguinea* contains a large amount of C_{22} ω-hydroxy fatty acid (0.38 μg/g) as well as α-hydroxy fatty acids, neither of which occurs in *Neothyris* sp., although C_{13} β-hydroxy fatty acid is present in *Neothyris* sp.

The Carboniferous brachiopod *Daviesiella llangollensis* did not yield an insoluble fraction, and, therefore, it was not possible to compare the BIL fraction with that of the New Zealand fossils. The dominant compounds present in the IFL fraction are squalene, pristane, and phytane, indicating postdepositional ingress. The FIL fraction contains a homologous series of *n*-alkanes, *n*-C_{24} being the most abundant. There is a dominance of even *n*-alkanes. The presence of pristane and phytane in the FIL fraction indicates some postdepositional ingress.

The living brachiopods contain the highest concentration and range of lipids with a significant reduction for recent and fossil shells for both the free and unbound fractions. Although lipids have been isolated and characterized from living, recent, and fossil brachiopod valves, the source or role of these lipids is unknown. The epithelial cells of the mantle are the most likely source of the lipids, which may be important for biomineralization or may simply be trapped during deposition of the shell.

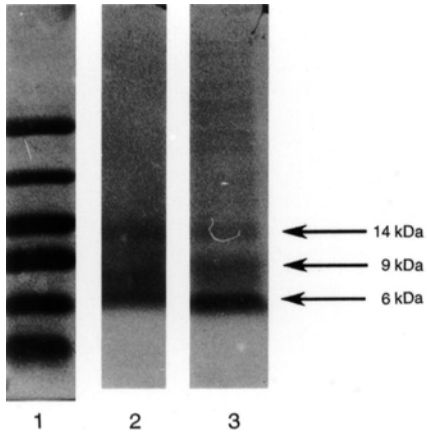

FIG. 217. Separation of proteins from *Discinisca tenuis* valves by SDS PAGE as described in the caption of Figure 208. Lane 1 contains proteins of known molecular weight (see caption of Figure 208). The sample in lane 2 has been treated with sodium hypochlorite before EDTA dissolution while the sample in lane 3 has not (new).

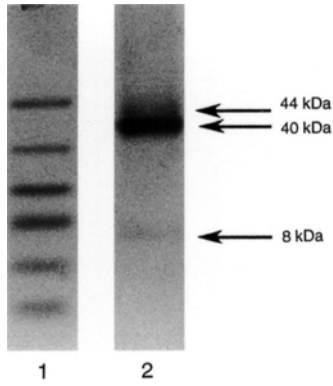

FIG. 218. Separation of mineral-associated proteins from *Neocrania anomala* valves by SDS PAGE as described in the caption of Figure 208 (new).

TABLE 26. The intercrystalline free lipids of *N. lenticularis*, *C. inconspicua,* and *T. sanguinea* as identified by GC-MS (new; data from Clegg, 1993).

Compound	*N. lenticularis* μg/g	*C. inconspicua* μg/g	*T. sanguinea* μg/g
24-norcholesta-5, 22E-dien-3β-ol	0.52	0.80	0.72
24-methyl-27-norcholesta-5,22-dien-3β-ol	0.25	0.28	0.54
cholesta-5,22E-dien-3β-ol	1.08	1.30	2.06
cholesta-5-en-3β-ol	4.19	10.20	5.99
n-C_{28} alcohol	0.60	0.26	0.00
24-methylcholesta-5,22E-dien-3β-ol	1.48	2.99	2.33
24-methylcholesta-5,24(28)-dien-3β-ol	1.89	2.77	4.47
24-ethylcholesta-5,22E-dien-3β-ol	0.16	0.54	0.26
24-ethylcholesta-5-en-3β-ol	0.59	0.98	0.81

CARBOHYDRATES IN BRACHIOPOD VALVES

GENERAL

Carbohydrates are important biomolecules, since they are formed during photosynthesis and are thus the first intermediate in the incorporation of carbon, hydrogen, and oxygen into living matter. Commonly known as sugars, carbohydrates can occur as monosaccharides, oligosaccharides (2 to 10 monosaccharides), or polysaccharides (larger polymer carbohydrates). Carbohydrates occur in biominerals, including brachiopod valves (JOPE, 1965), although very little work has been done to characterize these molecules. BORMAN and others (1987) described methylated and dimethylated monosaccharides in the calcite of the coccolith *Emiliania huxleyi,* while neutral sugars were extracted from *Mercenaria mercenaria* (CRENSHAW, 1972). COLLINS, CURRY, and others (1991) detected neutral sugars in the EDTA-soluble fraction of recent *Neothyris lenticularis* by colorimetric assays using sulphuric acid and phenol. They also used immunological techniques to demonstrate the presence of carbohydrates in Pleistocene *Neothyris* sp. (Kupe shell bed, 0.45 Ma) using periodate oxidation to remove carbohydrate moieties. Neutral polysaccharides occur in the primary layer of *Glottidia pyramidata* valves (PAN & WATABE, 1988b) as well as the periostracum (PAN & WATABE, 1989).

TABLE 27. Free intracrystalline fatty acids from valves of *N. lenticularis* and *T. sanguinea* as identified by GC-MS (new; data from Clegg, 1993).

Fatty acid	*N. lenticularis* μg/g	*T. sanguinea* μg/g
$C_{12:0}$	0.16	0.18
$C_{13:0}$	0.00	0.02
$C_{14:0}$	0.08	0.14
$C_{15:0}$	0.04	0.04
$C_{16:1}$	0.03	0.05
$C_{16:0}$	0.83	1.10
$C_{17:0}$	0.04	0.02
$C_{18:1}$	0.02	0.02
$C_{18:1}$	0.04	0.05
$C_{18:0}$	0.25	0.11
$C_{20:2}$	0.02	0.00
$C_{20:1}$	0.03	0.00

Chitin

The monomer of the polysaccharide chitin, the amino sugar N-acetyl glucosamine, has been detected in the phosphatic valves of *Lingula anatina, Discina striata,* and, intriguingly, the carbonate valves of *Neocrania anomala* (JOPE, 1967a). X-ray diffraction has demonstrated that chitin in *Lingula* valves is in the β-form, i.e., the polysaccharide chains are parallel (DWELTZ, 1961; IIJIMA, MORIWAKI, & KUBOKI, 1991b). The fiber axis of β-chitin is coincident with the c-axis of apatite and parallel with the growth direction of the valves of *Lingula anatina* (KELLY, OLIVER, & PAUTARD, 1965) and *Lingula shantoungensis* (IIJIMA &

TABLE 28. The intracrystalline crystal-bound fatty acids and *n*-alcohols of *N. lenticularis, C. inconspicua,* and *T. sanguinea* as identified by GC-MS; measurements are μg/g (new; data from Clegg, 1993).

Compound	*Neothyris lenticularis*	*Calloria inconspicua*	*Terebratella sanguinea*
$C_{12:0}$	0.07	0.51	0.14
$C_{13:0}$	0.01	0.14	0.07
$C_{14:0}$	0.13	0.79	0.15
C_{12} β-hydroxy	0.00	0.96	0.00
$C_{15:0}$ *iso*	0.00	0.30	0.00
C_{13} β-hydroxy	0.00	0.25	0.00
$C_{15:0}$ normal	0.09	0.17	0.14
C_{13} β-hydroxy	0.00	0.42	0.00
$C_{16:1}$	0.23	0.70	0.36
$C_{16:0}$	3.85	6.06	6.26
n-C_{16} alcohol	0.05	0.16	0.16
$C_{17:0}$ *iso*	0.10	2.40	0.18
$C_{17:0}$	0.26	1.77	0.55
$C_{18:1}$	0.13	0.48	0.12
$C_{18:1}$	0.21	0.47	0.28
$C_{18:0}$	1.48	3.26	2.22
n-C_{18} alcohol	0.06	0.98	0.24
$C_{19:0}$	0.05	0.14	0.12
C_{17} β-hydroxy	0.00	0.26	0.00
C_{20} polyunsaturated	0.09	0.00	0.13
$C_{20:2}$	0.65	0.33	1.36
$C_{20:1}$	1.27	1.13	3.08
$C_{20:0}$	0.07	0.57	0.00
C_{18} α-hydroxy	0.00	0.00	0.19
$C_{21:0}$	0.06	0.10	0.13
$C_{22:2}$	0.27	0.10	0.73
$C_{22:0}$	0.31	0.35	0.47
$C_{23:0}$	0.00	0.24	0.00
C_{21} α-hydroxy	0.09	0.10	0.44
$C_{24:0}$	0.06	0.25	0.00
C_{22} α-hydroxy	0.06	0.00	0.90
C_{22} ω-hydroxy	0.06	0.23	0.00
C_{23} α-hydroxy	0.11	0.00	0.24
C_{24} α-hydroxy	0.00	0.00	0.11
Total	9.82	23.62	18.77

others, 1988; IIJIMA & MORIWAKI, 1990; IIJIMA, MORIWAKI, & KUBOKI, 1991).

Glycosaminoglycans (GAGs)

GAGs occur in the valves of *Glottidia pyramidata* (WATABE & PAN, 1984) where they are associated with the apatitic mineral (PAN & WATABE, 1988b). Alcian blue staining of sections of *Lingula anatina* valves indicates the pervasive presence of acidic GAGs (WILLIAMS, CUSACK, & MACKAY, 1994). TANAKA, ANNO, and SENO (1982) described a novel GAG from the pedicle of *Lingula anatina.* The GAG is sulphated and contains equimolar amounts of galactose and *N*-acetylgalactosamine. The carbohydrate is linked to the peptide portion through the *O*-glycosyl bond between threonine and *N*-acetylgalactosamine. TANAKA, ANNO, and SENO (1982) named this GAG lingulin sulfate.

TABLE 29. Fatty acids in the FIL fraction of *C. inconspicua* and *N. lenticularis* as determined by GC-MS (new; data from Clegg, 1993).

Fatty acid	*C. inconspicua* μg/g	*N. lenticularis* μg/g
$C_{14:0}$	0.01	0.03
$C_{15:0}$	0.00	0.02
$C_{16:1}$	0.04	0.04
$C_{16:0}$	0.00	0.19
$C_{17:0}$	0.00	0.02
$C_{18:1}$	0.00	0.03
$C_{18:0}$	0.01	0.08

Carbohydrates in Fossil Brachiopods

CLEGG (1993) analyzed in a preliminary way the carbohydrates in the EDTA-insoluble residue of *Neothyris* sp. from the Kupe shell bed (0.45 Ma). Table 33 lists the quantities and types of carbohydrate present. No amino sugars were detected. No recent material was analyzed.

IMMUNOLOGY OF BRACHIOPOD SHELL MACROMOLECULES

Immunological methods have been used to estimate the degree of biochemical similarity between biomolecules extracted from the shells of a wide range of brachiopods. These data are available predominantly for extant species, but the use of antibodies has also been extended to a number of fossil taxa. In all cases the antibodies have been prepared against intracrystalline biomolecules, as the extraction procedure excludes intercrystalline biomolecules.

TABLE 30. Identity and locality of fossil samples included in the survey of CLEGG, 1993 (new).

Age (Ma)	Taxa	Stratigraphical age	Location
0.12	*Neothyris* sp.	Rapanui	Castlecliff, N. Island
0.45	*Neothyris* sp.	Kupe shell bed	Castlecliff, N. Island
0.45	*T. sanguinea*	Kupe shell bed	Castlecliff, N. Island
0.45	*C. inconspicua*	Kupe shell bed	Castlecliff, N. Island
1.49	*Neothyris* sp.	Waipuru shell bed	Turakina Point, N. Island
1.47–1.7	*Neothyris* sp.	Wairarapa	The Reef, Castlepoint, N. Island
2.0	*Neothyris* sp.	Hautawa shell bed	Castlecliff, N. Island
2.2	*Neothyris* sp.	Parihauhau shell bed	Castlecliff, N. Island
2.5	*Neothyris* sp.	Waipipi	Castlecliff, N. Island
2.5	*T. sanguinea*	Waipipi	Castlecliff, N. Island
2.65	*Neothyris* sp.	Waipipi	Wapukura, N. Island
15	*Pachymagas* sp.	Gee Greensand	Old Rifle Butts, S. Island
23	*Pachymagas* sp.	Otekaike limestone	Trig Z, S. Island
300	*D. llangollensis*	Pen-yr-hendlas	Holywell, North Wales*

*all other localities in New Zealand.

VARIATION OF SKELETAL MACROMOLECULES IN RECENT BRACHIOPODS

A total of 26 different antibodies has been prepared against macromolecules extracted from brachiopod shells. Extraction of these macromolecules was achieved by powdering the shells, removing the intercrystalline material, and then releasing the intracrystalline organic material by etching the shells with EDTA. Antibodies were then prepared against bulk extracts from each taxon for which sufficient quantities of shell were available. Measurements of immunological cross-reactivity and hence overall biochemical similarity were determined using enzyme-linked immuno-sorbent assay using a fluorescent substrate (FELISA). The nature of the antigens detected by the antibodies is unknown, although it has been suggested that both proteins and carbohydrates are involved (COLLINS, CURRY, & others, 1991). Full descriptions of the techniques used are given in the references cited below. These antibodies were subsequently used in a range of experiments to assess the degree of biochemical similarity between representatives of approximately half of the total present-day brachiopod fauna.

The first immunological study utilized three antibodies, and the results suggested that the long-established subdivision of the largest living extant brachiopod order (the Terebratulida) into short- and long-looped groups was an oversimplification (COLLINS & others, 1988). Subsequently a larger number of antibodies was prepared, initially against nine brachiopod genera (COLLINS, MUYZER, CURRY, & others, 1991) and then against eleven genera (CURRY, QUINN, & others, 1991). The availability of these additional antibodies allowed the calculation of immunological distances between major brachiopod groups. The data from these investigations were assessed by a variety of different clustering methods, and the resulting dendrograms and cluster diagrams confirm the earlier results and provide strong evidence for a primary three-fold subdivision of the living terebratulids, with the cancellothyridoids

TABLE 31. Fatty acids in the FIL fraction of fossil *Neothyris* sp. Fatty acids identified by the retention times of the trimethyl silyl ethers (new; data from Clegg, 1993).

Fatty acid	Kupe shell bed µg/g	Waipuru shell bed µg/g	Wairarapa formation µg/g
$C_{12:0}$	0.003	0.002	0.00
$C_{13:0}$	0.01	0.004	0.00
$C_{14:0}$	0.03	0.005	0.002
$C_{15:0}$	0.015	0.00	0.001
$C_{16:0}$	0.04	0.005	0.002
$C_{18:0}$	0.003	0.001	0.001

TABLE 32. Amount of lipids (*mg/g*) in BIL fraction of fossil brachiopods; *A,* Rapanui *Neothyris* sp. (0.12 Ma); *B,* Kupe *Neothyris* sp. (0.45 Ma); *C,* Kupe *T. sanguinea* (0.45 Ma); *D,* Kupe *Calloria inconspicua* (0.45 Ma); *E,* Waipuru *Neothyris* sp. (1.49 Ma); *F,* Wairarapa *Neothyris* sp. (1.47–1.7 Ma); *G,* Hautawa *Neothyris* sp. (2.0 Ma); *H,* Parihauhau *Neothyris* sp. (2.2 Ma); *I,* Upper Waipipi *Neothyris* sp. (2.5 Ma); *J,* Upper Waipipi *T. sanguinea* (2.5 Ma); *K,* Lower Waipipi *Neothyris* sp. (2.65 Ma); *L,* Gee Greensand *Pachymagas* sp. (15 Ma); *M,* Otekaike Limestone *Pachymagas* sp. (23 Ma); *ND,* not determined (new; data from Clegg, 1993).

	A	B	C	D	E	F	G	H	I	J	K	L	M
$C_{12:0}$ fatty acid	0.02	0.03	0.06	0.04	0.01	0.01	0.06	0.03	0.03	0.03	0.15	ND	ND
$C_{13:0}$ fatty acid	ND	0.10	0.01	0.02	0.05	0.05	ND	0.08	0.01	ND	0.15	ND	ND
$C_{14:0}$ fatty acid	0.07	0.20	0.08	0.13	0.24	0.22	0.14	0.33	0.09	0.12	0.48	0.07	0.04
$C_{15:0}$ *iso* fatty acid	0.01	0.01	0.01	0.03	ND	ND	0.01	ND	ND	ND	ND	ND	ND
$C_{15:0}$ fatty acid	0.05	0.06	0.03	0.08	0.06	0.05	0.07	0.09	0.04	0.06	0.09	0.03	0.02
C_{13} β-hydroxy fatty acid	ND	0.04	0.04	0.06	0.07	0.08	ND	0.05	0.01	ND	ND	ND	ND
$C_{16:1}$ fatty acid	ND	0.06	0.02	ND	0.09	0.05	0.03	0.05	0.06	0.08	ND	0.03	0.03
$C_{16:0}$ fatty acid	0.55	0.65	0.54	1.09	0.60	0.70	0.52	0.61	0.41	0.64	1.16	0.44	0.37
$C_{17:0}$ *iso* fatty acid	0.01	0.02	0.03	ND	0.02	0.02	ND	ND	ND	ND	ND	ND	ND
$C_{17:0}$ fatty acid	0.02	0.03	0.01	0.03	0.04	0.03	0.04	0.04	0.03	0.05	0.05	0.03	0.03
$C_{18:1}$ fatty acid	ND	0.07	0.01	ND	0.06	0.03	0.01	0.03	0.04	0.20	ND	0.16	0.08
$C_{18:1}$ fatty acid	ND	ND	0.01	ND	0.01	0.02	0.04	0.01	ND	ND	ND	0.06	0.01
$C_{18:0}$ fatty acid	0.10	0.24	0.07	0.11	0.19	0.21	0.13	0.23	0.14	0.24	0.39	0.20	0.16
$C_{13:0}$ hydroxy fatty acid	ND	ND	0.02	ND	ND	ND	ND	ND	ND	ND	ND	ND	ND
$C_{19:0}$ fatty acid	ND	ND	ND	0.01	ND	ND	ND	0.01	ND	0.01	ND	0.01	0.02
$C_{20:0}$ fatty acid	0.01	0.03	0.06	0.09	0.02	0.02	0.03	0.02	0.03	0.06	0.05	0.04	0.03
$C_{21:0}$ fatty acid	0.04	0.01	0.01	0.01	0.01	0.01	0.01	0.01	ND	0.02	ND	0.01	0.01
$C_{22:0}$ fatty acid	0.02	0.03	0.02	0.08	0.02	0.01	0.05	0.02	0.02	0.07	0.02	0.05	0.04
$C_{23:0}$ fatty acid	0.01	0.01	ND	0.02	0.01	ND	0.01	0.01	0.01	0.02	ND	0.01	0.01
C_{21} α-hydroxy fatty acid	ND	0.01	ND	ND	ND	0.01	ND	ND	ND	0.02	ND	0.02	0.01
$C_{24:0}$ fatty acid	0.02	0.01	0.03	0.05	0.01	0.01	0.03	0.01	0.03	0.01	0.02	0.02	0.01
C_{22} hydroxy fatty acid	ND	0.16	ND	ND	0.08	0.07	ND	ND	ND	0.38	ND	0.21	0.03
C_{24} α-hydroxy fatty acid	ND	0.04	ND	ND	0.02	0.01	ND	ND	ND	0.05	ND	0.05	0.03
$C_{26:0}$ fatty acid	ND	ND	0.02	0.10	ND	ND	0.01	0.04	0.01	ND	ND	ND	ND
C_{26} α-hydroxy fatty acid	ND	0.02	ND	ND	0.01	0.01	ND	ND	ND	0.06	ND	0.04	0.02
C_{28} fatty acid	ND	ND	0.01	0.05	ND	ND	0.01	ND	0.01	ND	ND	ND	ND
$C_{30:0}$ fatty acid	ND	ND	ND	0.02	ND	ND	ND	ND	ND	ND	ND	ND	ND
$C_{32:0}$ fatty acid	ND	ND	ND	ND	ND	ND	ND	ND	ND	ND	ND	ND	ND

plotting separately from the long-looped terebratelloids and predominantly short-looped terebratuloids (Fig. 219–220).

Immunological techniques were also used to investigate the extent of biochemical similarity between skeletal biomolecules from twelve species and one subspecies of *Terebratulina* (ENDO & CURRY, 1991). These species were collected from worldwide localities, and, where possible, morphometric analysis allowed an integrated molecular and morphological investigation of their relationships. The immunological results revealed two main clusters of *Terebratulina* species (ENDO & CURRY, 1991). These clusters are not determined geographically or ecologically, because both Japanese and North Atlantic species of the genus appear in the two subclusters. It has been suggested that these two subclusters reflect a major vicariance event during the evolution of the genus, possibly representing an older group of species and a more recently evolved group that has also undergone considerable geographic dispersal. In addition it was discovered that two sympatric Japanese species were morphologically indistinguishable and very closely related at the molecular level and, hence, are best considered as synonymous (ENDO & CURRY, 1991). The morphometric analysis

TABLE 33. Sugars in EDTA-insoluble fraction of *Neothyris* sp. (Kupe, 0.45 Ma) (new; data from Clegg, 1993).

Sugar	mg/g	% of total
Rhamnose	0.001	0.79
Fucose	0.001	0.79
Ribose	0.006	4.76
Arabinose	0.002	1.59
Xylose	0.008	6.35
Mannose	0.005	3.97
Galactose	0.003	2.38
Glucose	0.1	79.37

also revealed ecophenotypic differences in the species surveyed, with clear differentiation apparent between species with heavy shells and small pedicle foramens and those with light shells and large pedicle foramens (ENDO & CURRY, 1991). The former association of characters is usually taken to indicate a tendency toward a free-lying mode of life, while the latter suggest a more pedicle-dependent life habit.

The most unexpected result of the immunological investigation was the clustering of the long-looped kraussinid genera with the short-looped terebratulids (Fig. 219), and several other anomalous relationships (Fig. 220) were revealed by an investigation of immunological responses in a wide range of other brachiopod taxa for which reciprocal data are not yet available (CURRY, QUINN, & others, 1991). Such results point to a level of biochemical similarity between these taxa that would not be expected, which warrants further investigation.

At higher taxonomic levels, the pattern of immunological cross-reactivity proved to be entirely consistent with the traditional view of brachiopod evolution based on shell morphology and the fossil record. Thus representatives of different orders were strongly separated by immunology, indicating that there was considerable biochemical differentiation between groups that last shared a common ancestor as far back as the Paleozoic Era.

ENDO and others (1994) extended the range of the immunological survey to investigate 44 species from the most abundant, extant brachiopod order, the terebratulides. This study confirmed and reinforced the conclusions of the previous studies and identified four groups of terebratulid taxa that were consistently differentiated on the basis of shell biochemistry. ENDO and others (1994) demonstrated that these four groups were also distinct morphologically and, from detailed consideration of the morphology and stratigraphic distribution of fossil terebratulid brachiopods, proposed a reconstruction of evolutionary history that was consistent with the immunological data (Fig. 221).

The advantage of the immunological approach is that it can be applied to small fragments of shell, even those that have been

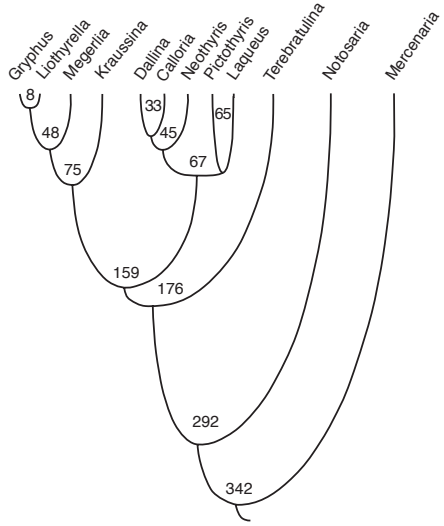

FIG. 219. UPGMA (unweighted pair-group method using arithmetic averages) dendrogram based on immunological distance data for the following brachiopod genera: *Gryphus vitreus* (BÖRN), Mediterranean Sea; *Liothyrella neozelanica* (THOMSON), New Zealand; *Megerlia truncata* (GMELIN), Mediterranean Sea; *Kraussina rubra* (PALLAS), South Africa; *Dallina septigera* (LOVEN), Scotland; *Calloria inconspicua* (SOWERBY), New Zealand; *Neothyris lenticularis* (DESHAYES), New Zealand; *Pictothyris picta* (DILLWYN), Japan; *Laqueus rubellus* (SOWERBY), Japan; *Terebratulina retusa* (LINNAEUS), Scotland; *Notosaria nigricans* (SOWERBY), New Zealand; and the bivalve *Mercenaria* as an outgroup. The numbers are immunological distances (Curry, Quinn, & others, 1991).

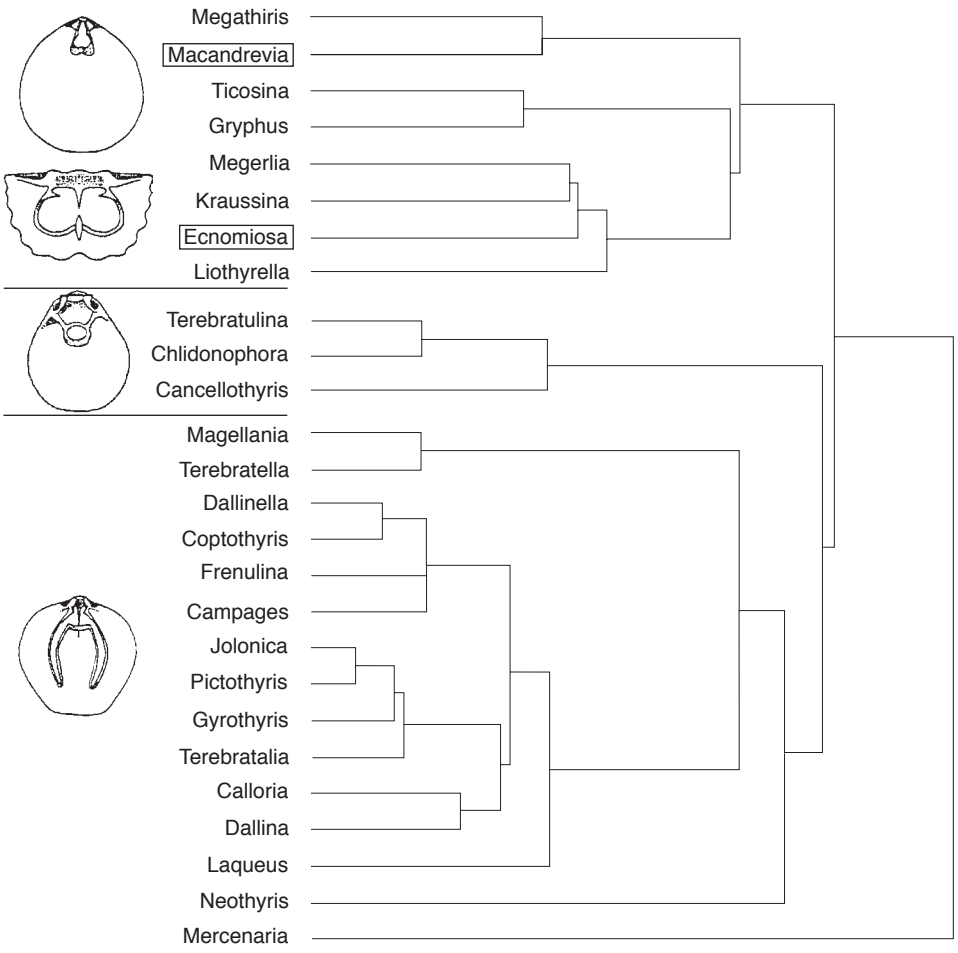

FIG. 220. Single-linkage cluster analysis of 25 terebratuloid brachiopods with the three major groups outlined and represented by stylized loop sketches. The anomalous positions of *Macandrevia* and *Ecnomiosa* (i.e., long-looped genera clustering with short-looped stocks) are indicated by *boxes;* the bivalve *Mercenaria* is included as the outgroup (Curry, Quinn, & others, 1991).

stored in museum collections. Consequently a large number of taxa could be included in this study, many more than could have been included in a survey using any other molecular method. The main disadvantage is that, for taxonomic purposes, the resolution of immunological data is lower than some of the other available techniques. For the shell macromolecules of brachiopods, immunological techniques appear to be most effective at the generic level and above, although species-level discrimination was possible in the long-lived genus *Terebratulina* (ENDO & CURRY, 1991).

APPLICATION OF IMMUNOLOGY TO FOSSIL BRACHIOPODS

Immunological techniques applied to fossil brachiopods have provided unequivocal evidence of the survival of antigenic determinants in brachiopod shells over 2 million years old (COLLINS, CURRY, & others, 1991; COLLINS, MUYZER, WESTBROEK, & others, 1991). The immunological approach was

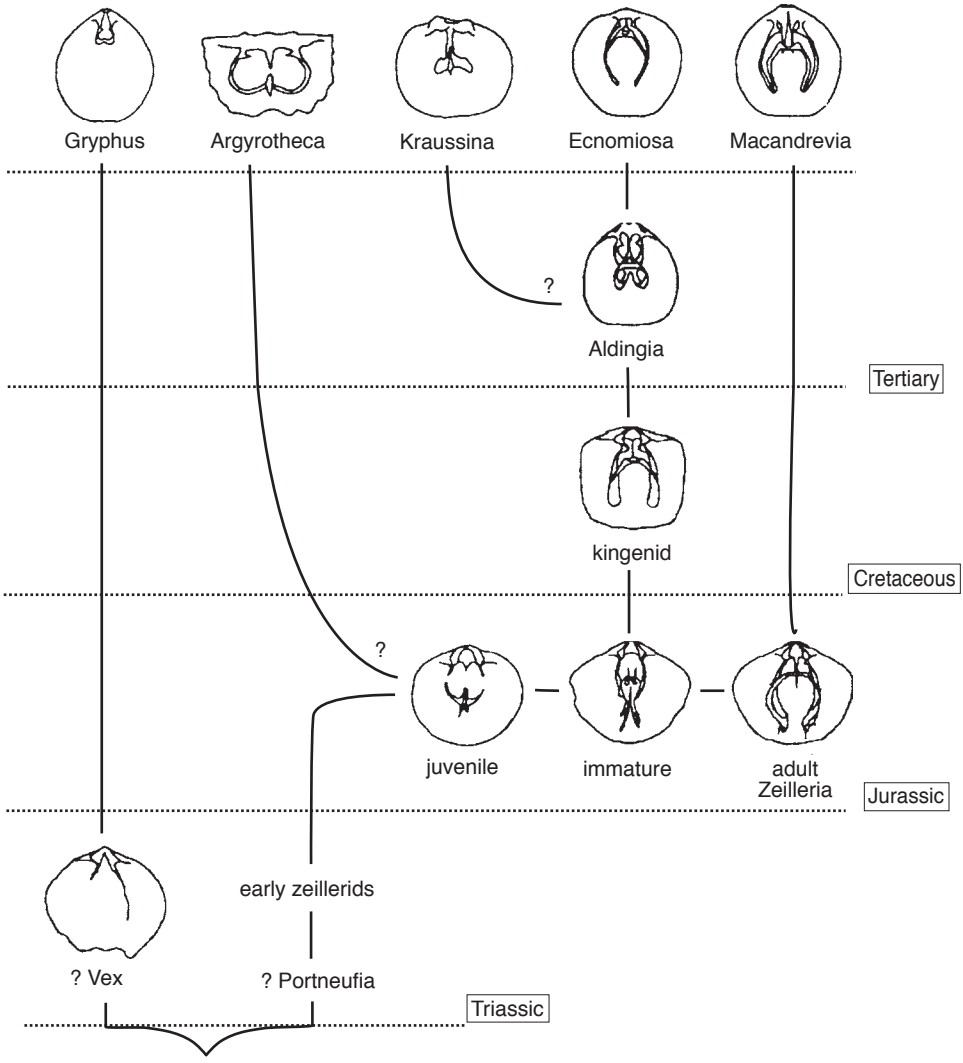

FIG. 221. A possible terebratulide phylogeny, based on immunological data (Endo & others, 1994).

also applied to investigate the biochemical similarity between extant taxa and a related, extinct Pleistocene brachiopod from Japan (ENDO, 1992). The technique allowed the extinct taxon to be linked to one of four extant species of *Terebratulina.* This relationship was not evident from morphology alone.

SHELL STRUCTURE

ALWYN WILLIAMS
[University of Glasgow]

INTRODUCTION

The integument of the living brachiopod consists of the epidermis and all surface layers secreted by it, the most striking of which is the biomineralized shell. The main constituents of the shell are aggregations of biominerals (with intracrystalline proteins) and their matrices or membranes, which are composed of glycosaminoglycans (GAGs), proteins, and chitin. So far as we know, only the biominerals and a few stable polymers, like collagen, normally survive fossilization in a recognizable state. Even so, there are two advantages to considering the skeletal successions of extinct groups in conjunction with those of living species. First, biominerals are the main components of the subperiostracal shell of all brachiopods and largely determine its structural frame (fabric). These biomineralized successions are invariably secreted in a well-stratified order and, under favorable conditions, have been preserved more or less in the original state throughout the skeletal fossil record. Second, the fabric of all brachiopod shells conforms to a standard stratiform succession (Fig. 222). This consists of a periostracum underlain by

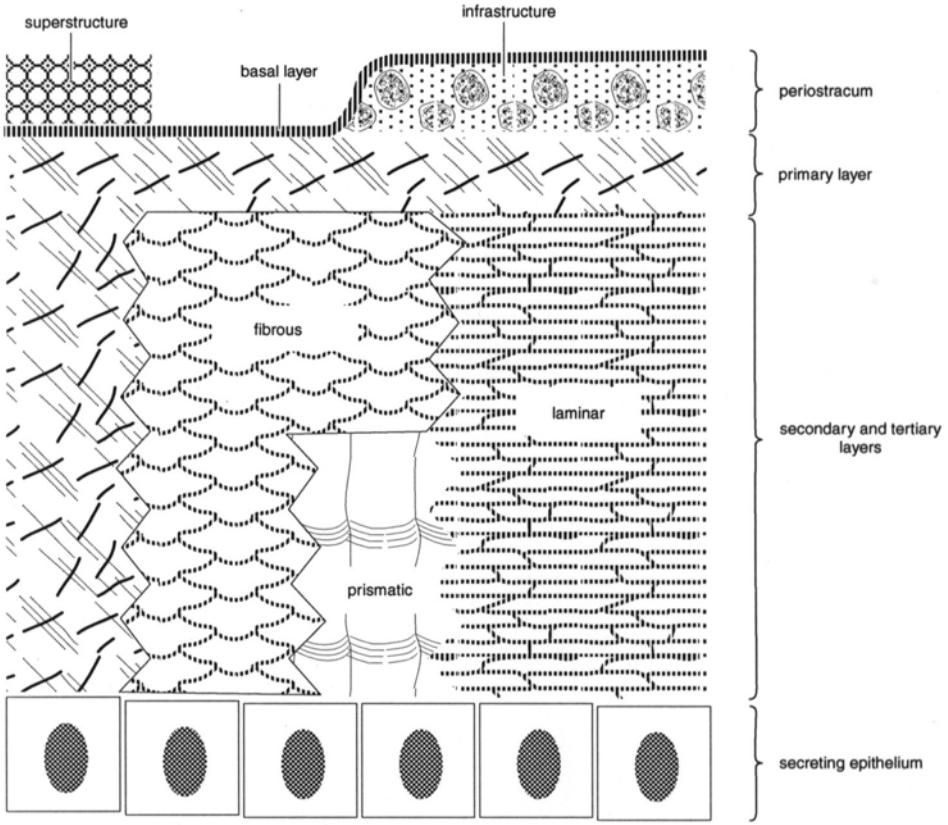

FIG. 222. Stylized representation in the form of a chronostratigraphic succession of the main components of the integument of calcitic-shelled brachiopods (new).

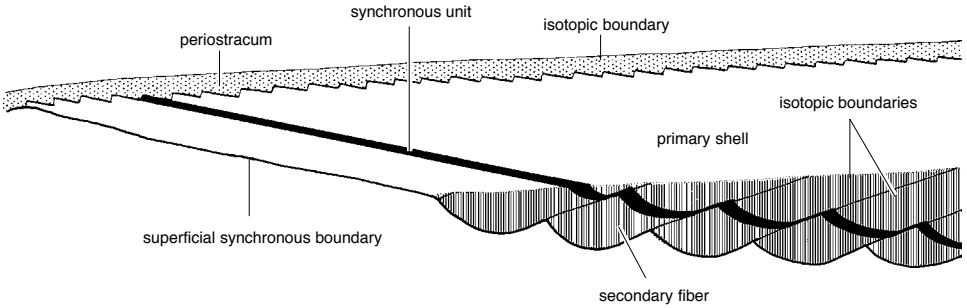

FIG. 223. Stylized medial longitudinal section of the valve edge of a young rhynchonellide, *Notosaria nigricans* (SOWERBY), showing the relationship between various isotopic and synchronous surfaces (Williams, 1971a).

biomineralized primary, secondary, and tertiary layers, of which only the periostracum and the primary layer are always present, the secondary layer being almost entirely absent in living thecideidines and the tertiary layer mainly restricted to a minority of living and fossil species (Fig. 222).

The standard succession of the brachiopod shell reflects the inherent homogeneity of the fabric of each layer, which forms an isotopic unit (WESTBROEK, 1967). The isotopic interfaces bounding such layers are quite different from surfaces of active shell deposition or resorption, which are isochronous

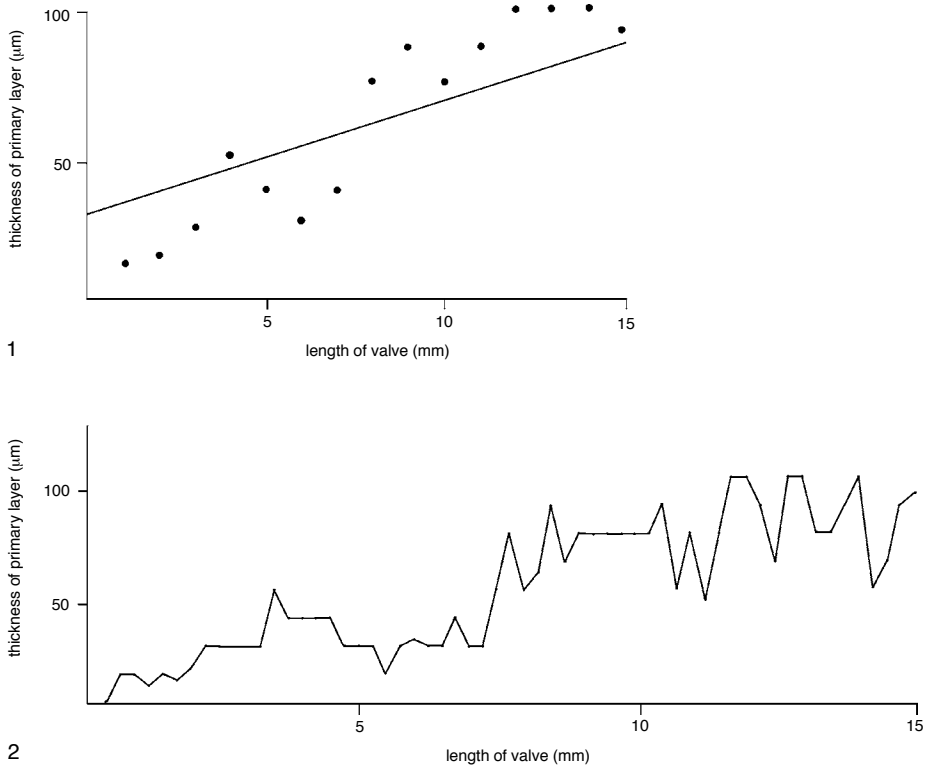

FIG. 224. Maximum thickness of the primary shell, *1,* per mm and *2,* per 0.25 mm, measured along a medial section of a dorsal valve of the rhynchonellide *Notosaria nigricans* (SOWERBY) (Williams, 1971a).

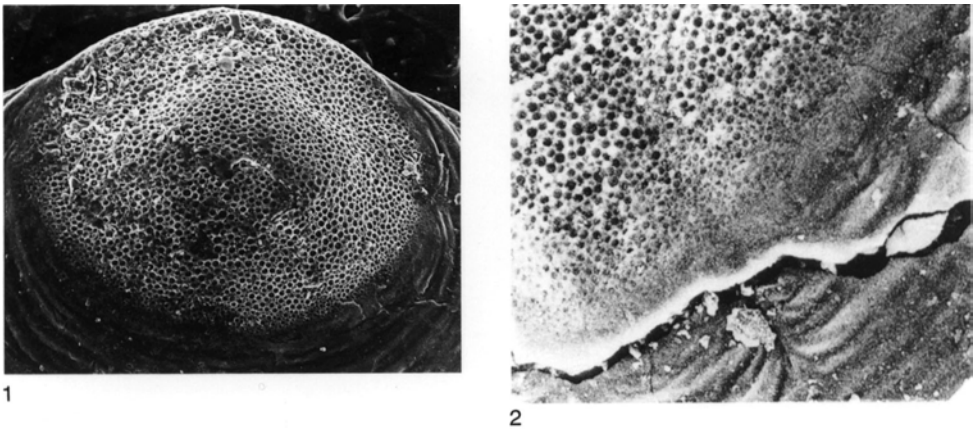

FIG. 225. Pitted larval shells of acrotretoids; *1,* dorsal valve of *Scaphelasma mica* POPOV indented by hemispherical pits, ×43 (new); *2,* diminution and loss of hemispherical pits toward the margin of a dorsal larval shell of *Angulotreta postapicalis* PALMER, ×516 (Williams & Holmer, 1992).

and anisotopic (WILLIAMS, 1971a) as is illustrated by the entire shell interior at the moment of death (superficial synchronous boundary; Fig. 223). With respect to cumulative growth, the primary layer differs from other biomineralized isotopic units in being subject only to incremental increases in thickness from umbo to anterior margin (Fig. 224). In a dorsal valve of *Notosaria* 15.5 mm long, periodic retraction of the outer mantle lobe continually reduced the primary layer to negligible thicknesses. Even so the maximum thicknesses of the primary layer increased steadily from the umbo by about 12 μm per mm of surface length (WILLIAMS, 1971a). The primary layer of organophosphatic brachiopods is also fairly constant in thickness. In a dorsal valve of *Lingula,* the thickness of the primary layer ranged from 31 to 46 μm (mean of 40 μm) for 15 measurements along half of a transverse section through the midregion (WILLIAMS, CUSACK, & MACKAY, 1994).

PERIOSTRACA

Periostraca have rarely been found in the fossilized state. The most remarkable preservation so far reported is the organic cover of a Late Cretaceous species of the terebratulid *Sellithyris* (GASPARD, 1982). Sufficient fabric has survived to confirm that the *Sellithyris* periostracum was openly vesicular like that of its living relative *Liothyrella* (WILLIAMS & MACKAY, 1978). More commonly, however, features that are feasibly interpreted as casts of periostraca ornament the shell exteriors of fossil and living species.

Larval shells of acrotretoids are indented by hemispherical or flat-bottomed, circular pits (Fig. 225) ranging from 250 nm to more than 5 μm in diameter and varying in distribution from hexagonal, close packing in two sizes (*Torynelasma*) to less regular arrangements with overlapping pit boundaries (*Opsiconidion*). The pits are like negatives of bubble rafts or of the labyrinthine superstructure of terebratelloid periostraca (WILLIAMS, 1968b). They have therefore been interpreted (Fig. 226) as impressions of vesicular periostraca cast in polymerizing primary layers (BIERNAT & WILLIAMS, 1970; POPOV, ZEZINA, & NOLVAK, 1982). This would require the accumulation of vesicles infrastructurally beneath the basal layer in a succession homologous with that of *Notosaria.* Their absence from the adult shell of acrotretoids has been attributed to the postlarval secretion of a rapidly thickening, inner bounding membrane, which would have blanketed the vesicular microtopography of

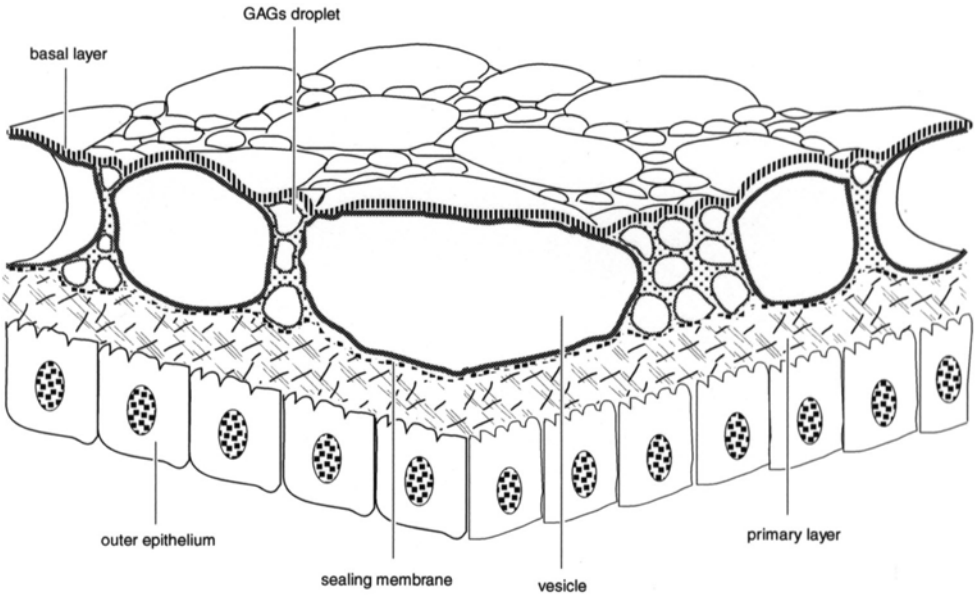

FIG. 226. Diagrammatic restoration of the acrotretoid periostracum to show its inferred relationship with the apatitic primary layer (new).

the mature periostracum (WILLIAMS & HOLMER, 1992). This is consistent with the casts of hemispherical vesicles becoming smaller and shallower toward the margin of the larval shell (Fig. 225).

An alternative interpretation of the flat-bottomed, overlapping pits, such as those of *Opsiconidion,* is that they were formed by selective resorption of successive laminae composing the larval shell (LUDVIGSEN, 1974; VON BITTER & LUDVIGSEN, 1979). This explanation is unlikely for two reasons (Fig. 227). First, surfaces undergoing biogenic resorption become pitted with irregular depressions with frayed, not sharp, edges. Second, pits that overlap like craters on biogenic surfaces do not necessarily constitute chronological successions, an essential criterion of selective resorption. Vesicles in a terebratelloid periostracum can vary from spherical bodies up to 2 μm in diameter to flattened disks no more than 250 nm thick, which are commonly stacked against one another. The overlapping arrangement of similar bodies in an acrotretoid periostracum would therefore indicate the way they were packed during exocytosis and not their relative ages.

Pits, interpreted as casts of periostracal vesicles, also indent the postlarval shells of other extinct organophosphatic brachiopods, including the linguloid *Rowellella* (HOLMER, 1989) and the discinoid *Orbiculoidea* (WILLIAMS & CURRY, 1991). In the latter genus they form closely packed, concentric bands becoming segregated distally into radial sets, with up to 8 pits in a row, which periodically dichotomize. The association of these radially aligned sets of pits with microscopic isoclinal folds with radial axial traces suggests that their disposition was determined by the distribution of setae at the mantle edge (Fig. 228).

Another kind of cast, found on the external surfaces of brachiopod shells, is that of the microtopography of the inner periostracal surface, which serves as a seeding substrate for the primary layer (Fig. 229). In

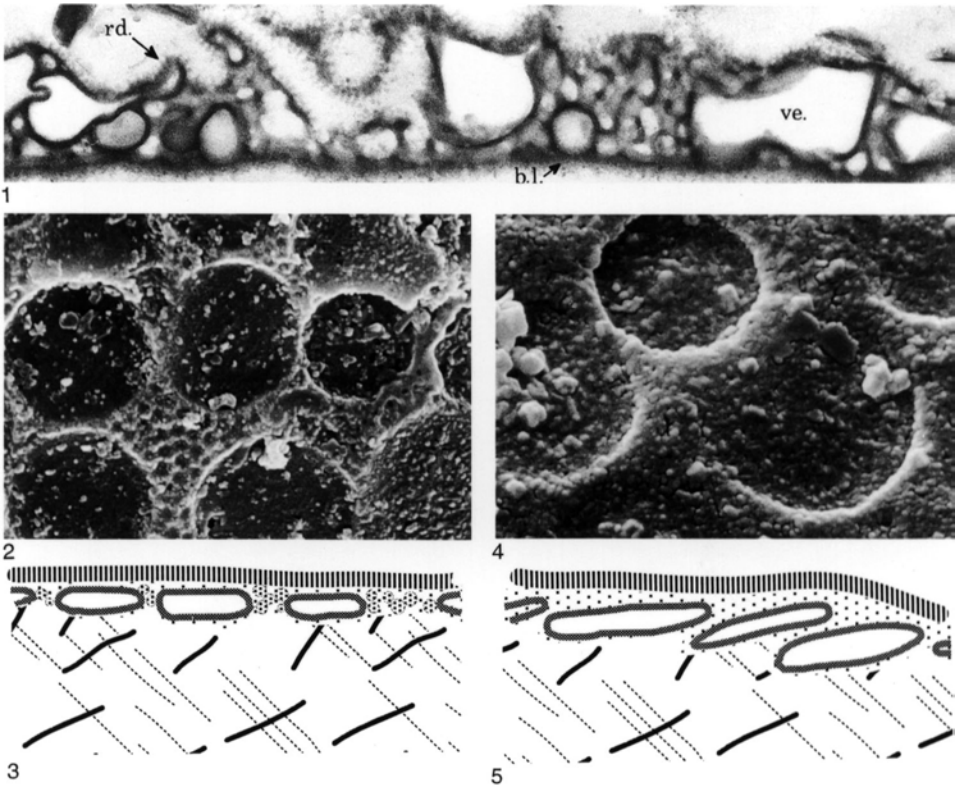

FIG. 227. Comparison of sections of the reconstructed periostracum (*3, 5*) of the acrotretoid *Opsiconidion aldridgei* (COCKS), as inferred from the surface of the dorsal larval shell (*2, 4*), ×4,000, with a section of the periostracum of the terebratulide *Magellania australis* (QUOY & GAUMARD) (*1*) showing the basal layer (*b.l.*) surmounted by vesicles (*ve.*) and proteinaceous rods (*rd.*), ×36,000 (new).

terebratelloids calcitic rhombs may accrete on the basal layer of the periostracum simultaneously with the continuing exudation of proteinaceous ridges along intercellular spaces of the secreting epithelium. Consequently molds of vesicular cell outlines are commonly found on the external, primary calcitic shell surface when stripped of periostracum (WILLIAMS & MACKAY, 1978). Molds originating in the same way and delineating elongate, parallel-sided vesicular cells also occur sporadically on acrotretoid shell surfaces (WILLIAMS & HOLMER, 1992). Vesicular cell outlines are probably sporadically but widely preserved on the surfaces of brachiopod shells throughout the Phanerozoic.

PRIMARY LAYER

Differences in the composition of the primary layers of organophosphatic and calcitic brachiopods are responsible for striking dissimilarities in their fabrics. There are also compositional differences among species within these two groups. Thus the proportion of finely granular apatite present in the primary layer of living organophosphatic species is greater in discinids than in lingulids; but the matrix, which is mainly GAGs, determines those characteristics of greatest morphological interest. Accordingly, irrespective of the levels of concentration of the dispersed apatite, the layer acts as a

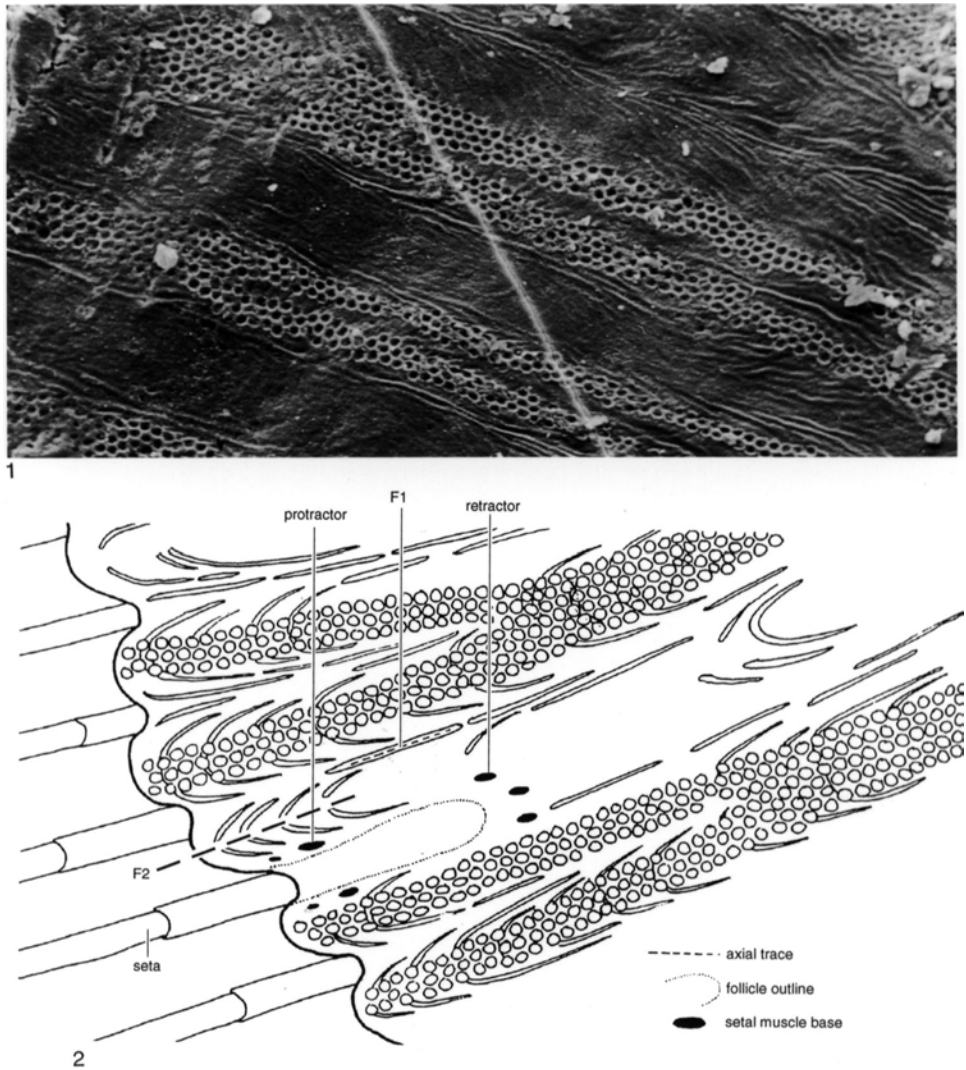

FIG. 228. *1,* Radial arrays of pits on the surface of a dorsal valve (×570) of the discinoid *Orbiculoidea nitida* (PHILLIPS) and *2,* their inferred relationship in life with setae and their principal muscle systems at the mantle edge (Williams & Curry, 1991).

flexible, plastic body that polymerizes slowly enough to preserve not only impressions of the overlying periostracum but also microscopic fold systems resulting from stress fields operating at the shell margin. These include the differential pull at sites along the outer mantle lobe by protractor and flexor muscles activating setae and the variation in rates of secretion of the periostracum relative to the migration of associated vesicular cells. Stress fields set up by setae are believed to be responsible for deforming concentric folds of primary shell (fila) into sets of discrete arcs (drapes) (Fig. 230–231; WILLIAMS & HOLMER, 1992), while complex fold systems, found on the surfaces of many well-preserved fossil and living shells, represent the latter (Fig. 232).

The primary layer of calcareous-shelled brachiopods is essentially a brittle crystalline

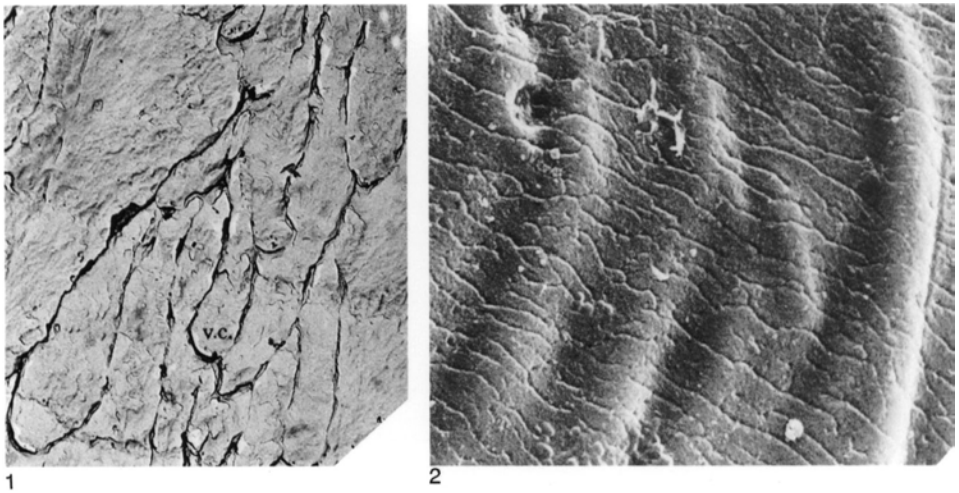

FIG. 229. Vesicular cell (*v.c.*) casts on primary shell surfaces; *1,* external surface of the terebratulide *Calloria inconspicua* (SOWERBY), ×7,100 (Williams & Mackay, 1978); *2,* external surface of the acrotretoid *Prototreta* sp., ×2,050 (Williams & Holmer, 1992).

medium, and its fabric is normally finely granular or acicular (Fig. 233; WILLIAMS, 1968a, 1973; MACKINNON & WILLIAMS, 1974), although it can also be sporadically tabular or lenticular with aggregates of crystallites up to 2 μm in size as in *Neocrania* (WILLIAMS & WRIGHT, 1970). Even so, radial sections of the layer commonly show synchronous shell units as a distinct banding inclined at acute angles to the primary-secondary isotopic interface. Such bands are traces of old depositional surfaces and are parallel with the section of the superficial synchronous boundary, on which the outer face of the outer mantle lobe rests (WILLIAMS, 1971a; GASPARD, 1991).

The nature of these surfaces is well shown by sections of valves of living thecideidines, which are composed almost entirely of primary shell (Fig. 233). In *Thecidellina* the

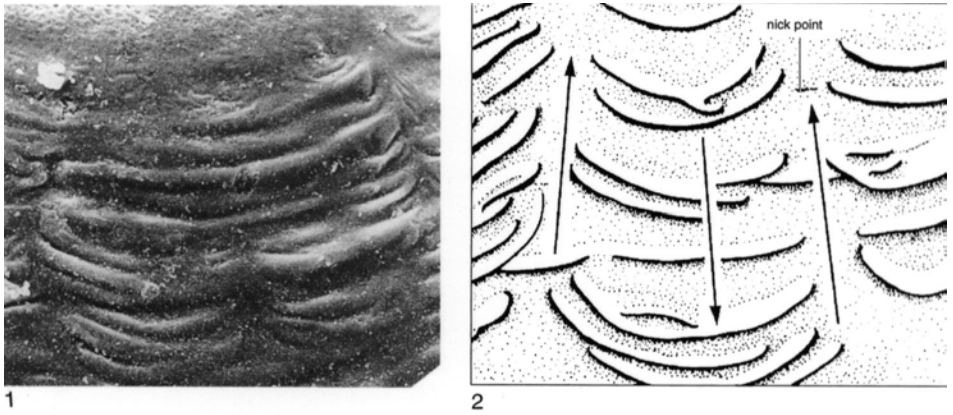

FIG. 230. *1,* Discrete folds interrupting fila on the external surface of the dorsal valve of the acrotretoid *Angulotreta triangulatus* PALMER, ×700; *2,* diagram of the inferred stress couples responsible for the folds, ×700 (Williams & Holmer, 1992).

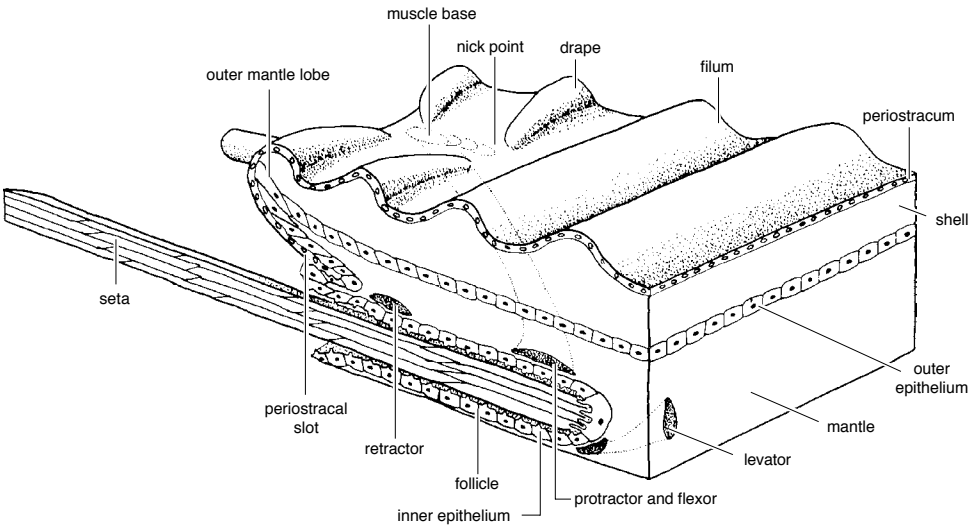

FIG. 231. Inferred structure of the outer mantle lobe of a living acrotretoid in relation to the shell, a follicle, and the muscles controlling the seta; all features are assumed to have been arranged as in *Lingula* (Williams & Holmer, 1992).

basic constituents are calcitic crystallites between 250 and 400 nm thick and up to 15 μm long with rhombic or scalenohedral terminal faces, which tend initially to be disposed as overlapping rows. As the shell thickens, crystallites frequently amalgamate into

FIG. 232. Isoclinal folds affecting the periostracum and primary layer of *Glottidia pyramidata* (STIMPSON); the folds close in a posteromedian direction, ×140 (new).

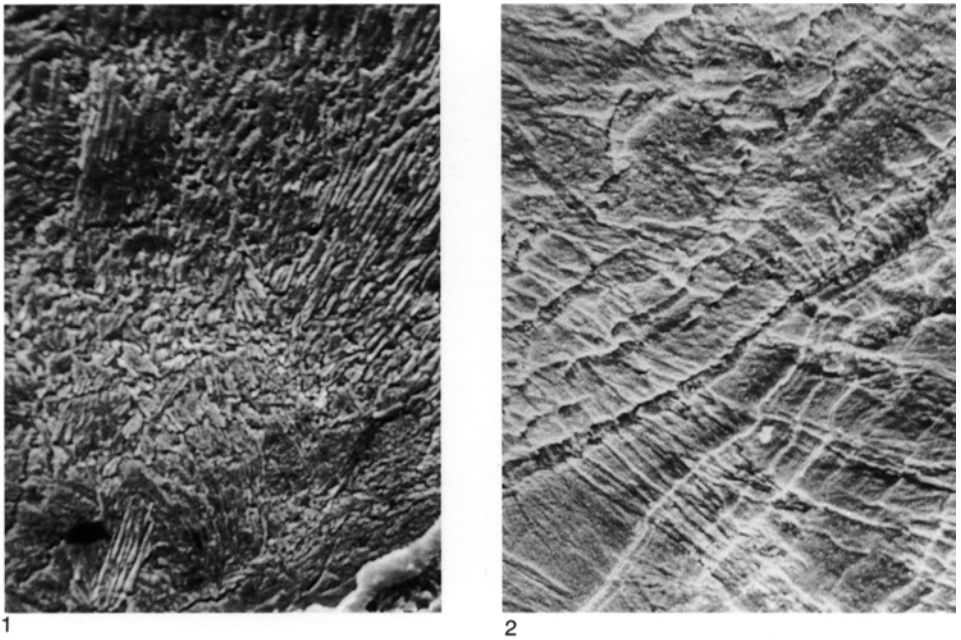

FIG. 233. The ultrastructural fabric of the primary layer; *1,* etched section of the ventral valve of *Neocrania anomala* (MÜLLER) with periostracum and underlying substrate in bottom right-hand corner, ×2,400 (new); *2,* etched section of the dorsal valve of *Thecidellina barretti* (DAVIDSON) showing a transgression of one set of growth bands over another, ×1,300 (Williams, 1973).

impersistent lenticular blades or mosaics, but the overall fabric is that of acicular crystallites in epitaxial continuity even across transgressive growth surfaces. The microtopography of this primary fabric of *Thecidellina* consists of tubercles up to 30 μm high, made up of crystallites that are disposed normal to the outer surface and closely packed groups of rhombs composed of acicular crystallites aligned parallel with cleavage planes (Fig. 234).

Despite the fact that any biomineralized succession always includes a first-formed layer secreted on an external organic substrate (periostracum), such a primary layer is not always found in fossilized shells. Comprehensive studies have confirmed its existence in most of the early brachiopod stem groups (WILLIAMS, 1968a; HOLMER, 1989) but occasionally only with great difficulty for two reasons. First, the biomineralized primary layer may have been so thin and of such an open microtexture in the original state as to facilitate replacement by entombing rock matrix (WILLIAMS, 1970a). Second, the primary layer of organophosphatic fossil species may have been largely organic (as in some living *Lingula anatina*) and therefore subject to prediagenetic degradation. The sporadic occurrence of the primary layer in some linguloid species described by HOLMER (1989) may be evidence of this circumstance.

SECONDARY LAYER

The secondary layer is the most variable succession of the brachiopod shell within as well as among species groups. Six different kinds of fabrics are already known with two being characteristic of wholly extinct groups, and more are expected to be discovered as study of early Paleozoic stocks progresses. The three fabrics of the organophosphatic brachiopods are inherently the most diverse but are more obviously related to one another than to those of calcitic brachiopods, which are less variable in composition.

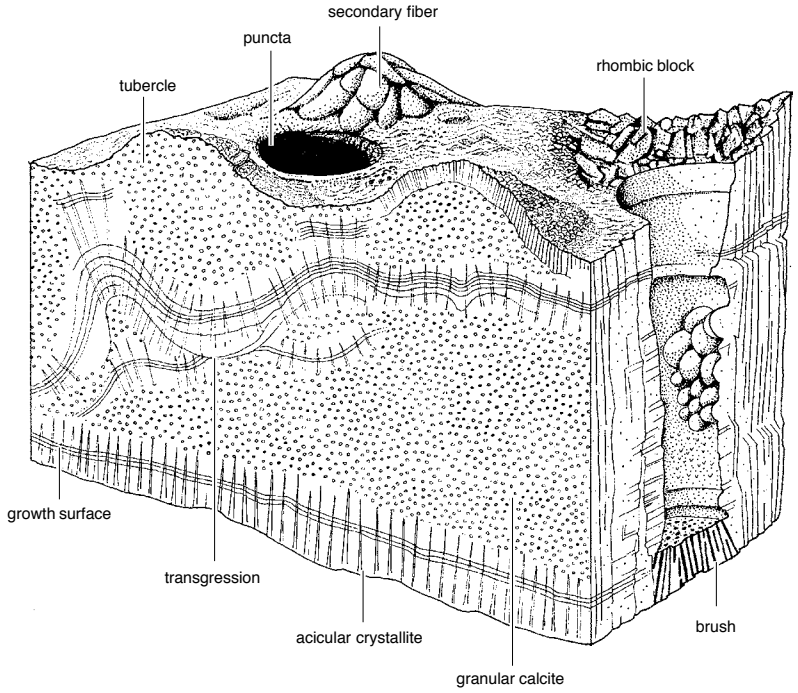

FIG. 234. Diagrammatic view of a sectioned block of *Thecidellina* shell showing some of the microtopographic and fabric features, approximately ×640 (Williams, 1973).

ORGANOPHOSPHATIC LAMINATION

The compositional and structural diversity of the secondary organophosphatic shell is well displayed in living lingulids. In *Lingula,* four constituents identifiable at ultrastructural level (Fig. 235)—apatitic granules, chitinous strands, fibrillar collagens, and all-pervading GAGs—are assembled into a succession of isotopic and isochronic laminae with thicknesses measured in microns compared with areas frequently of several square millimeters (Fig. 236). Compact laminae composed of closely packed spheroidal aggregates of apatitic granules (spherules) are succeeded by botryoidal or walled laminae, in which apatitic aggregates form botryoidal masses or vertical walls in a GAGs matrix, or by rod and plate laminae with apatitic rods accreting into anastomosing ridges disposed transversely on the body platform and radially in peripheral regions (Fig. 235, 237). Membranous laminae in GAGs can occur throughout the succession, while stratified laminae, characterized by gently inclined, alternating organic and apatitic units, each about 1 μm thick, are especially well developed at the junction with the primary layer.

These laminae can pass laterally from one kind to another. Even so, they usually group into well-defined rhythmic sets passing gradually from a mainly apatitic lamina to a terminating membrane(s) that is a substrate for the next set. The laminar fabric of living *Lingula* is also characteristic of fossil lingulids (CUSACK & WILLIAMS, 1996).

The fabric of *Glottidia,* however, is distinguishable from that of *Lingula* in including laminae consisting of regular arrays of rods (baculi) coated with spherular apatite that commonly subtend acute angles with one another and are generally inclined at high

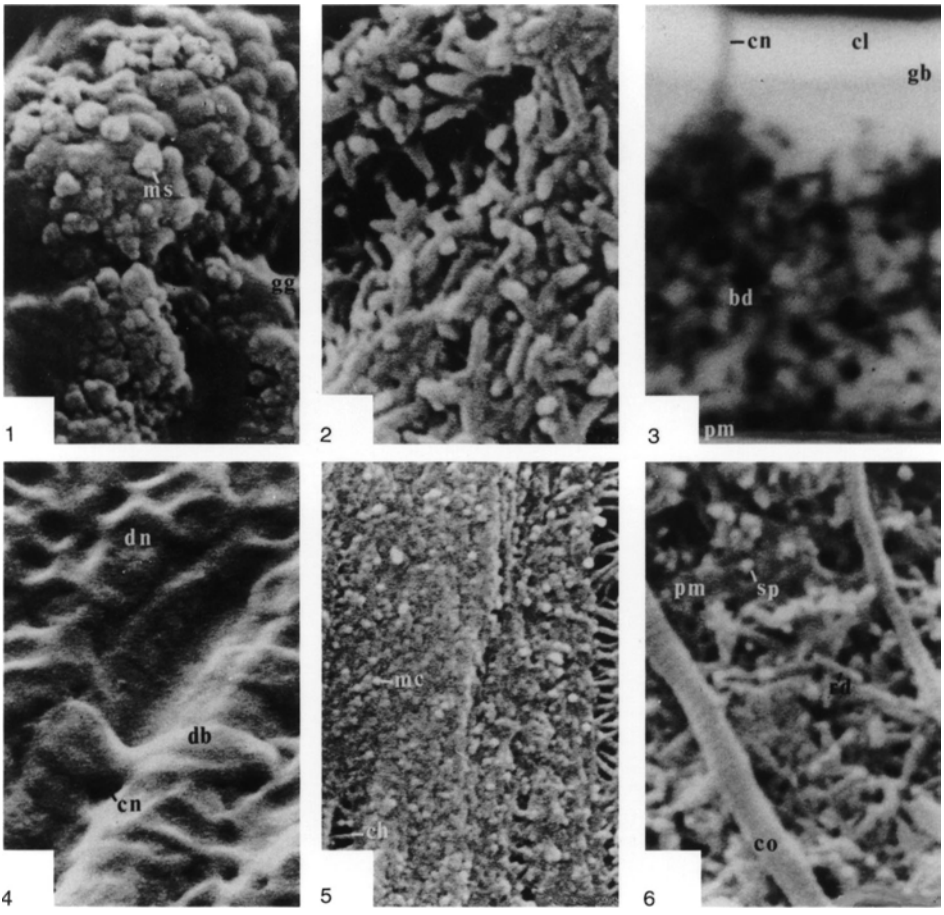

FIG. 235. The ultrastructure of the main constituents of the shell of *Lingula anatina* LAMARCK; *1,* botryoidal aggregates of apatitic mosaics (*ms*) in a matrix of GAGs (*gg*), ×11,552; *2,* rods and mosaics of apatite, ×11,552; *3,* backscattered electron micrograph of a laminar set showing a rhythmic unit of secretion from a predominantly apatitic base (*cl*) of packed mosaics (*white band* at top of micrograph), penetrated by the organic contents of a canal (*cn*) and terminated by a boundary (*gb*) marking the onset of GAGs secretion through a zone of dispersed mosaics and rods (*bd*) to an organic lamina (*pm; black band* at bottom), ×4,043; *4,* residual GAGs with contraction depressions (*dn*) and discoidal bodies (*db*) on ridges of apatite with a canal (*cn*), ×8,056; *5,* chitinous fibers (*ch*) coated with apatitic mosaics (*mc*), exposed in tension cracks, ×8,664; *6,* collagen fibrils (*co*) associated with apatitic rods (*rd*) and spherules (*sp*) in a muscle scar membrane (*pm*), ×20,216 (Williams, Cusack, & Mackay, 1994).

angles to the surfaces of bounding laminae (Fig. 238.1). A baculate lamina appears to have been a primitive fabric as it has been found in such Ordovician linguloids as *Ungula* and *Pseudolingula* (HOLMER, 1989).

The discinid secondary fabric, as typified by that of *Discina,* differs from that of lingulids mainly in the higher biomineral content (Fig. 239). As a result, compact laminae are usually about twice as thick (6 to 7 μm) as those of *Lingula;* and the botryoidal and walled laminae of *Lingula* are normally represented by poorly bedded (rubbly) successions of mosaics and lenticles up to 2 to 3 μm in lateral spread. Stratified laminae, however, are present immediately below the primary

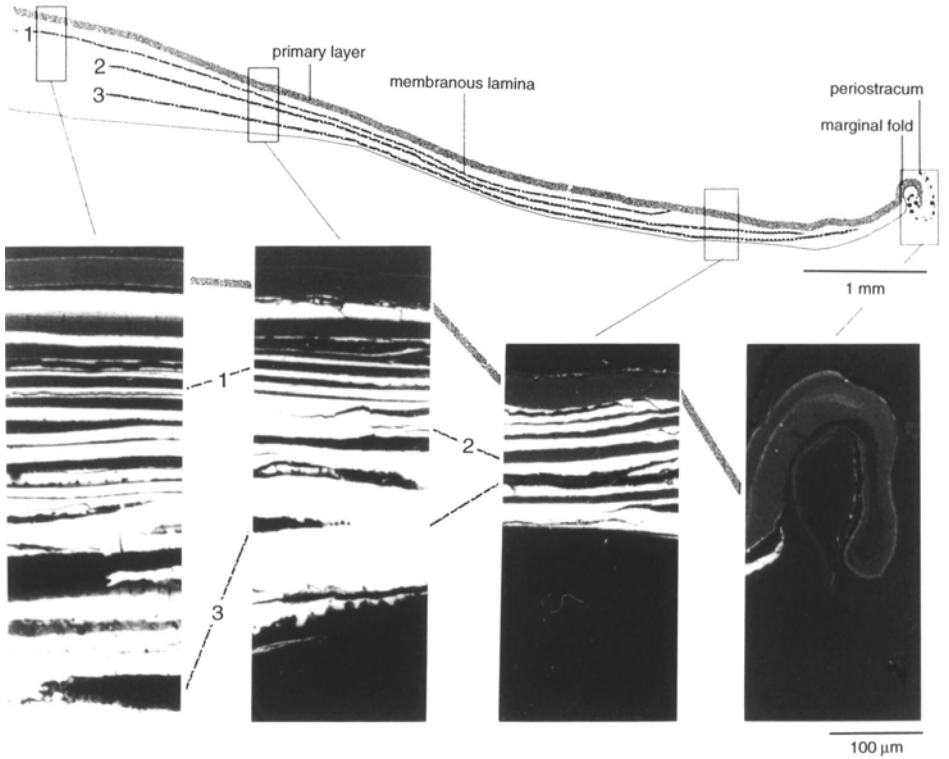

FIG. 236. Back-scattered electron micrographs of the successions at four indicated traverses of a transverse section of half of a valve of *Lingula anatina* LAMARCK showing variations in the apatitic content (*white*) and in three numbered prominent organic laminar sets (*black*) (Williams, Cusack, & Mackay, 1994).

layer, and baculate laminae are as well developed as they are in *Glottidia,* confirming the early phylogenetic origin of this fabric (WILLIAMS, MACKAY, & CUSACK, 1992)

The most extraordinary secondary fabric yet found is that of the lower Paleozoic acrotretoids (Fig. 240; POULSEN, 1971; HOLMER, 1989). The secondary shell consists of an overlapping stack of laminae, each of which can normally be traced throughout the skeletal succes(„internal of its subcircular junction with the primary layer. Each lamina is separated from its neighbors by a continuous, slotlike space (presumably the site of a membranous sheet) and consists of a pair of granular, apatitic lamellae (Fig. 241). The lamellae, which are contiguous medially, open up outwardly to form a wedgelike laminar margin enclosing variably developed spaces. In some acrotretoids, the apatitic walls of these spaces are studded with domes (Fig. 240.3) and connected by apatitic columns (Fig. 240.1–240.2) with hollow cores (columnar laminae). In others, the spaces are divided into boxlike compartments by vertical partitions of apatite (Fig. 240.4) with narrow (200 nm) medial spaces (camerate laminae). These medial spaces coincide with intercellular spaces found in the primary layer and are assumed to have been occupied by membranes in life. In determining how spaces with domes and columns and membrane-covered empty boxes of apatite originate, it has to be assumed that in life the spaces were filled with discrete bodies of granular apatite in a GAGs matrix; and this apatitic mesh contributed to the biomineralized coats of camerate membranous partitions and organic strands that formed the substrates for domes and columns (Fig. 241).

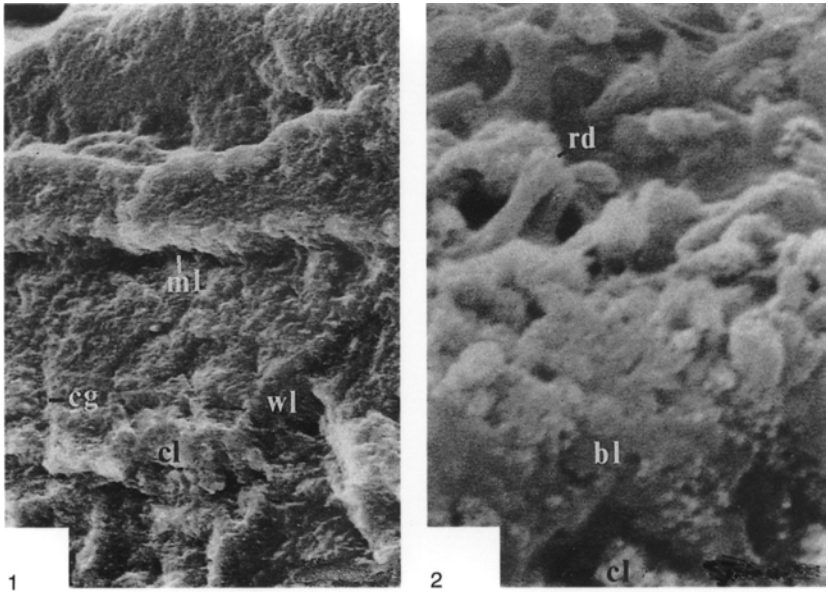

FIG. 237. Sections of the shell of *Lingula anatina* (LAMARCK) showing rhythmic laminar sets; *1,* three cleaved (*cg*) sets, each consisting of a compact lamina (*cl*) passing into a walled lamina (*wl*) and a capping membranous lamina (*ml*), ×1,300; *2,* compact lamina (*cl*) passing through a botryoid (*bl*) into a lamina of rods and plates (*rd*) embedded in GAGs, ×14,000 (Williams, Cusack, & Mackay, 1994).

The secondary fabric of the problematic organophosphatic paterinides is also anomalous although more readily interpretable (POPOV & USHATINSKAYA, 1987). The secondary layer, which constitutes the sole succession of the genera described (*Cryptotreta,*

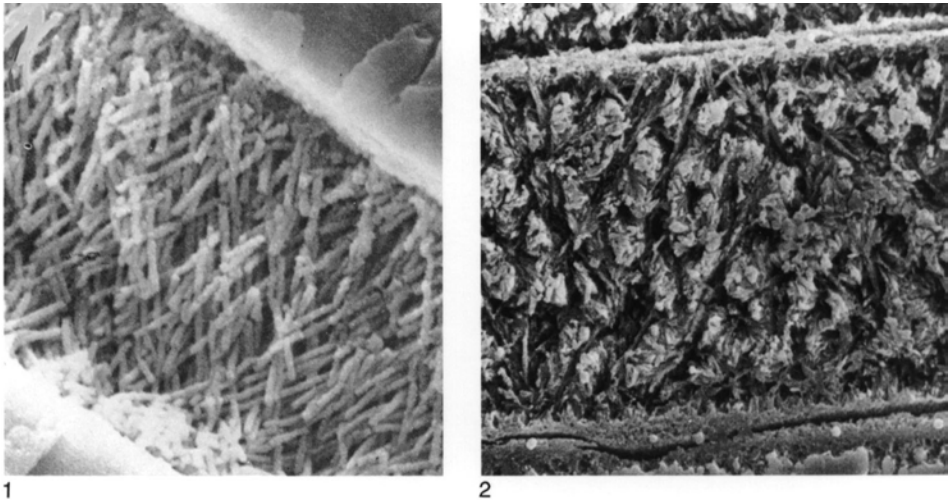

FIG. 238. Sections of linguloid shells showing the disposition of baculi between compact laminae; *1,* recent *Glottidia pyramidata* (STIMPSON), ×2,200 (Iwata, 1982); *2,* Early Ordovician *Ungula ingrica* (EICHWALD), ×3,300 (Holmer, 1989).

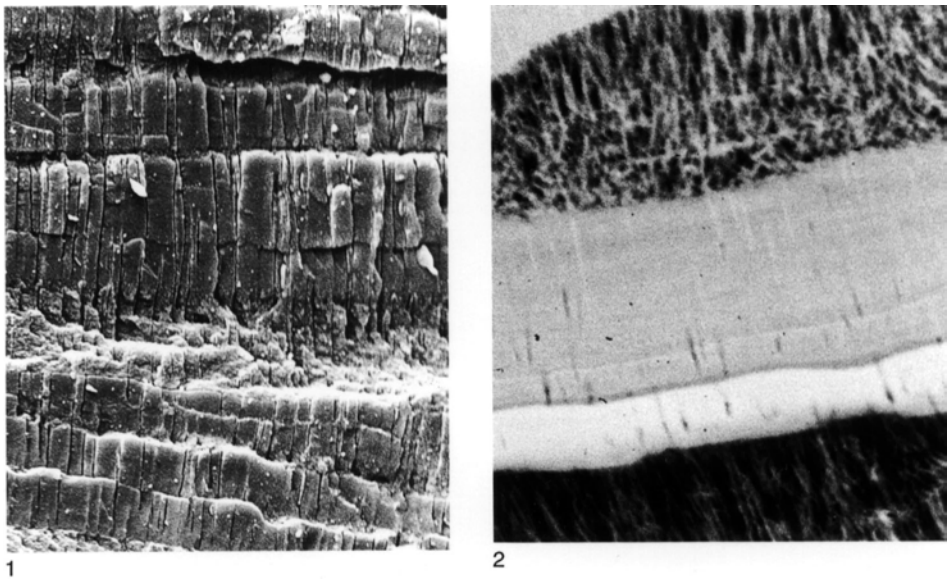

FIG. 239. Sections of the shell of *Discina striata* (SCHUMACHER); *1,* SEM showing thick apatitic laminae seamed by canals with rubbly laminae in midsection indicative of discrete apatitic components including baculi, ×720; *2,* back-scattered electron micrograph of compact laminae (*white*) between baculate laminae (*vertically striped*), ×1,260 (new).

Micromitra), consists of almost horizontal laminae up to 40 μm thick, composed of hexagonal, closely packed vertical prisms about 7 to 8 μm thick. In *Dictyonina,* the laminar microtexture is known to be spherular in aggregates up to 1 μm across (WILLIAMS, MACKAY, & CUSACK, 1992). If the apatitic prisms with their surrounds were secreted by cuboidal epithelium (POPOV & USHATINSKAYA, 1987), one can also assume that the primary layer, which together with the periostracum would have been exuded by elongate vesicular cells of the outer mantle lobe, consisted mainly of GAGs and would not have been preserved. In such a setting the paterinide prismatic fabric would have been analogous with that of the terebratulid tertiary layer.

CALCITIC FABRICS

The three kinds of secondary fabric found in calcitic-shelled brachiopods differ not only in their structure but also in their relative importance within the phylum as a whole. A fibrous fabric has always been the dominant feature of articulated shells except possibly during the Permo-Carboniferous when the cross-bladed, laminar strophomenides (*s.l.*) attained the peak of their diversity. In comparison with these major groups, the inarticulated calcitic species characterized by tabular laminae had a relatively modest distribution in the lower Paleozoic but, unlike the strophomenides, they survive to the present day and their living representative, *Neocrania,* furnishes an insight into laminar secretion.

CALCITIC FIBERS

The fabric of a fibrous, secondary shell is unmistakable in surface view and in section (WILLIAMS, 1966, 1968a, 1971b). On the internal surfaces of a valve, the transition from primary to secondary fabric is relatively sudden. In *Notosaria,* for example, the radial distance between the first traces of the arcuate fronts of newly formed fibers and fully developed ones is less than 20 μm. As the secondary shell thickens, these discrete patches of calcite (about 10 μm across) with

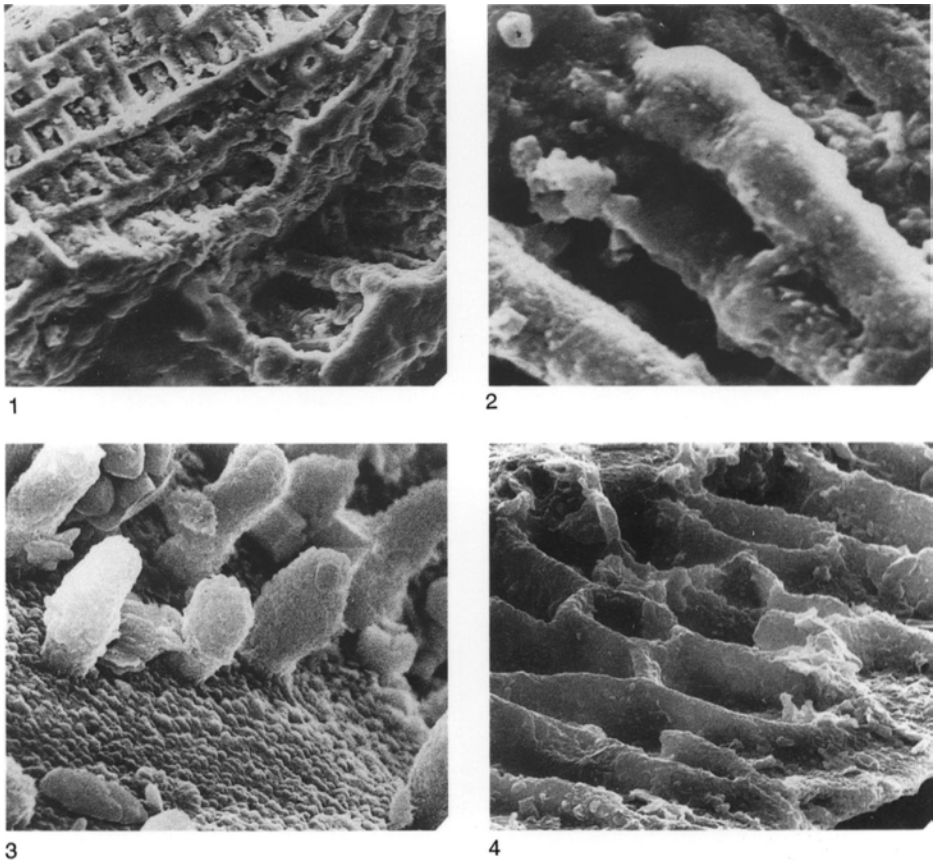

FIG. 240. Columnar and camerate fabric structures in acrotretoid secondary shell; *1,* general view of a columnar laminate succession, ×710, with *2,* details of columns, ×3,000, and *3,* of domes in a section of a ventral valve of *Angulotreta postapicalis* PALMER, ×4,100; *4,* internal margin of a dorsal valve of *Hisingerella tenuis* showing the disposition of partitions in a camerate lamina, ×2,200 (Williams & Holmer, 1992).

their surrounding membranes become elongated into fibers ensheathed in proteinaceous sheets. In this way the internal surface of secondary shell is fashioned into a distinctive mosaic that is really a protein-calcite cast of the secreting plasmalemmas of outer epithelium (Fig. 242).

The mosaic has a discernible lineation reflecting the incremental growth relationship of fibers that can be graphically represented by plotting the long axes of exposed parts of fibers (keels) as growth vectors. The resultant growth maps are informative (Fig. 243–244). For example, they show that extensions of fibers normal to the edges of convex valves are only characteristic of a narrow peripheral zone. Inwardly the terminal faces of fibers become reoriented more or less parallel to the valve margin. Accordingly, each fiber tends to grow in a spiral arc directed clockwise in the right half of a valve and counterclockwise in the left half (WILLIAMS, 1968a; BAKER, 1970b). Modifications of this pattern, the characteristic trace (WILLIAMS, 1971a), include the formation of microscopic whorls, in which individual fibers can be bent into open spirals (see Fig. 274). Such configurations can be regarded as solid-state summaries of the dynamics of epithelial migration during shell growth as each traces

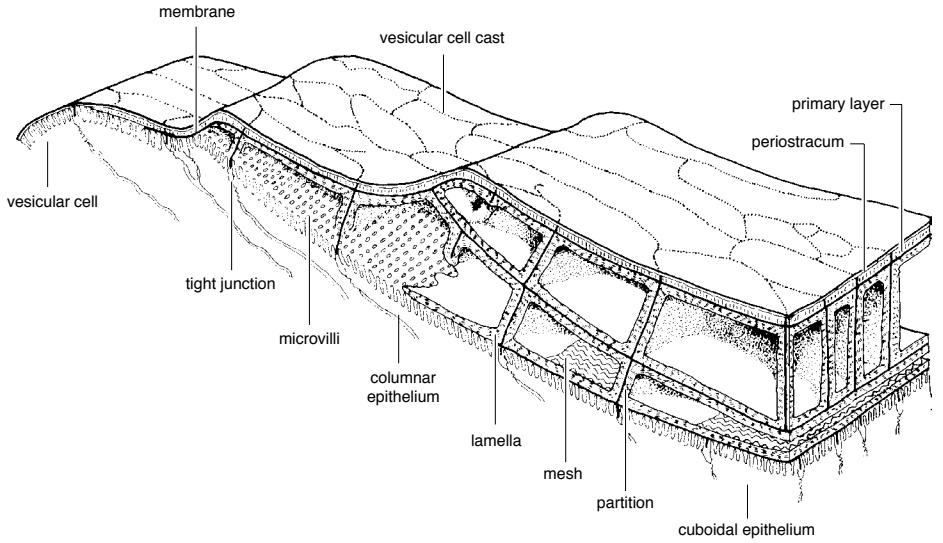

FIG. 241. Inferred relationships between the mantle and its outer lobe and the valve margin of the acrotretoid *Hisingerella* in life (Williams & Holmer, 1992).

successive loci of a secretory cell. All internal outgrowths of secondary shell result from accelerated rates of secretion and are built up of fibers lengthened and reoriented in this way.

Differential growth of the fibrous secondary shell is facilitated by the mode of stacking of the fibers (Fig. 242). Fibers within their membranous sheaths remain segregated from one another throughout life and interlock to achieve the best possible fit without impeding localized variations in growth. The arrangement is best understood in terms of shape of the fibers. In medial longitudinal section, fibers appear as blades that gradually become wider toward their terminal faces in phase with the increasing size of the maturing cells secreting them. The fibers are initially inclined outward at about 10° to the isotopic interface with the primary layer but may become reoriented with further growth. In contrast to this relatively simple longitudinal profile, cross sections of a typical fiber show that it is bounded by an inner, keeled surface that is flatly to roundly concave outward and an outer surface made up of two lateral arcs and a medial saddle, all also concave outwardly. This profile corresponds to the topography of the mosaic. The inner surface with its keel represents the terminal face of the fiber and its exposed posterior trail respectively, while the outer lateral areas rest on the two adjacent halves of fibers in the immediately younger row, and the saddle accommodates the keel of the next younger fiber. During the growth of a fiber, its transverse outline also changes and usually flattens as it enlarges laterally. A composite picture of these changes is provided by any transverse section of a secondary layer.

A fibrous fabric is invariably characteristic of the secondary shell of living rhynchonellides and terebratulides and is well developed in earliest known genera, such as the Devonian *Mutationella* and the Ordovician *Rostricellula,* respectively. It is also the standard fabric for all spire-bearing brachiopods, pentamerides, and most orthides (Fig. 245; WILLIAMS, 1968a). Even the problematic dictyonellidines have been shown to have some fibrous secondary shell (WRIGHT, 1981).

The secondary fibrous layer is, of course, variably developed in all groups; but no such changes are so spectacular as the neotenous

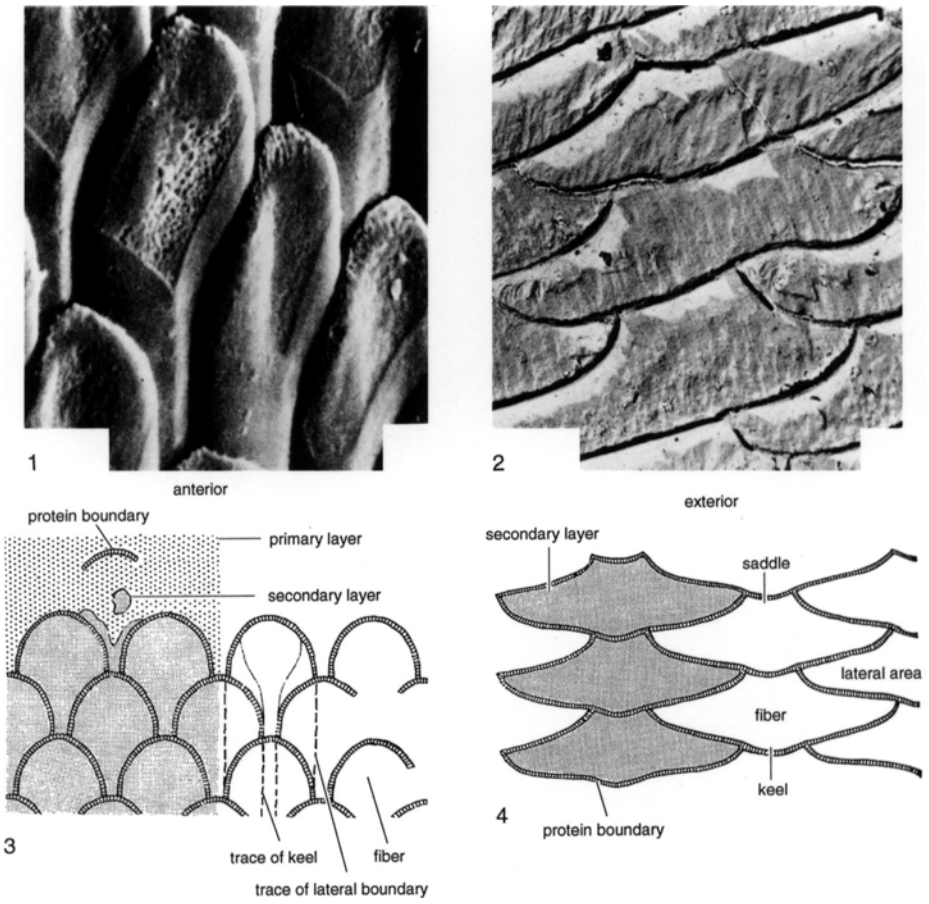

FIG. 242. Mosaic of the fibrous secondary shell of the rhynchonellide *Notosaria nigricans* (SOWERBY); *1,* terminal faces of fibers exposed in the floor of a valve, ×2,000; *2,* transverse section of orthodoxly stacked fibers, ×4,000 (Williams, 1968d); *3–4,* morphology of terminal faces and transverse sections respectively of orthodoxly stacked fibers (Williams, 1966).

reduction of the layer in the thecideidines (Fig. 246; WILLIAMS, 1973; BAKER, 1991). Such early Mesozoic thecideidines as *Davidsonella* and *Moorellina* have continuous layers of fibrous secondary shell. Post-Jurassic members of all lineages, however, were affected by a heterochronous, progressive loss of secondary shell so that, in living *Thecidellina* and *Lacazella,* orthodoxly stacked fibers are restricted to the teeth and additionally occur in the sockets and as microscopic patches on internal tubercles of the former genus. On the other hand, the shell continues to thicken throughout life so that the acicular and granular calcite of the primary layer is seamed with growth banding bearing frequent signs of interrupted accretion or absorption and widely distributed microscopic features like tubercles and closely packed rhombic blocks on mature internal surfaces.

During the evolution of the fibrous secondary sheet, fibers have varied in shape from large rods with lenticular cross sections of the spiriferide *Koninckina* to broad, flat structures commonly interleaved with lenses

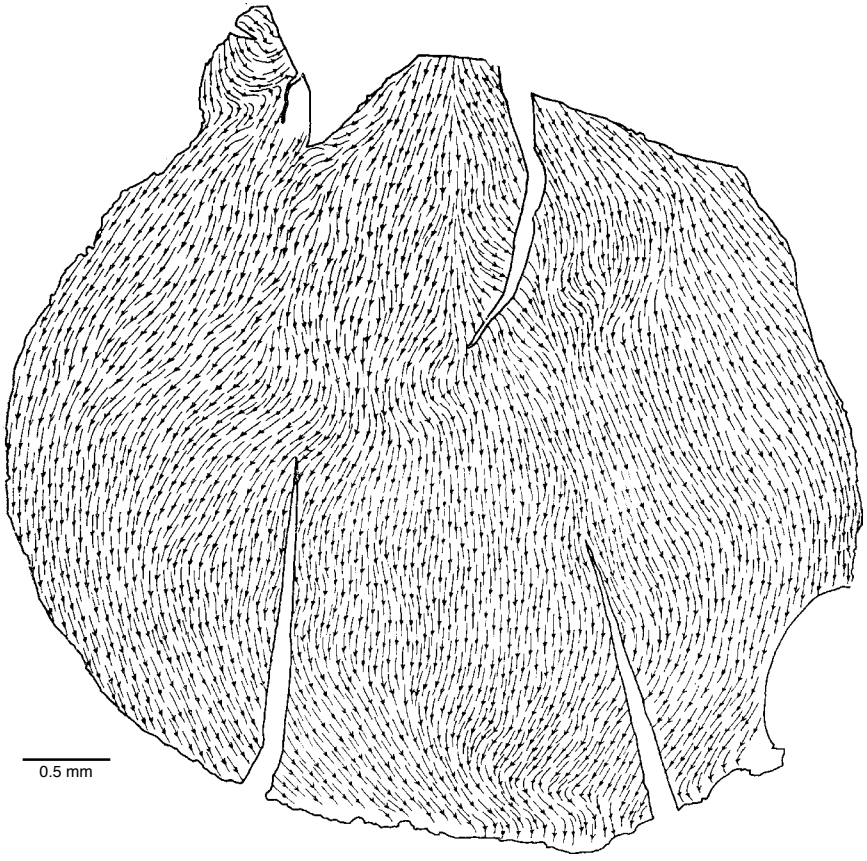

FIG. 243. Growth map of the mosaic of the dorsal valve of the rhynchonellide *Notosaria nigricans* (SOWERBY), using the long axes of exposed fibers as vectors of growth (Williams, 1968a).

of prismatic calcite as in pentameroids and many spire-bearing species. Yet there is no doubt that this fabric was typical of some of the oldest-known calcitic brachiopods like *Nisusia* and *Kotujella* (WILLIAMS, 1968c) and was the dominant fabric among articulated brachiopods.

CALCITIC TABULAR LAMINATION

The secondary fabric of the remaining articulated brachiopods, the extinct billingselloids and strophomenides, is more easily interpreted if that of the living inarticulated calcitic brachiopod *Neocrania* is considered first.

The secondary shell of *Neocrania* has a laminar fabric, seen in section as a succession of calcitic plates (Fig. 247.1) separated from one another by interconnected proteinaceous membranes. On the internal surface of a valve, the laminae are seen as overlapping tablets that are rarely perfectly rhombohedral (Fig. 247.2). They normally occur as single or double screw dislocations with fine growth banding on the tablet faces. The banding registers the incremental (possibly diurnal) growth of tablets recording, for example, sudden increases in corner angles from 75° to 135° or 150° so that extra hexagonal and dihexagonal edges are added by spiral growth to impart a subrounded outline to large laminae. If adjacent nuclei are crystallographically aligned, they may amalgamate into a composite tablet with a common

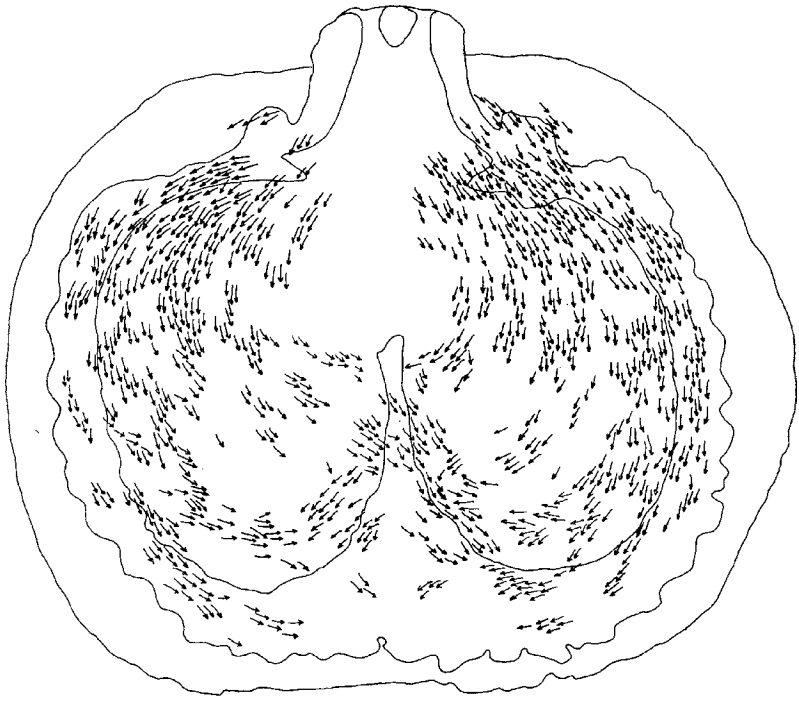

FIG. 244. Reconstruction of the secondary growth mosaic of the thecideidine *Moorellina granulosa* (MOORE), plotted from 25 superimposed peels (Baker, 1970a).

accretionary border. More usually, laminae are not aligned, and the junctions between neighboring units persist as cracks or notches. Where the edges of three or more laminae meet, triangular or trapezoidal enclosures occur.

Two constraints must be taken into account when considering how such a laminar shell is deposited as an alternating succession of tablets and membranes. First, discrete biomineral tablets require an organic substrate on which to seed and expand. Second, as nearly all tablets are affected by screw dislocation, they grow spirally by calcitic accretion along dislocation edges. Consequently as a calcitic lamina undergoes lateral accretion, it simultaneously presents an expanding inner surface for settlement by proteins, which polymerize into a new membrane. But the lamina is normally part of an expanding helicoid spiral so that its newly accumulating proteinaceous coat is also part of one continuous strip rotating just behind the dislocation front around the helicoid axis. Hence, the membrane acts as a cover for one calcite surface and a foundation for a later-forming calcitic tablet in the manner shown in Figure 248 (WILLIAMS, 1970b).

Secondary shell deposition in *Neocrania,* therefore, involves simultaneous secretion of protein and calcite by outer epithelium at different levels within a laminar succession. In effect, the succession thickens and expands laterally by spiral growth, which is a continuous, not an episodic, process. Spiral growth of this kind also affords sufficient biomineral continuity between levels within a shell succession to ensure a general crystallographic alignment (epitaxy) even when intervening proteinaceous membranes are imperforate.

This secondary laminar fabric of tablets is characteristic of all cranioids although it is variably developed in the ventral valve, by

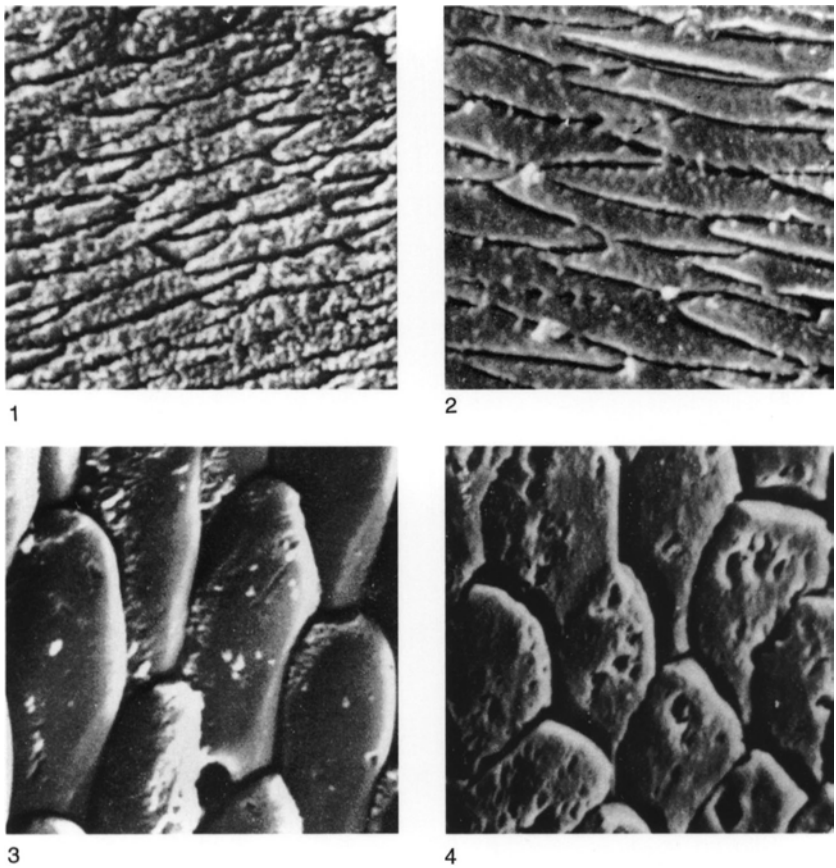

FIG. 245. Sections and internal surface views of the fibrous secondary shell of articulated brachiopods; *1,* Ordovician rhynchonellide *Rostricellula lapworthi* (DAVIDSON), ×2,600; *2,* late Silurian terebratulide *Mutationella podolica* (SIEMIRADZKI), ×2,700; *3,* Jurassic spiriferide *Spiriferina walcotti* (SOWERBY), ×1,300; *4,* Pennsylvanian enteletoid *Rhipidomella* sp., ×1,300 (Williams, 1971b).

which all but the oldest cranioids are cemented to the substrate. Indeed the ventral valve is commonly represented only by primary shell, and even this biomineralized layer may be absent as in species of *Craniscus.* Primary and secondary fabrics, however, were developed in both valves of the oldest known cranioid, the Ordovician unattached *Pseudocrania* (WILLIAMS & WRIGHT, 1970).

Two other inarticulated groups have calcitic shells with well-developed primary and secondary layers (WILLIAMS & WRIGHT, 1970). The fabric of the craniopsoid secondary shell, as typified by a mid-Silurian species of *Craniops,* is finely and regularly laminar with units about 300 nm thick (Fig. 249). The succession is so like that of Paleozoic cranioids as to make it likely that the craniopsoid laminae were also tablets interleaved with interconnected membranes.

The secondary layer of the obolellide *Trematobolus,* on the other hand, is more coarsely and irregularly laminar with lenticular units (folii) up to 500 nm thick and 10 μm across (Fig. 249). The fabric is further complicated by the presence of regularly dis-

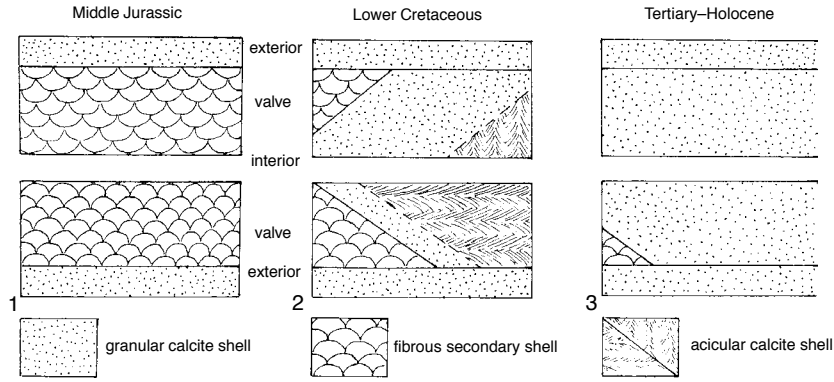

FIG. 246. Selected chronological states in the evolution of thecideidine shell structure; *1, Moorellina* with a continuous fibrous secondary shell in both valves; *2, Thecidiopsis* with a reduced fibrous secondary shell and well-developed acicular crystallites associated with the primary granular fabric; *3, Lacazella* with vestigial fibrous secondary shell on teeth and inner socket ridges (adapted from Baker, 1990).

tributed hemispherical nodules of coarsely crystalline calcite up to 40 μm across and convex externally. Nodules also occur in the cranioid secondary shell, but they are convex internally and more readily identifiable as temporary muscle bases. On balance, the obolellide secondary folii were probably ensheathed in membranes and more like fibers than laminae in origin.

CALCITIC CROSS-BLADED LAMINATION

The laminar secondary fabric of the strophomenides (*s.l.*) and billingselloids is not tabular in the cranioid style. The basic unit is a long, lath- or blade-shaped crystallite of variable length (but commonly traceable for more than 100 μm) and with a width

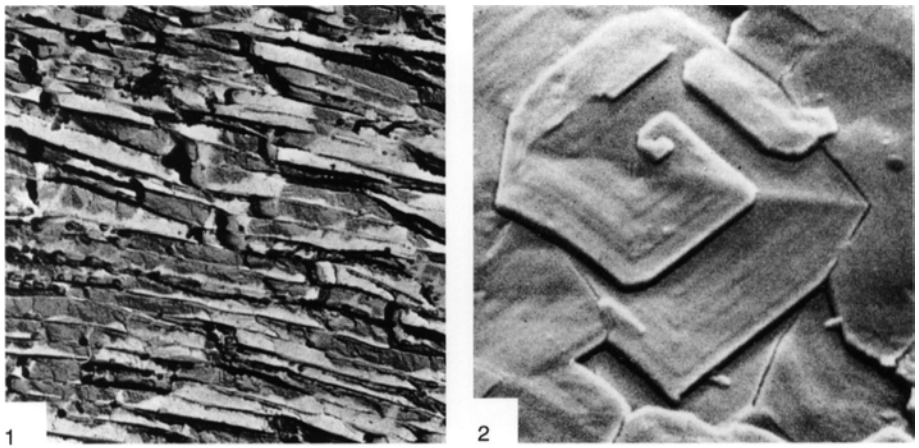

FIG. 247. The laminar secondary shell of living *Neocrania anomala* (MÜLLER); *1,* section of a succession of laminae with acutely triangular and trapezoidal outlines representing different aspects of spiral growth, ×7,000; *2,* internal surface of a dorsal valve showing three successive laminae of a single spiral growth unit with concentric growth bands, ×5,900 (Williams, 1970b).

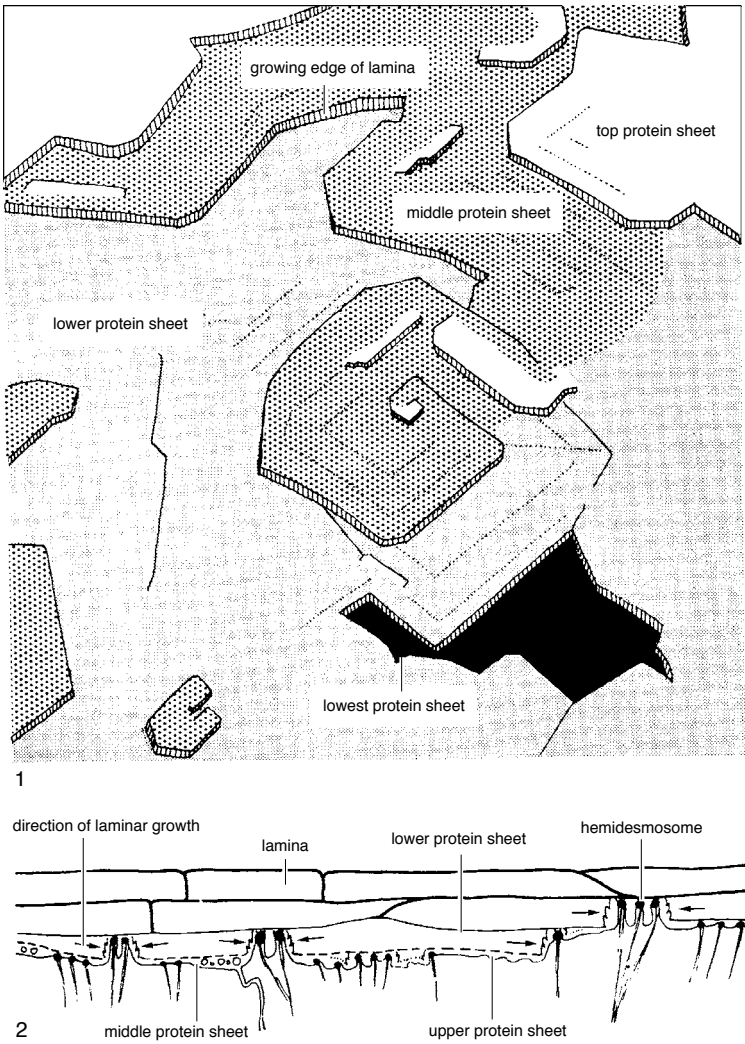

FIG. 248. Stylized reconstruction of several laminae, shown in Figure 247.2, in association with their proteinaceous covers as seen on the internal surface of the dorsal valve (*1*), together with the inferred relationship with secreting outer epithelium (*2*) (Williams, 1970b).

ranging from 2 μm to 6 μm and a thickness from about 100 nm to 500 nm (WILLIAMS, 1970a). Each lamina consists of a set of contiguously aligned blades with their lateral junctions in various stages of amalgamation (Fig. 250). Accordingly, although traces of these junctions on a laminar surface are normally parallel with one another, they vary from breaks cutting through the lamina (Fig. 250.1–250.2) to faint ridges on the inner surfaces (Fig. 250.3). Such traces of blade sets may be disposed at acute angles to one another in successive laminae (the cross-bladed fabric of ARMSTRONG, 1969) and act as optical diffraction gratings to give the nacreous sheen of loosely foliated shells like those of *Pholidostrophia* (TOWE & HARPER, 1966). The other noteworthy feature of

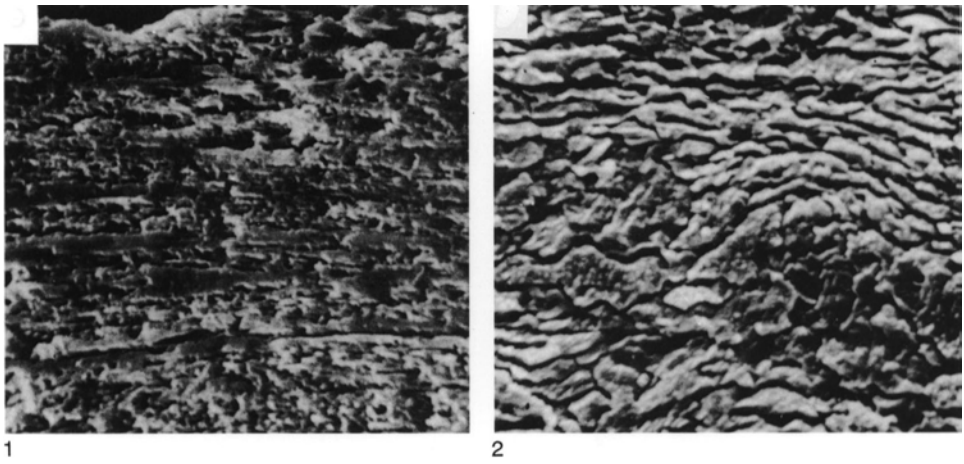

FIG. 249. Sections of the calcitic secondary shell of inarticulated brachiopods; *1,* ventral valve of the craniopsoid *Craniops implicata* (SOWERBY) showing the laminar structure of the secondary shell, ×1,140; *2, Trematobolus pristinus bicostatus* GORYANSKY with a coarse and irregularly laminar (foliated) secondary shell, ×2,280 (Williams & Wright, 1970).

cross-bladed lamination is that even in such later-appearing groups as the productidines and orthotetidines, the external surfaces of blades, which are normally flat, may be gently convex with rounded or obtusely planar slopes (crested laminae) and appear to terminate in scalenohedral faces as opposed to the rhombohedral edges of flat blades (Fig. 251).

The recovery of amino acids from strophomenide shells by JOPE (1965) suggests that cross-bladed laminae were associated with proteinaceous membranes. The disposition of the calcitic components also suggests that the membranes were interleaved with laminae, comparable in that respect with cranioid secondary successions. However, it seems unlikely that the well-ordered blades of the strophomenide laminar fabric grew by screw dislocation. A more feasible assumption is that the growth of this kind of lamina involved simultaneous deposition of protein and calcite on the surfaces and along the rhombohedral edges (or scalenohedral faces) respectively of blade sets (Fig. 251). This is confirmed by the disposition of growth banding in individual blades, which is transverse to the long axes of the blades and parallel to their edges (Fig. 250.2–250.3). With respect to the origin of the cross-bladed laminar fabric, the nature of the secondary shell of two early Paleozoic groups has to be taken into account.

The orthidine *Billingsella* has a well-developed, albeit recrystallized, primary layer underlain by a secondary shell composed of parallel-sided laminae about 1 μm thick. The laminae are composed of blades that can be up to 35 μm wide, presumably recrystallized, amalgamated sets of four or five laths (Fig. 252).

The strophomenide plectambonitoids, on the other hand, have a fibrous secondary shell (Fig. 252–253). This anomalous condition is all the more intriguing in that typical chonetidines, which are likely to have evolved from the plectambonitoids, have a secondary shell with a cross-bladed laminar fabric. In this context it is noteworthy that plectambonitoid aegiromenines like *Aegiromena* and contemporaneous chonetidines (*Strophochonetes*), which are morphologically alike except for the presence of hinge-spines in the latter stock, have a similar secondary shell fabric (Fig. 253). In *Aegiromena* orthodoxly stacked fibers dominate the outer secondary shell fabric, but internally the

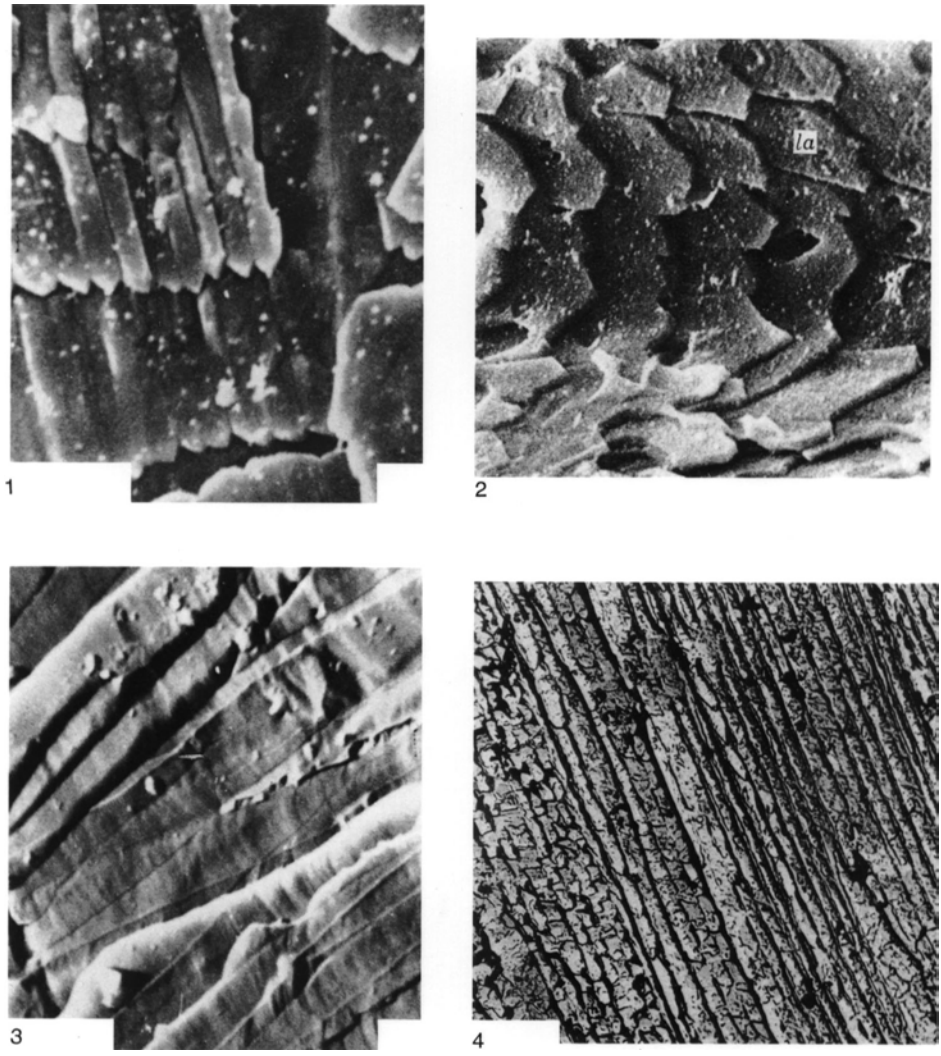

FIG. 250. The cross-bladed laminar secondary shell of strophomenides; *1,* contiguous laths in various stages of amalgamation to form laminae in a fracture surface of the ventral valve of the orthotetidine *Gacella insolita* WILLIAMS, ×2,600 (Williams, 1970a); *2,* internal surface of a ventral valve of the orthotetidine *Schellwienella* cf. *aspis* (SMYTHE) showing the overlapping arrangement of laminae composed of laths (*la*) along their terminal faces, ×2,800 (Williams, 1973); *3,* cross-bladed laminae composed of amalgamated laths in a fracture surface of a ventral valve of the strophomenoid *Strophomena oklahomensis* COOPER, ×2,600 (Williams, 1970a); *4,* section of a cross-bladed laminar succession in a valve of the stropheodontoid *Pholidostrophia* cf. *geniculata* IMBRIE, ×2,500 (Williams, 1968a).

fibers (about 14 μm wide) are lathlike and typically flattened in cross section with their edges commonly overlapping. In *Strophochonetes,* the basic constituents of the secondary shell are also lath-shaped (6 to 10 μm wide) and overlap like those of *Aegiromena* or lie in contiguity without lateral fusion. These discrete laths are the dominant fabric of Sil-

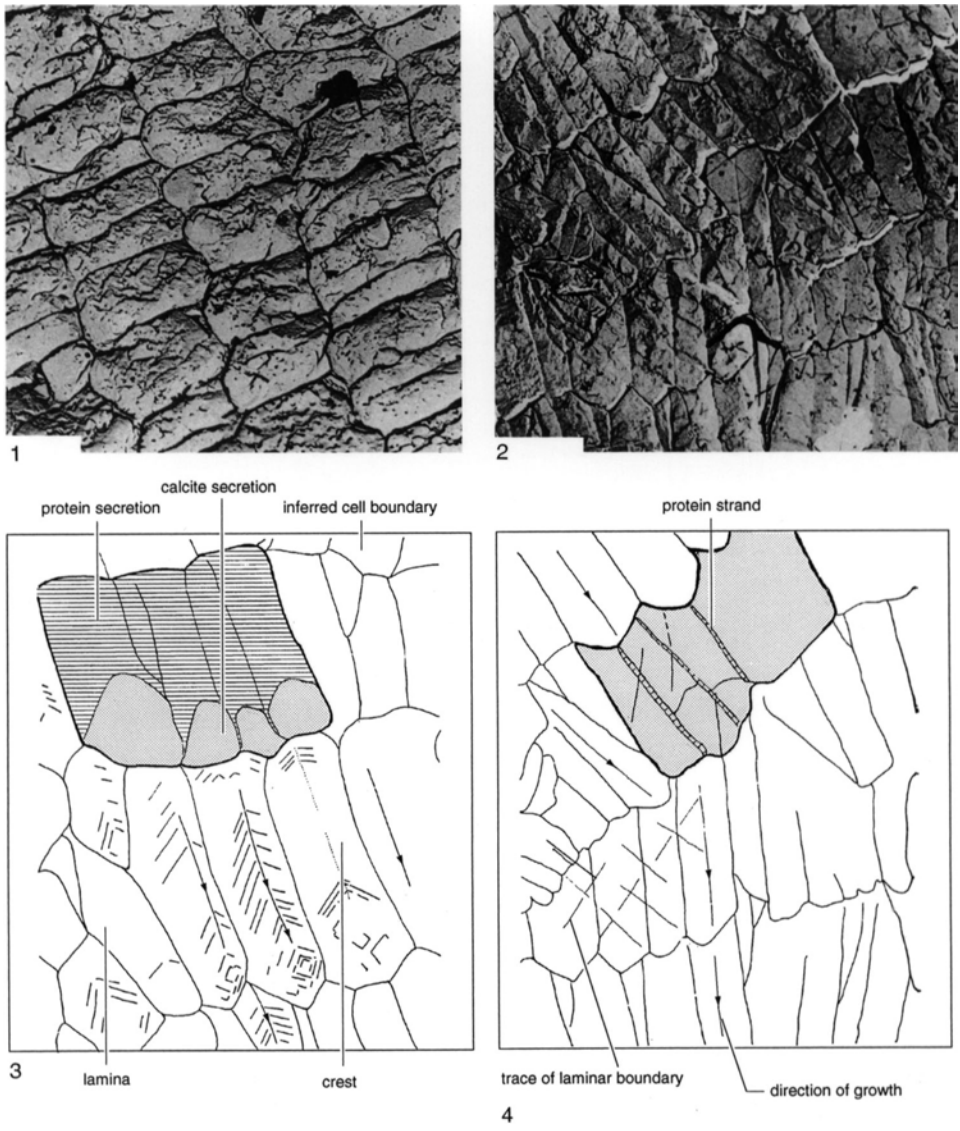

FIG. 251. Mosaics on the internal surfaces of valves with cross-bladed laminar secondary layers and their inferred relationships with interleaved proteinaceous membranes and secreting outer epithelium; *1, 3,* angular ridges along terminal faces giving rise to crested laminae, ×2,500; *2, 4,* flat terminal faces of typical, cross-bladed laminae, ×2,500. Both sets of terminal faces in a dorsal valve of the productidine *Juresania* sp. (Williams, 1968a).

urian chonetidines. They were not fully fused into laminar sheets until the Devonian and did not become wholly cross-bladed until the Carboniferous (BRUNTON, 1972).

The ancestry of cross-bladed lamination is clearly complicated. There are good morphological grounds for assuming a close affinity between *Billingsella* and the

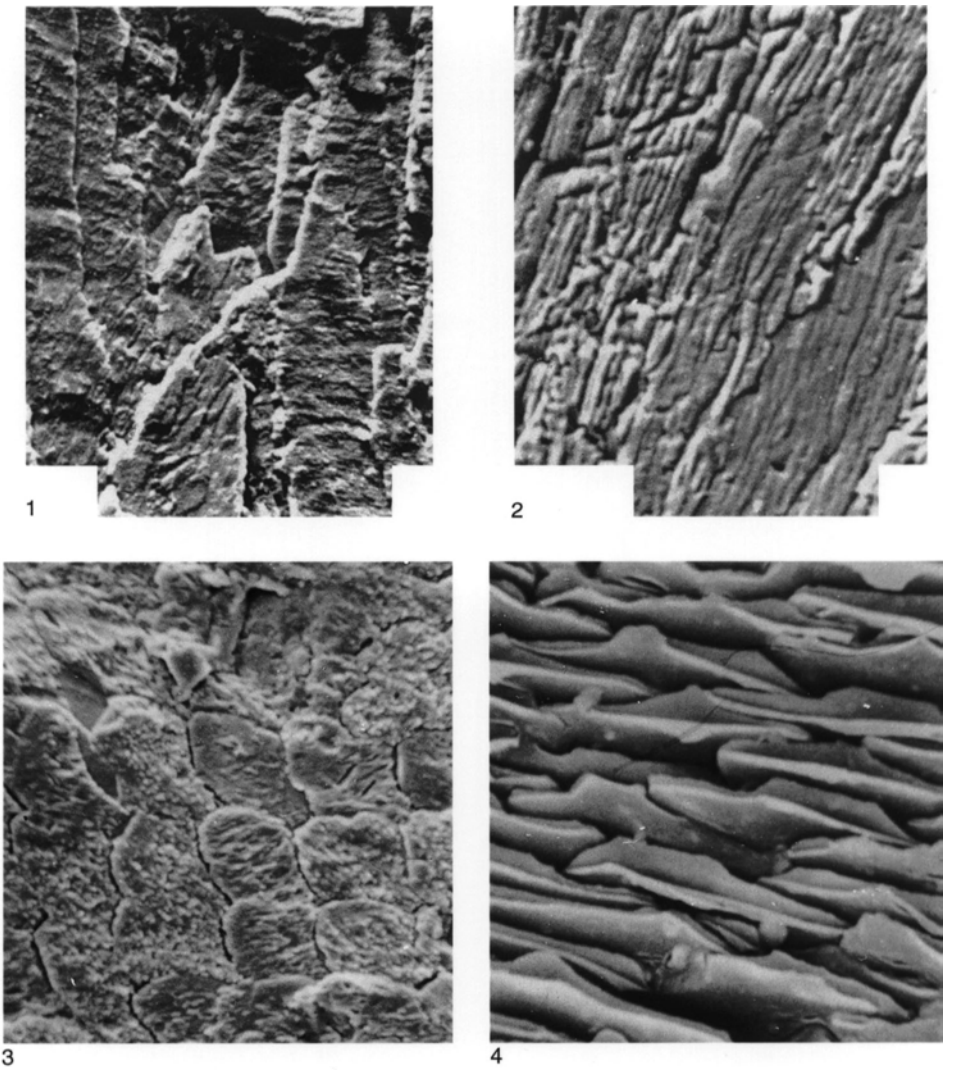

FIG. 252. Secondary shell fabrics; *1,* fracture surface (×1,700) and *2,* section (×800) of the laminar shell of the orthide *Billingsella lindströmi* (LINNARSSON) (Williams, 1970a); *3,* internal surface (×600) and *4,* section (×830) of the pseudopunctate fibrous shell of the plectambonitoid *Sowerbyella variabilis* COOPER (new).

impunctate, early orthotetidines and triplesiidines and to a lesser extent between *Billingsella* and the pseudopunctate early strophomenoids. There are equally good grounds for believing that plectambonitoids and strophomenoids are more closely related to each other than to any other known brachiopod stock. The conclusion, therefore, is that the cross-bladed laminar fabric is homoplastic with billingselloids and chonetidines originating in late Precambrian and Late Ordovician times respectively and the strophomenoids possibly in the Early Ordovician from plectambonitoids (WILLIAMS,

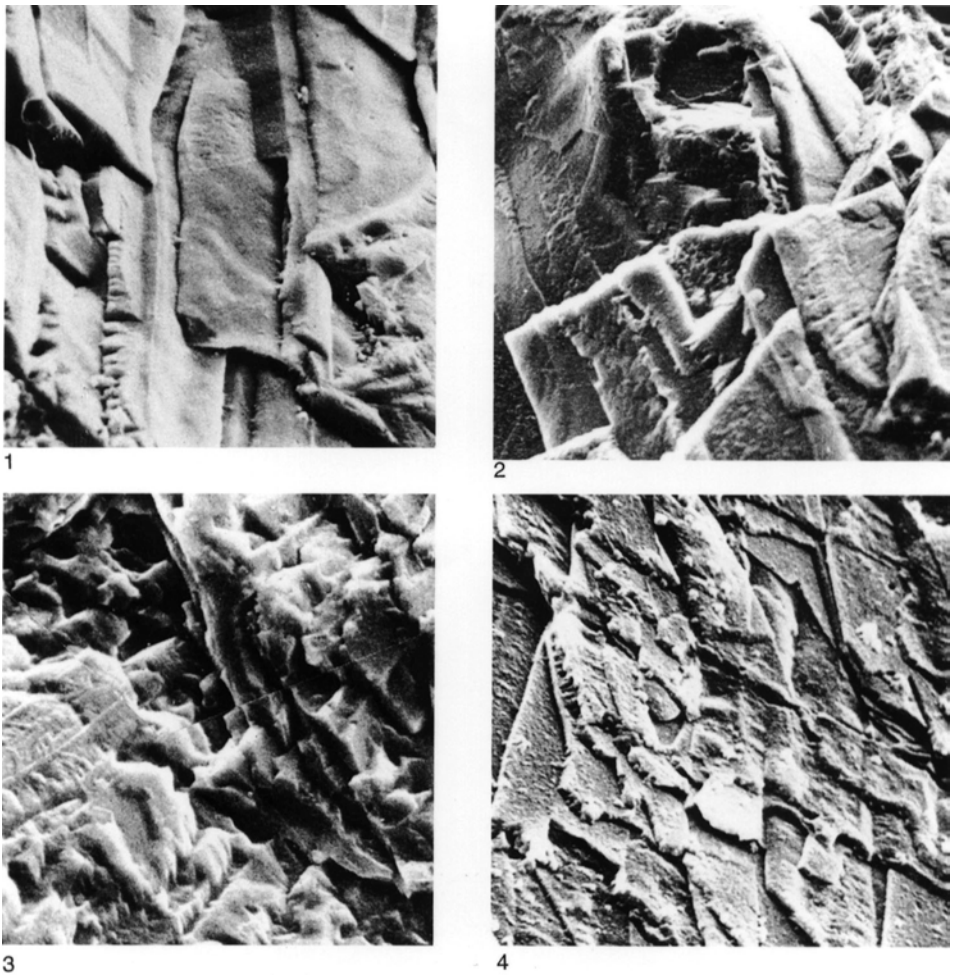

FIG. 253. Secondary shell fabrics; *1,* orthodoxly stacked, flattened fibers in the outer part of the secondary succession of the plectambonitoid *Aegiromena aquila* (BARRANDE), ×1,200; *2,* flattened fibers forming laminar sheets around a taleola in the middle part of the secondary succession of *Aegiromena aquila,* ×1,100; *3,* flattened fibers forming laminar sheets in the secondary succession of the chonetidine *Strophochonetes primigenius* (TWENHOFEL), ×1,000; *4,* secondary laminae of chonetidine *Rugochonetes silleesi* BRUNTON, ×2,100 (Brunton, 1972).

1970a). In any event, it seems likely that a fibrous shell was ancestral to a cross-bladed laminar one.

TERTIARY LAYER

The term tertiary is given to a continuous layer of shell that is sufficiently different from the overlying secondary succession to have been deposited by outer epithelium with a distinctive secretory regime. There is a continuity in secretion from the periostracum to the tertiary layer, which suggests that differences in the successions reflect physiological changes in the secretory regimes of distinctive outer epithelia (Fig. 254). Thus in such living terebratulids as

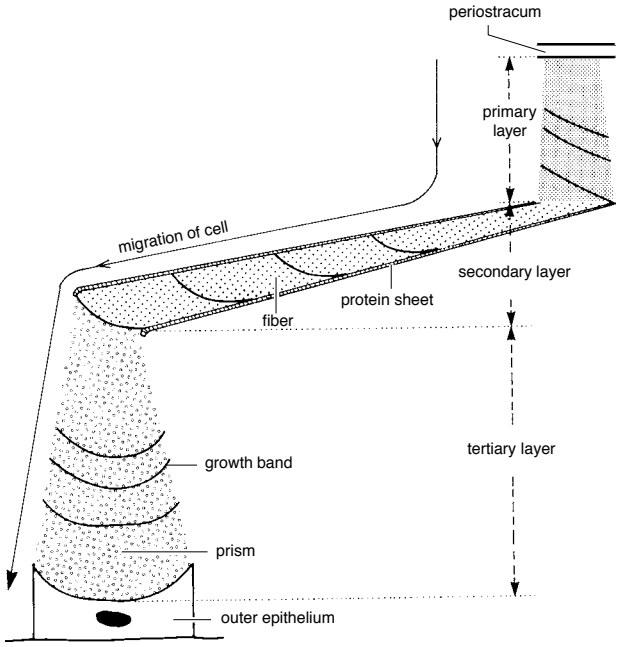

FIG. 254. Diagrammatic longitudinal section of integument of the terebratulide *Liothyrella* showing the migration of an outer epithelial cell during its secretion of succeeding biomineral components (Williams, 1990).

Gryphus and *Liothyrella,* prismatic calcite forms a continuous tertiary layer immediately distinguishable from the overlying fibrous secondary shell (MACKINNON & WILLIAMS, 1974). The origin of the tertiary layer has been traced in *Gryphus.* In the transitional zone, a flat-lying fiber becomes transformed by a lateral spreading of its terminal face, which is then extended vertically by accretion into a prism, normally corrugated by strong growth banding (Fig. 255). The prisms are discrete units, up to 20 μm thick. They have interlocking boundaries but are not separated from one another by extensions of the proteinaceous membranes ensheathing the fibers. The amalgamation of prisms, therefore, may be inhibited by sheets of water-soluble polymers or by crystallographic nonalignment of contiguous prisms. This change in cell secretion must be reversible to account for interdigitations of fibrous and prismatic fabrics along the interface between the secondary and tertiary layers of *Liothyrella* (Fig. 255.2).

The terebratulid tertiary layer was acquired gerontomorphically by the group as a whole, but no chronostratigraphic order has yet been discerned in its phylogeny. Isolated lenses of prismatic calcite are common in the fibrous secondary shell of fossil terebratulids and may have been precursory to the development of a continuous tertiary layer within the stocks concerned. A tertiary layer has also been identified in Mesozoic megathyrids and terebratellids, which confirms the homoplastic origin of this prismatic fabric even within an ordinal group of brachiopods (SMIRNOVA & POPIEL-BARCZYK, 1991).

Lenses of prismatic calcite also commonly occur within the fibrous secondary shell of many pentamerides and spire-bearing brachiopods. A fully developed, prismatic tertiary layer is found in the koninckinoids and reticularioids and in some atrypoids, athyroids, and pentameroids and must have evolved repeatedly.

So far as is known, a tertiary layer, as here defined, is rare in organophosphatic

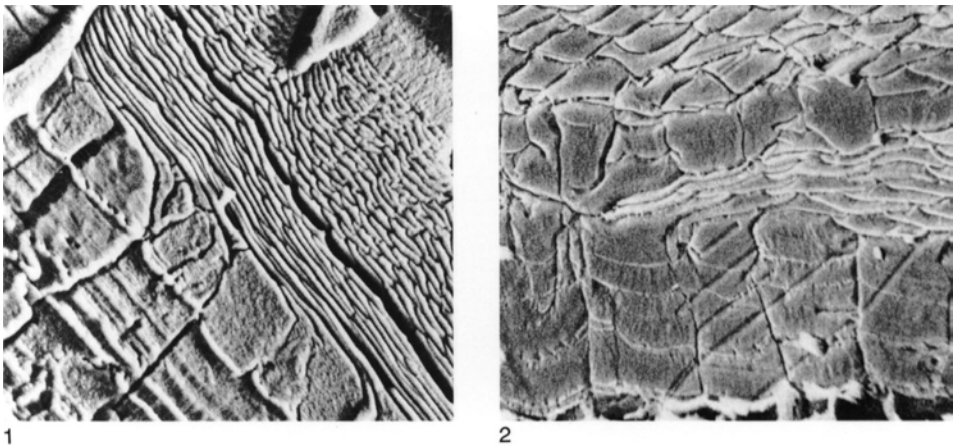

FIG. 255. Secondary and tertiary shell fabrics; *1,* fibrous secondary layer passing into prismatic tertiary layer (bottom left of micrograph) of a dorsal valve of the terebratulid *Gryphus vitreus* (BÖRN), ×565; *2,* relationship between the tertiary layer and an earlier-formed lens of prismatic calcite enclosed by secondary fibers in the dorsal valve of *Liothyrella neozelanica* THOMSON, ×1,175 (MacKinnon & Williams, 1974).

brachiopods. HOLMER (1989) described a continuous tertiary layer of columnar laminae succeeding a camerate secondary shell in such acrotretoids as *Acrotreta* and *Torynelasma.* This distinction in fabric is enhanced by the transgressive encroachment of the horizontal tertiary columnar laminae across the wedge-shaped sectors of the secondary camerate laminae. Similar structural discontinuities affect shell successions of *Ephippelasma* and *Biernatia,* which consist entirely of columnar laminae. However, they do not alone signify a basic distinction between secondary and tertiary layers (WILLIAMS & HOLMER, 1992).

SHELL PERFORATIONS

Conspicuous features of the fabric of many brachiopod shells are caused by persistent extensions or localized attachments of the mantle. The consequential microscopic perforations or protuberances are common features of extinct and living brachiopods and have developed in many different ways. In general, however, shells that are permeated by canals are referred to as punctate, and stratified fabric penetrated by them is deflected as perforated cones pointing externally. Shells with protuberances formed within evaginations of the mantle are pseudopunctate when stratified fabric is puckered into cone-in-cone microstructures pointing internally. Shell fabric that is free of all such complications is described as impunctate.

PUNCTAE

There are three kinds of perforations (see Fig. 261)—endopunctae, punctae (*s.s.*), and canals—all of which are developed in living species. Endopunctae permeate terebratulides and thecideidines and, as described in the section on anatomy (p. 33), accommodate caecal extensions of the entire outer epithelium, which act as storage centers for the mantle. Endopunctae are relatively large canals, although they vary greatly in maximum diameter from about 5 μm in *Terebratulina* to 20 μm in *Macandrevia* (OWEN & WILLIAMS, 1969) or as much as 40 μm in megathyrids (SMIRNOVA & POPIEL-BARCZYK, 1991). An endopuncta is usually funnel-shaped in longitudinal section with the maximum diameter just proximal of the distal, perforated canopy of primary shell (1 μm and 7 μm thick in *Macandrevia* and *Thecidellina* respectively) separating the caecum from the periostracum (Fig. 256). The

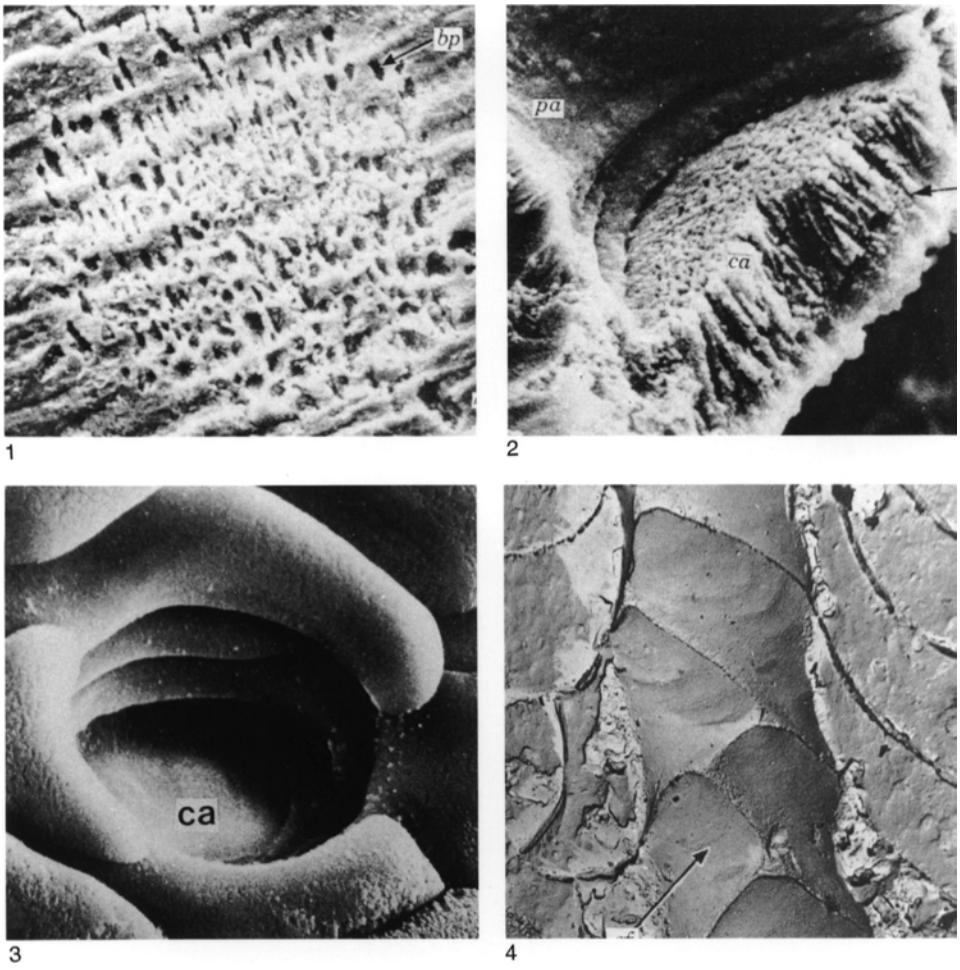

FIG. 256. Endopunctation; *1,* perforations of the brush (*bp*) seen externally (×1,400) and *2,* as perforations and canals (*arrow;* ×3,000) in the fracture section of the canopy (*ca*) of an endopuncta (*pa*) of *Lacazella mediterranea* (RISSO) (Williams, 1973); *3,* disposition of fibers defining an endopuncta and its canopy floor (*ca*) near the primary-secondary shell junction of the terebratulid *Liothyrella neozelanica* THOMSON, ×2,800 (Williams, 1990); *4,* resin cast of endopuncta of *Calloria inconspicua* (SOWERBY) showing the overlap of fibers (*arrow*) in the wall, ×5,000 (Owen & Williams, 1969).

narrowing of an endopuncta proximally is the result of the thickening of the secondary shell relative to the growth of a constant number of caecal peripheral cells, which become very attenuated (Fig. 257.2). With respect to its morphology, the definitive feature of an endopuncta is its perforated canopy. This is a calcitic cast of the microvillous plasmalemmas by which several storage cells become temporarily attached to the periostracum during their differentiation into a caecum at the outer mantle lobe (STRICKER & REED, 1985b). The perforated canopy is assumed to be a unique feature of the brachiopod shell (WILLIAMS, 1973) and, therefore, a reliable guide to the close affinities of various stocks with punctae capped by such a structure.

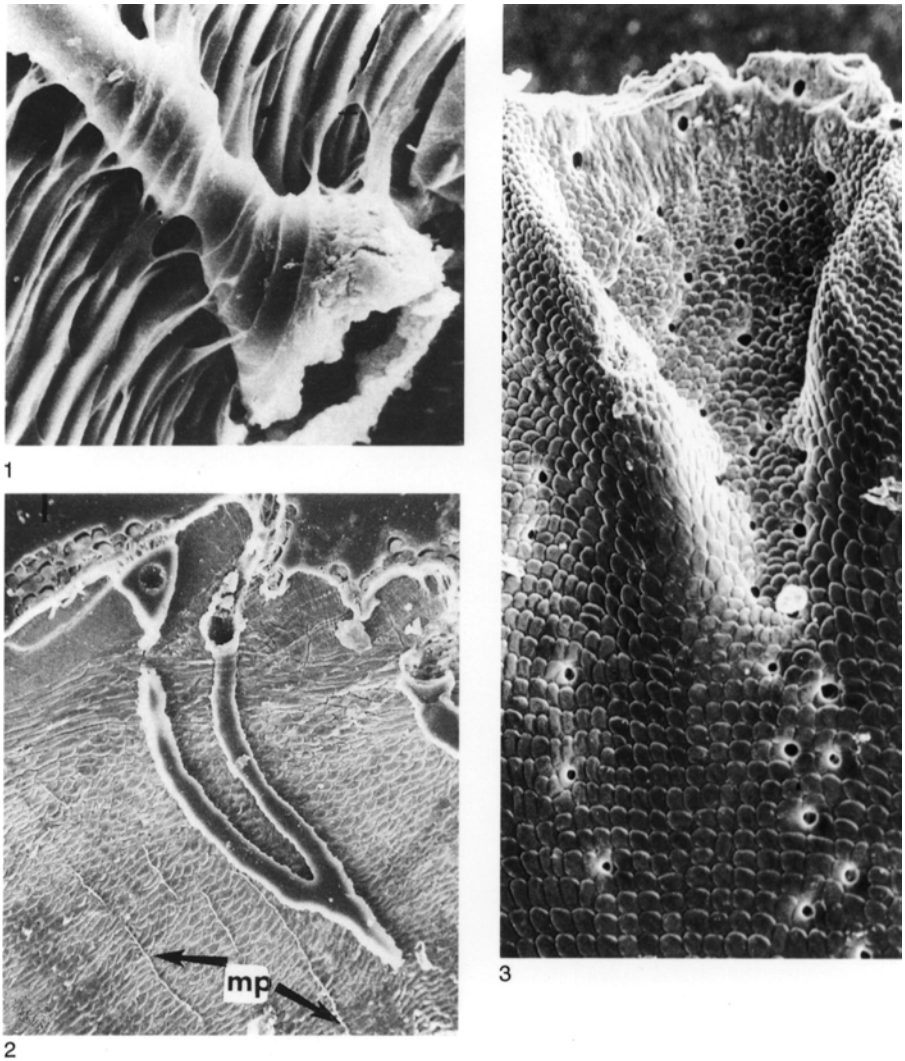

FIG. 257. Terebratulide punctation; *1,* fracture section of *Macandrevia africana* COOPER showing the typical outline of caecum associated with membranes of the secondary shell, ×2,000; *2,* section of *Megerlia truncata* (LINNÉ) showing branched punctae (filled with resin) and micropunctae (*mp*), ×350 (Gaspard, 1990); *3,* interior of the dorsal valve of *Terebratulina retusa* (LINN.) showing how the more numerous, regularly spaced endopunctae at the valve margin converge, as a result of secondary fibrous shell thickening, to form a smaller number of radially distributed bases, ×200 (new).

The distribution densities of endopunctae within the shell of living species are variable, but the pattern of distribution is essentially regular, as would be expected of features originating at the growing edge of a valve. The pattern is likely to be a mixture of hexagonal close packing (COWEN, 1966) and alternations in concentric rows (KEMEZYS, 1965) as was shown by BAKER (1970b) for the thecideidine *Moorellina* (Fig. 258). In *Thecidellina,* unbranched endopuncta (25 μm in maximum diameter) are arranged at

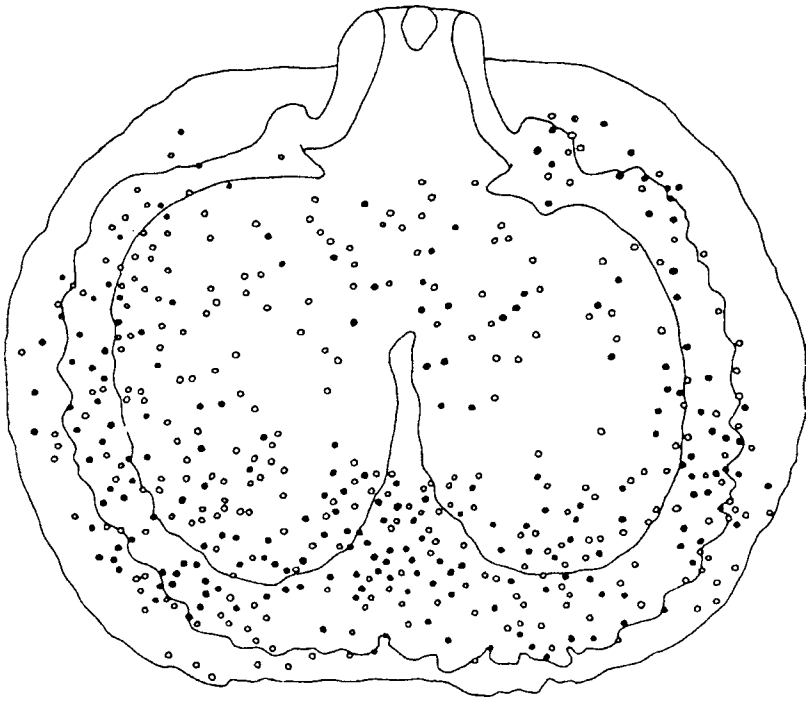

FIG. 258. Plot of endopunctae identified during horizontal serial sectioning of a dorsal valve of the thecideidine *Moorellina granulosa* (MOORE); *closed circles,* persistent punctae; *open circles,* impersistent punctae (Baker, 1970a).

intervals of about 45 μm in a dominantly hexagonal, close-packing pattern (WILLIAMS, 1973). This pattern is also the standard arrangement for terebratulides although it can be greatly modified by differential growth in such genera as *Terebratulina* where endopunctae are more densely distributed in radial sectors corresponding to the crests of ribs (Fig. 257). However, some indication of frequency differences even in regular, closely packed arrays is given by counts in the evenly contoured, median sector of the dorsal valve of *Magellania* where the frequency of endopunctae in quadrants with radii of 1 mm varied from 80 to 125 within 7 mm of the umbo (WILLIAMS & ROWELL, 1965b, p. 69).

Shell thickening and the microtopography of the external surface as well as the density of distribution and size of endopunctae determine whether endopunctae become branched in the manner shown in Figure 257.2. Endopunctae branch freely by converging to share a common, attenuated stalk of outer epithelium, which is pinched up from the mantle by deposition of the surrounding secondary shell. This accounts for the relatively few, radially arranged internal openings of endopunctae compared with the greater number of their more widely dispersed distal heads in *Terebratulina* (Fig. 257.3). Such differences in the density distributions of punctae in outer and inner successions of strongly ribbed shells are clearly evident in the enteletoid *Dicoelosia* (WRIGHT, 1966). In this stock, the distal ends of punctae, which lie normal to the sharply folded surfaces of the strong ribs, were quickly coalesced by shell thickening into a smaller number of more openly distributed trunks in simulation of the arborescent canal system of the inarticulated craniids.

Endopunctae are characteristic of all terebratulides throughout their geological history. They also permeate the shells of theci-

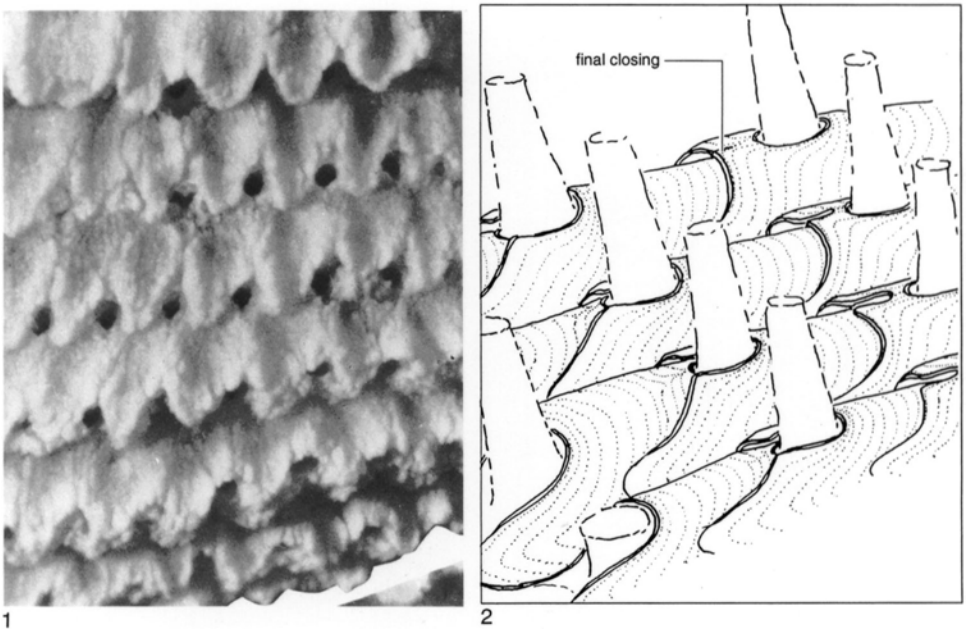

FIG. 259. Punctation in the atrypidine *P. (Punctatrypa) nalivkini* HAVLIČÉK from the Lower Devonian Zlichov Limestones, Czech Republic; *1,* fenestrae within the lamella on the exterior of a ventral valve, ×30; *2,* fenestrae interpreted as perforations accommodating setae (adapted from Wang, Copper, & Rong, 1983).

deidines but are sporadically suppressed as in the adult shell of *Bifolium* (BAKER & LAURIE, 1978). Endopunctae with perforated canopies have also been found in Jurassic spiriferinoids (MACKINNON, 1971). This suggests that the thecideidines, terebratulides, and some endopunctate spiriferides are monophyletic with a stem group of pre-Devonian age, a phylogeny supported by other, morphological considerations (WILLIAMS, 1973).

This phylogenetic relationship, however, does not necessarily support an assumption that punctae found in other spire-bearing brachiopods accommodated caeca with retractable apical microvilli. The fibrous secondary layer of *Punctatrypa* is pierced by very coarse, unbranched canals (fenestrae) that can also breach overlapping lamellae of primary shell (Fig. 259). Fenestrae that are up to 80 μm in diameter have been interpreted as having accommodated erect setae around the bases of which lamellae were secreted eventually to form a complete ring of primary shell by fusion of crenulations of the outer mantle lobe during forward growth (WANG, COPPER, & RONG, 1983).

This interpretation cannot be correct as setae (and their follicles) have always lain internal of the entire outer mantle lobe and, therefore, could not have been incorporated as appendages of the mantle itself. However, the persistence of fenestrae as canals suggests that they contained, temporarily at least, papillose outgrowths of the mantle. Moreover, the forward growth of lamellae to form by fusion complete, circular enclosures delineating fenestrae at the external surface indicate that these holes were filled in life with organic material. (There are no signs of perforated canopies or recrystallized primary shell.) Such material would have had to serve as a protective cover to any mantle extensions within the underlying canals. An obvious possibility is that the holes were filled with plugs of thickened periostracum, comparable with those closing the distal

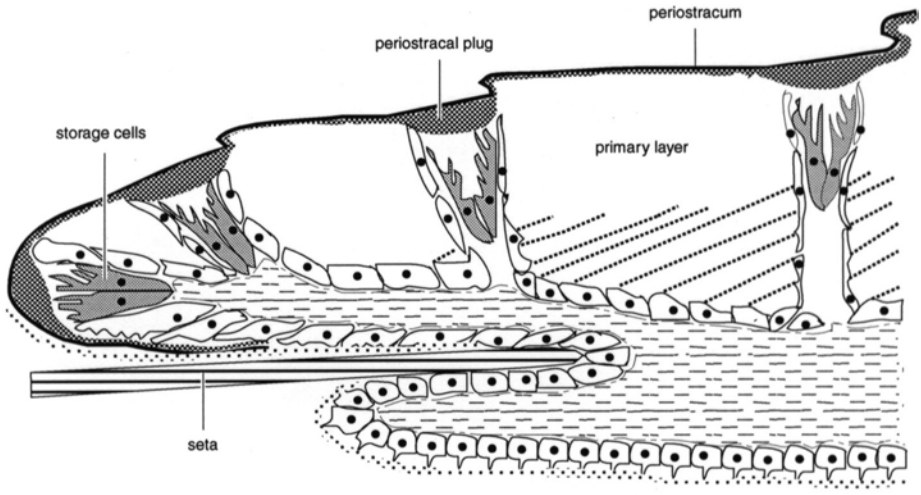

FIG. 260. Punctation in the atrypidine *P. (Punctatrypa) nalivkini* HAVLIČEK interpreted as repositories for storage cells, capped by plugs of infrastructural periostracum (new).

apertures of punctae in the cyclostomate bryozoan *Crisidia* (WILLIAMS, 1984), and were, therefore, true punctae (Fig. 260). It is noteworthy that living rhynchonellides, like *Notosaria,* differ from contemporaneous terebratulides in having a greatly thickened infrastructure of GAGs underlying the basal layer of the periostracum.

There is even a form of endopunctation that is not homologous with that of the terebratulides. The fibrous, secondary shells of the Carboniferous rhynchonellides, the Rhynchoporidae, are permeated by canals that do not penetrate the primary layer (Fig. 261). In *Tretorhynchia,* the canals, which are about 20 μm in diameter, end blindly just below a primary layer at least 30 μm thick (BRUNTON, 1971). The primary shell has been recrystallized, but there are no signs of perforations of any kind emanating from the distal ends of the canals. In any event, any organic contents of such endopunctae would not have been differentiated at the outer mantle lobe and could not have been more than columnar protuberances of outer epithelium. The rhynchonellide endopuncta was a short-lived phylogenetic novelty that may well be unique to the order.

The precise nature of punctation in orthide enteletidines is also unknown. Enteletidine shells are always permeated by punctae (Fig. 262), which usually fall within the same size range and commonly have the same disposition and funnel-shaped outline as terebratulide endopunctae. However, no perforated canopies have yet been found in enteletidines, and they are best referred to as punctae although their presence throughout the primary layer precludes any homology with rhynchonellide endopunctae.

The nature of dictyonellidine punctation is even more controversial. The network of rhombohedral to hexagonal ridges on the shell surface of *Dictyonella* itself normally defines deep cavities that connect with the interior by narrow canals. These composite structures have been interpreted as gross caeca; but the absence of such cavities in other genera has suggested that they were lined with periostracum and the caeca confined to the narrow proximal part of the structure (WILLIAMS, 1968a). However, it has now been shown (WRIGHT, 1981) that the pits of well-preserved *Dictyonella* are quite shallow, and their floors can be penetrated by up to nine fine canals. This suggests that the

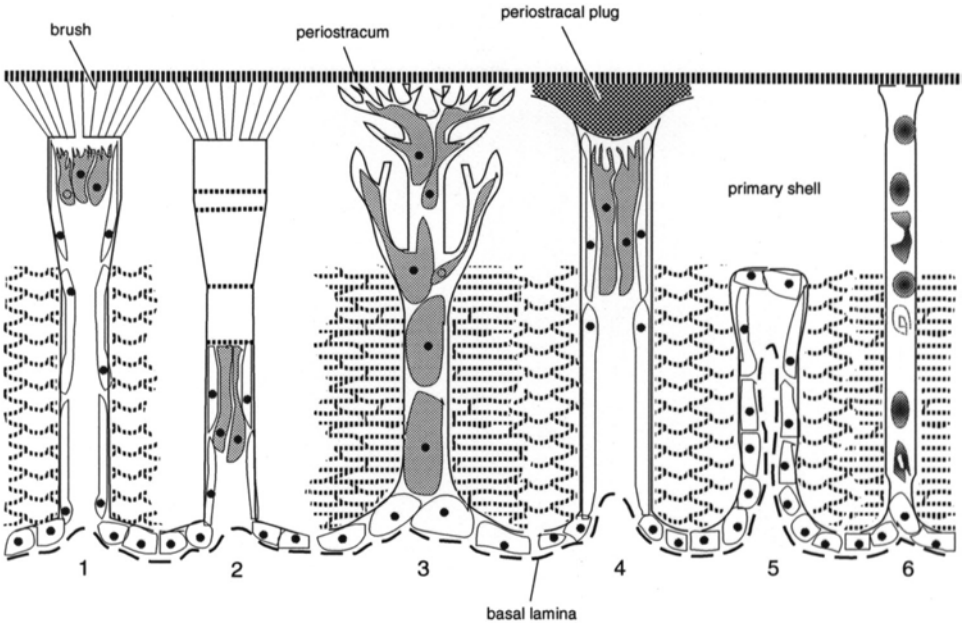

FIG. 261. Perforations of the brachiopod shell; *1–2,* canopied endopunctae with storage cells hanging distally in lumen or restricted to proximal locations by proteinaceous partitions in terebratulides and thecideidines respectively; *3,* branched puncta of cranioids perforating the entire shell, with storage cells throughout; *4,* puncta of atrypidine punctatrypids interpreted as having been plugged distally by a swelling of the infrastructural layer of the periostracum; *5,* endopuncta of the rhynchonellide rhynchoporids interpreted as originating at the primary-secondary shell boundary and therefore filled with cylindroid infolds of outer epithelium; *6,* canals of lingulids and discinids containing no extensions of the mantle, only secreted bodies (new).

canals contained branches of mantle outgrowths that converged centrally into large nodes more or less below the surface pits and that would form cavities in fossilized shells. The craniid puncta with its distal canopy of fine branches is a reasonably close model.

The many-branched canal systems of living *Neocrania* are certainly punctate in the strict sense as they terminate distally as finely divided branches more or less contiguous with the inner surface of the periostracum, to which they are connected by fibrils (Fig. 263). The fine branches are mainly restricted to the primary layer where they form a flat-topped arborescent zone because they coalesce within 50 μm of the periostracum into a series of relatively widely spaced trunks that, in turn, converge as the secondary shell thickens. Like terebratulide endopunctae, the canals accommodate storage outgrowths of the mantle, and the finest terminal branches (tubules) may indeed be long microvilli. Apart from having originated at the outer mantle lobe, however, they have little in common with endopunctae, must have evolved independently, and have always been characteristic of cranioids except for their suppression in the cemented ventral valve of the Paleozoic *Petrocrania* (Fig. 264).

Petrocrania, incidentally, is well known as a fossil that reproduced topographic details of its substrate on the external surface of the dorsal valve. The Ordovician *P. scabiosa,* which frequently settled on the strophomenide *Rafinesquina,* replicated the parvicostellate ornamentation of that stock with remarkable clarity. Three factors promoted such mimicry. First, the ventral valve was thin and lacked any thickened margin that would have elevated the dorsal mantle edge

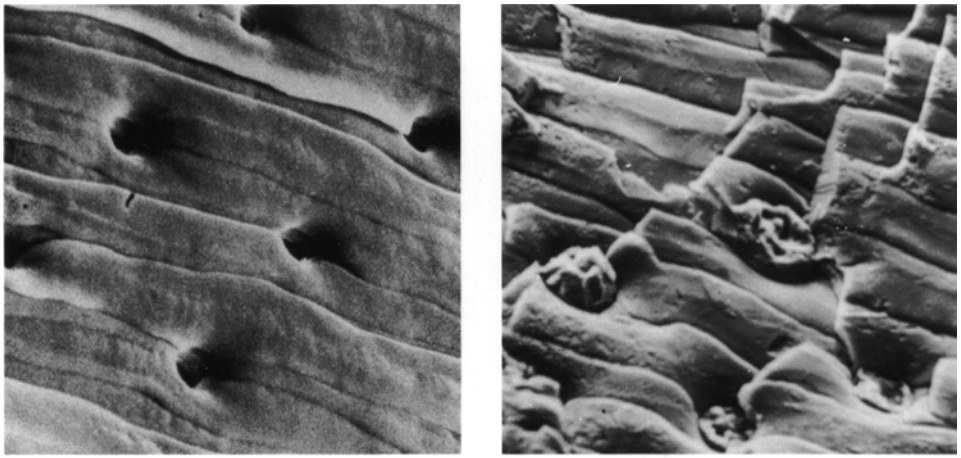

1 2

FIG. 262. Endopunctation in internal fracture surfaces showing the similarity between the endopunctate fibrous secondary shell of *1, Liothyrella neozelanica* THOMSON, ×1,600 (Williams, 1990) and *2,* of the enteletoid *Rhipidomella* sp., ×630 (new).

above the substrate. Second, the dorsal valve invariably overlapped the margin of the ventral valve. Third, in the absence of setae the subperiostracal layer at the margin of the dorsal valve must have constantly polymerized to form a cast of the substrate, over which it expanded (Fig. 264; WILLIAMS & WRIGHT, 1970).

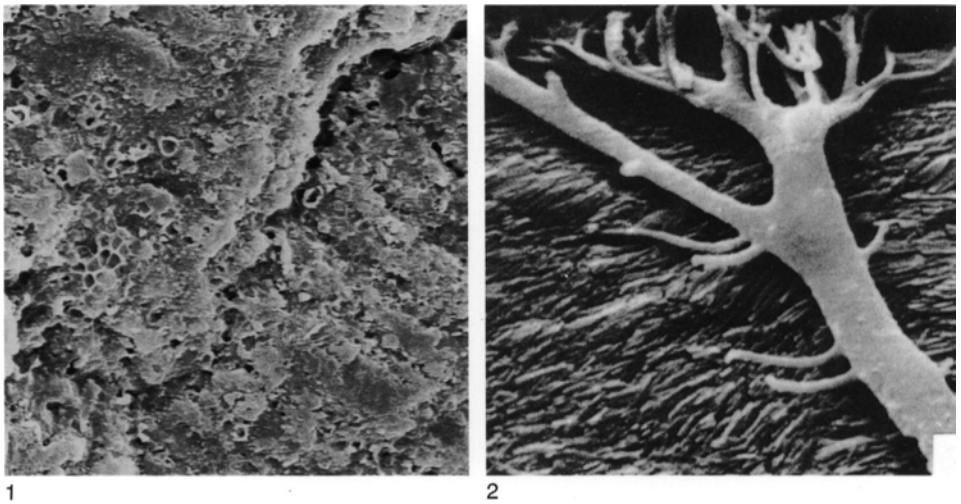

1 2

FIG. 263. Punctation of the cranioid *Neocrania anomala* (MÜLLER); *1,* external surface of the primary shell of a dorsal valve showing perforations (many with thickened organic surrounds) of the terminal branches of punctae, ×1,050 (new); *2,* section of the primary layer of a dorsal valve showing the main branches and tubules of a puncta filled with resin, ×2,600 (Williams & Wright, 1970).

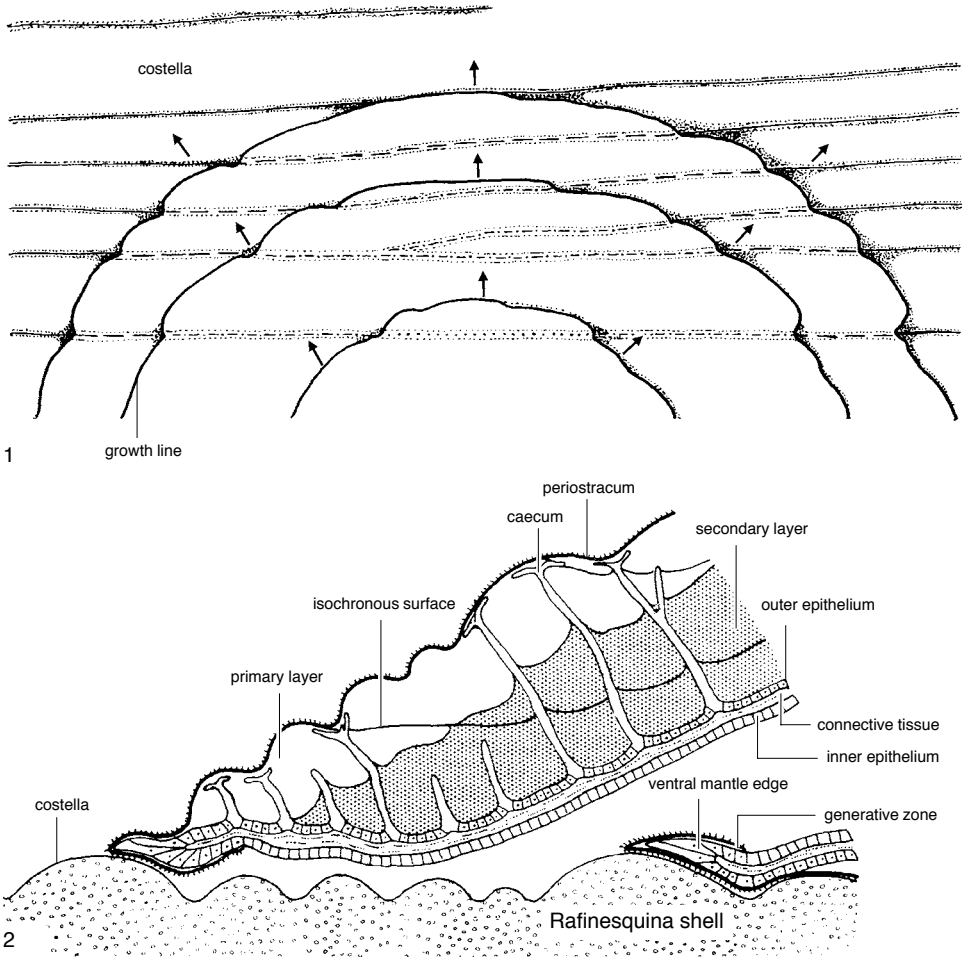

FIG. 264. *1,* Stylized external view and *2,* longitudinal section of the edge of the dorsal valve of the cranioid *Petrocrania scabiosa* (HALL) showing how details of substrate topography are reproduced on the dorsal external surface (Williams & Wright, 1970).

CANALS

The canals permeating the organophosphatic shell of living lingulids and discinids are fundamentally different from the punctation of calcitic-shelled brachiopods (Fig. 265.1–265.2). They are significantly finer with diameters ranging between 300 nm and 500 nm for *Discina* (WILLIAMS, MACKAY, & CUSACK, 1992) and between 180 nm and 850 nm (with bimodal peaks at 530 nm and 740 nm) for *Lingula* (WILLIAMS, CUSACK, & MACKAY, 1994). They contain only exocytosed materials and short extensions of apical plasmalemmas; and, although they are sporadically associated with recumbent cylindroid extensions and chambers several microns high, the protuberances of outer epthelium contained within these structures are not charged with storage vesicles as are caeca. Canals terminate with slightly expanded, flattened heads at the interface between the organic primary and biomineralized secondary layers of *Lingula*

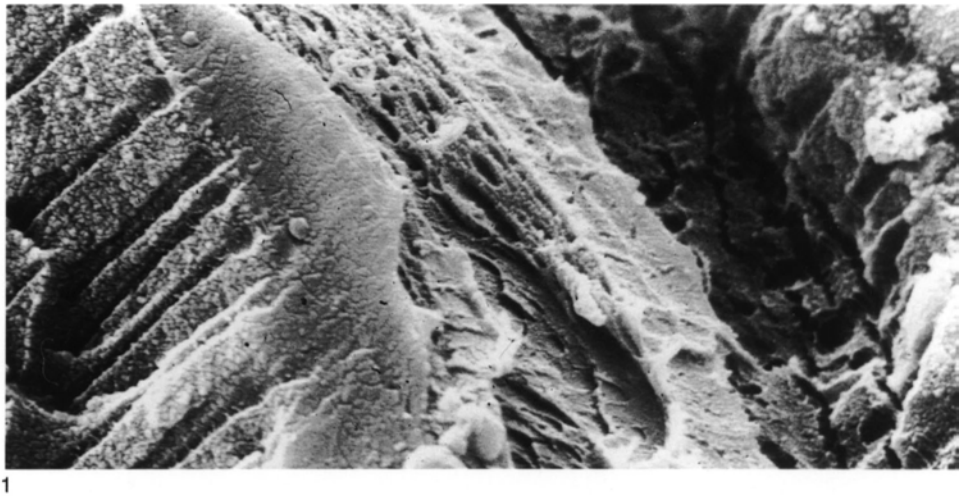

1

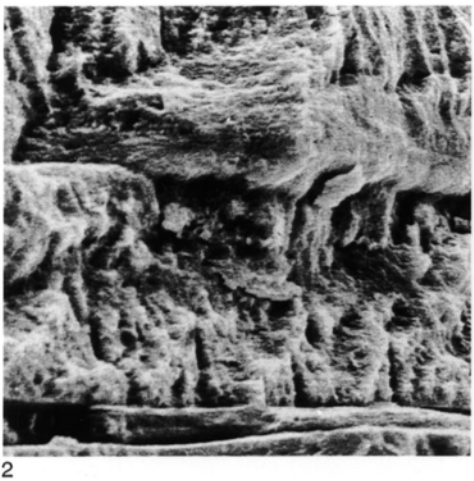

2

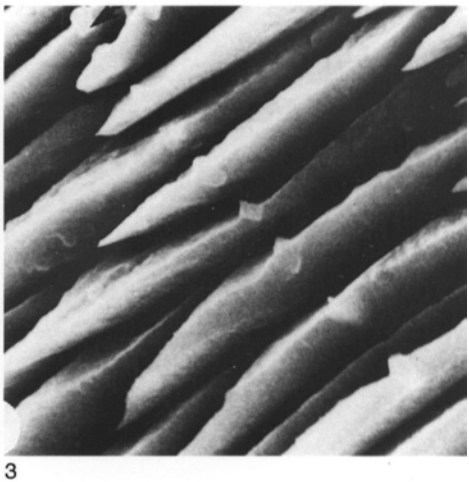

3

4

5

FIG. 265. *For explanation, see facing page.*

and in the narrow subperiostracal zone of GAGs terminating the mainly biomineralized primary layer of *Discina.* They are seldom (if ever) continuous throughout the secondary layer, as they are frequently interrupted especially, but not invariably, at intercalations of membranous laminae within successions. Canals also branch and, although they tend to be radially arranged at least in *Lingula,* the spacing can vary from 1 μm to 16 μm.

It is possible that this fine, canaliculate system is widely but sporadically developed among extinct organophosphatic groups. Thus they are found in acrotretoids but not in related spinose siphonotretoids (BIERNAT & WILLIAMS, 1971). However, the shell fabric of early Paleozoic stocks has not yet been comprehensively subjected to such studies as would reveal the existence and nature of these microscopic structures.

The only perforations in calcitic shells that are fine enough to be compared with lingulid canals are those found in late Mesozoic to recent endopunctate terebratulides and rarely in Silurian pseudopunctate plectambonitidines. The terebratulide micropunctae (GASPARD, 1978, 1982; SMIRNOVA & POPIEL-BARCZYK, 1991) occur in varying densities in terebratulids (Fig. 265.3), megathyrids, kraussinids, and some living terebratellids and range in diameter from 200 nm to 4 μm, significantly less than the 10 μm to 20 μm diameters of coexisting endopunctae. There is, however, some doubt about their true nature. Many figured micropunctae may vertically penetrate several fibers and their membranous sheaths without causing displacement of their biomineral-organic interfaces. If such canals represented the trails of impersistent strands secreted by outer epithelium, they would have been aligned with the long axes of fibers. Their vertical attitude should indicate that they originated at the outer mantle lobe and persisted in such a way as to cause thickening secondary shell to grow around them as it does around caeca. This is not so, and it is likely that at least some of the micropunctae are postmortem burrows of microorganisms comparable with those found by GASPARD (1989) infesting shells of recent terebratulides. The micropunctae of *Eoplectodonta,* on the other hand, are delineated by outwardly conical deflections of flattened, secondary fibers (BRUNTON, 1972) and are canaliculate (Fig. 265.4–265.5) although they have been formed like extropunctae.

PSEUDOPUNCTATION

Pseudopunctation is preeminently characteristic of the strophomenide shell. Even with a low-power light microscope, the secondary fabric of the great majority of strophomenides is clearly seen to be sharply crenulated by tight microscopic deflections. Yet pseudopunctation, initially interpreted as calcified punctation (CARPENTER, 1851), was not understood until it was shown to be conical puckerings of the shell fabric, which normally contain indigenous rods of calcite (taleolae) (KOZLOWSKI, 1929; WILLIAMS, 1956).

In its typical form, a pseudopuncta consists of a slightly arcuate, anteriorly inclined trail of cone-in-cone deflections affecting the entire secondary laminar (or fibrous) fabric and emerging at the internal surface of the valve as a tubercle (Fig. 266.1–266.2). The arcuate trace and inclination of a pseudopuncta are growth effects resulting from the mantle having been pushed outward radially in response to the thickening of the secondary shell and the marginal expansion of the

FIG. 265. Various fine perforations of the brachiopod shell; *1,* section across the interface between shell and mantle (top right-hand corner) of critical-point dried dorsal valve of the discinoid *Discina striata* (SCHUMACHER) showing the disposition of canals with exposed bases perforating stratified laminae, ×6,000; *2,* fracture section of the shell of *Lingula anatina* (LAMARCK) showing canals impersistently crossing laminae, ×1,400 (new); *3,* etched, resin-impregnated section of the secondary shell of *Sellithyris cenomanensis* GASPARD showing a micropuncta perforating a succession of fibers, ×4,000 (Gaspard, 1990); *4–5,* exfoliated internal surfaces of the secondary shell of the Silurian *Eoplectodonta transversalis* (WAHLENBERG) showing *4,* a general view of a micropuncta (at tip of *white arrow*), ×250 and *5,* a detail of the surface showing the externally deflected conical surround of a micropuncta, ×1,200 (Brunton, 1972).

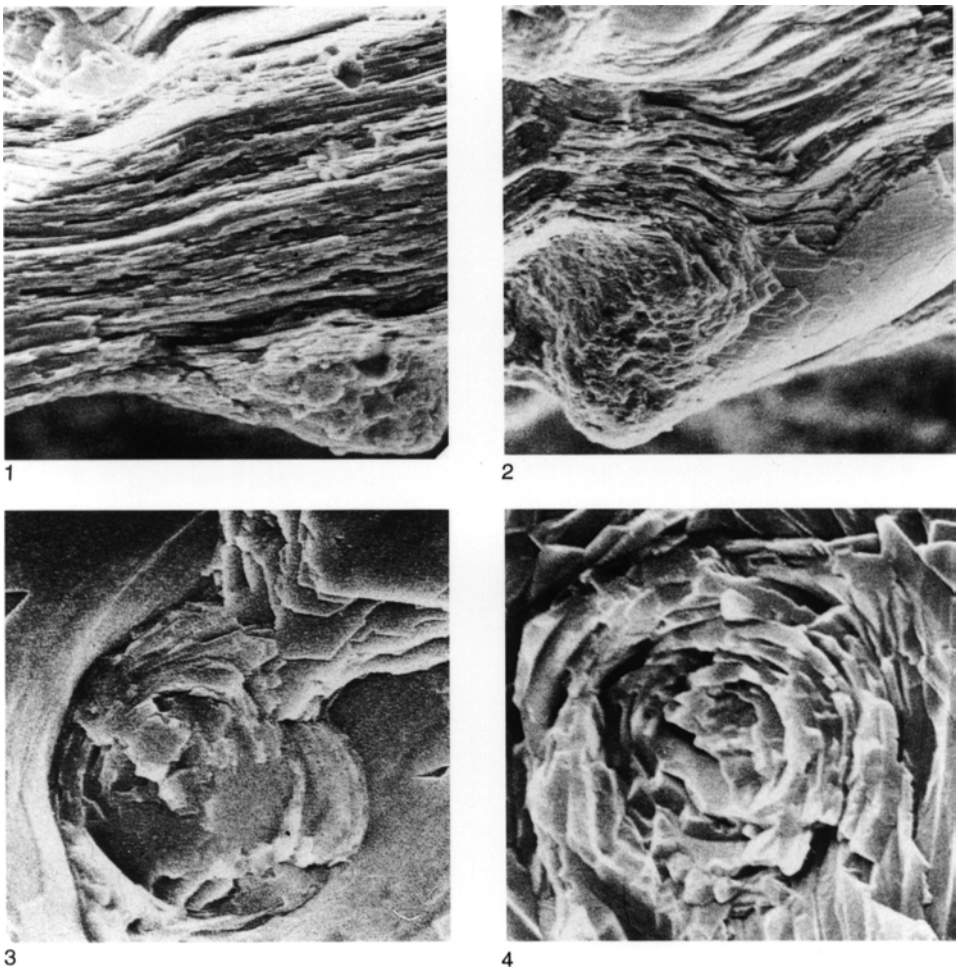

FIG. 266. Pseudopunctation in the laminar secondary shell of strophomenides; *1–3,* fracture sections and internal fracture surface of a ventral valve of the orthotetidine *Apsocalymma shiellsi* MCINTOSH showing *1–2,* the pseudopunctae indenting laminar surfaces and forming tubercles toward the tops and bottoms of micrographs, respectively, ×370, ×570, and *3,* an external view of a pseudopunctate core of obliquely and spirally arranged laminae, ×1,500; *4,* detail of a pseudopunctate core of spirally inclined laminae in ventral valve of *Strophomena planumbona* (HALL), ×3,000 (Williams & Brunton, 1993).

valve. Consequently a pseudopuncta is characteristically asymmetrical in longitudinal section with constituent laminae (or fibers) of the secondary shell deflected inwardly and inclined along the anterior and posterior sides of the pseudopuncta at narrowly and widely acute angles respectively. Pseudopunctae are usually hexagonally closely packed in varying densities (between 25 to 30 per mm^2 in orthotetids) and vary greatly in diameter as measured across all deflected laminae (or fibers) involved in their definition (rosettes).

There are two kinds of pseudopunctae (WILLIAMS & ROWELL, 1965b; MANANKOV, 1979). In orthotetidines and early strophomenoids, pseudopunctae consist exclusively of rosettes of conically disposed laminae. In

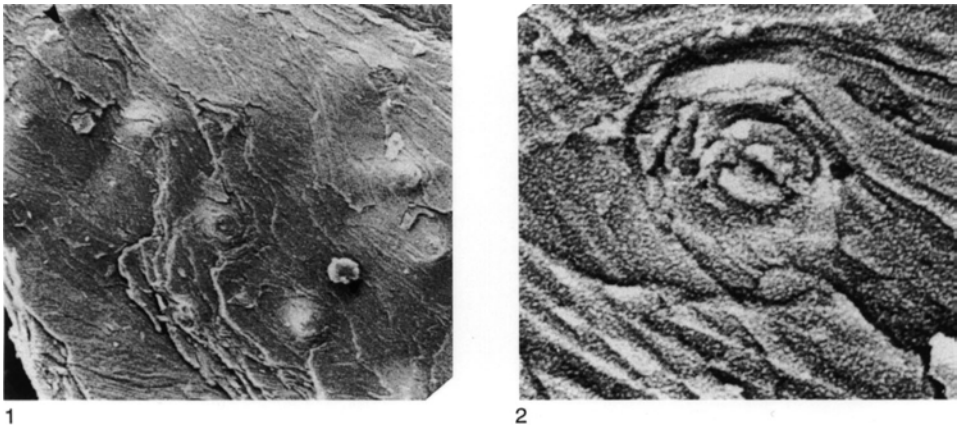

FIG. 267. Origin of orthotetidine pseudopunctation; *1,* general view (X170) and *2,* detail (X2,340) of internal surface of a fragment of the secondary shell of *Fardenia scotica* LAMONT showing incipient pseudopunctae breaking through cross-bladed laminae in spirally disposed arrangements (Williams & Brunton, 1993).

orthotetids up to 20 or so laminae can form a concentric layering (up to 50 μm across) with gently convex tops (tubercle) around a core (about 20 μm) of solid calcite or of tilted fragments of discrete laminar sets (Fig. 266.3). Well-preserved tubercles are completely covered by domed laminae that seem to have been unbroken in the original state. Arrays of these domed cones have been traced throughout shells along sinuous paths about 40 μm wide with cores consisting of amalgamated domes of successive laminar cones. The pseudopunctae of Ordovician strophomenoids (Fig. 266.4) are identical in structure with tilted blocks of laminae forming cores that, in *Rafinesquina,* can be 50 μm in diameter within rosettes about three times as big. Differentially preserved exteriors of *Strophomena,* which has radially disposed rosettes about 40 μm in diameter, reveal the nature of the first-formed parts of pseudopunctae. Interspatial depressions and pseudopunctate cores aligned within them are lined with granular primary shell, while cores of pseudopunctae exposed in the exfoliated crests of costellae consist of obliquely stacked, laminar blocks. In effect strophomenid pseudopunctae originated on a thin primary layer, probably in the same manner as those of *Fardenia* (WILLIAMS & BRUNTON, 1993).

The cross-bladed, laminar fabric of the Ordovician orthotetidine *Fardenia* is impunctate; but exceptionally shallow immature pseudopunctae develop (Fig. 267). The rosettes of these pseudopunctae are seldom more than 40 μm across with cores (about 10 μm in diameter) encircled by fewer than seven laminae. The core of one immature pseudopuncta was composed of two spirally continuous laminae inclined toward a central slit. The most likely way for this arrangement to have arisen would have been for a cell about 5 μm across to have started secreting on an interlaminar membrane fibrillar proteins (or filaments) connected by hemidesmosomes and to have continued to do so at a faster rate than the deposition of laminae by surrounding cells. These rapidly lengthening filaments would, in turn, have caused adjacent cells to secrete laminae in a steeply inclined coil around the strands to form the biomineralized core of the growing pseudopuncta (Fig. 268). From time to time the process would have been brought to a halt by cessation of secretion of the strand. This would account for tubercles being capped by entire as well as perforated domes and would

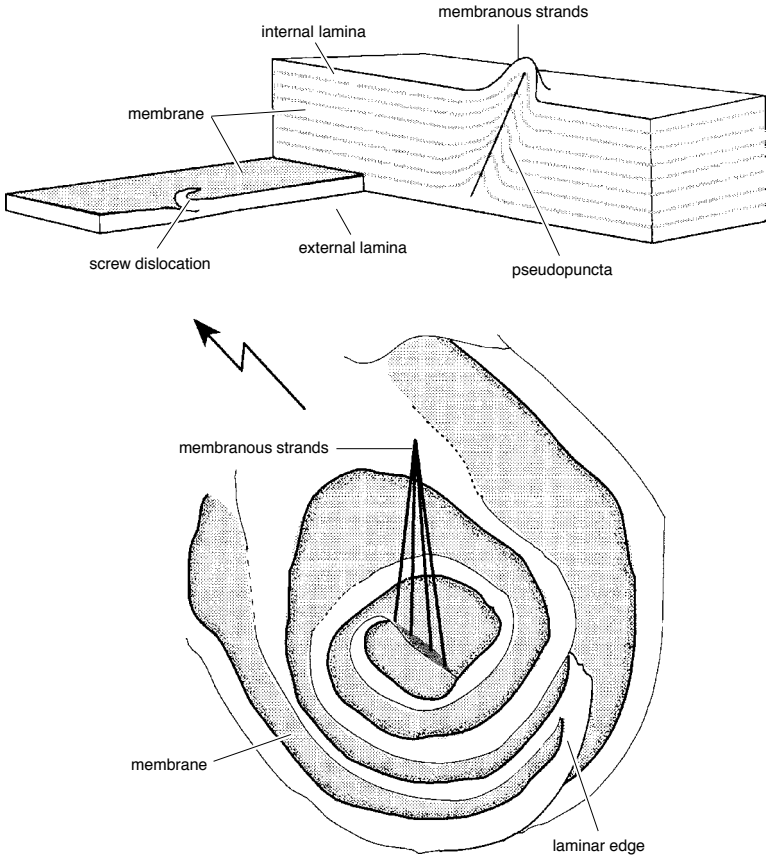

FIG. 268. Diagrammatic reconstruction of the origin and essential structure of a pseudopuncta, based on those found on internal laminae of *Fardenia scotica* LAMONT (see also Fig. 267) (Williams & Brunton, 1993).

not have precluded the growth of succeeding pseudopunctae on the same sites and at new loci.

The other kind of pseudopuncta, which is characteristic of plectambonitoids (Fig. 269.1), chonetidines, productidines, and oldhaminidines (Fig. 269.2), and such strophomenoids as leptaenids (Fig. 270) and stropheodontids, has a distinctive rod of calcite (taleola) at the core of a tubercle with a rosette of conically disposed laminae (or fibers in plectambonitoids). Thus the pseudopunctae of the Carboniferous leptaenid *Leptagonia* (Fig. 270) consist of rosettes of inwardly inclined laminae 75 μm or more in diameter grouped around taleolae (up to 30 μm across). A taleola is fully developed and differentiated from the fabric of its host shell when first formed, and its distinctiveness is further emphasized by the way its surface is a calcified patina that is sharply separated from the surrounding laminae. The most striking difference, however, between taleolae and the laminar infills of orthotetid pseudopunctae is brought out by the porous structure of etched taleolae. The pits of this porous fabric are commonly delineated by rhombohedral planes but are clearly part of an interlacing series of canals (up to 300 nm in diameter) permeating the entire structure. This suggests that a taleola, *in vivo,* consisted of a calcitic mesh permeated by intercon-

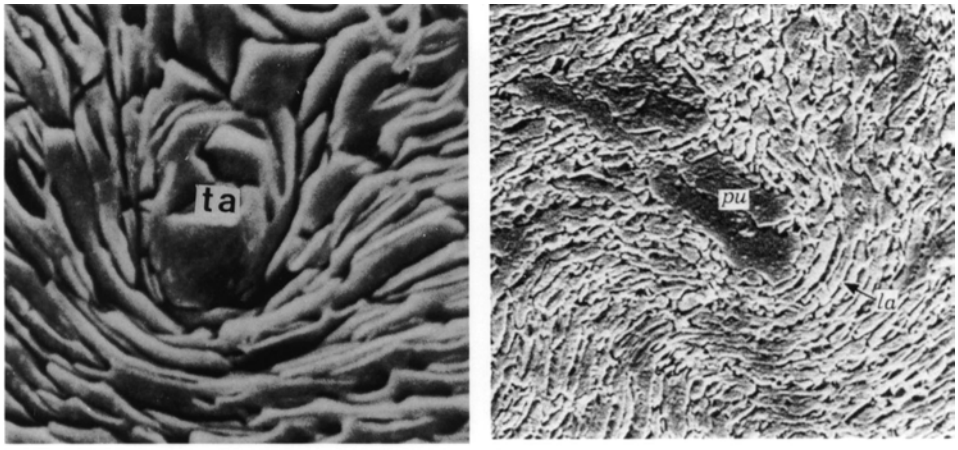

FIG. 269. Pseudopunctation in shell sections; *1,* transverse view of a taleola (*ta*) within the fibrous secondary shell of the plectambonitoid *Sowerbyella variabilis* COOPER, ×1,400 (Williams, 1990); *2,* outwardly directed pseudopuncta (*pu*) in a laminar (*la*), secondary shelled dorsal valve of the lyttonioid (oldhaminidine) *Leptodus* cf. *richthofeni* KAYSER, ×1,200 (Williams, 1973).

nected tunnels that were filled with organic materials and that it was probably bounded by a membrane continuous with those between the calcitic components of the laminar succession (WILLIAMS & BRUNTON, 1993).

The phylogenetic relationship between pseudopunctae with or without taleolae has yet to be determined. Both kinds have been reported in the same shells of many species. But in view of the subtle, albeit fundamental, difference between taleolar and amalgamated laminar cores there is abundant opportunity for misidentification. Pseudopunctae lacking taleolae are certainly homoplastic, having appeared independently on at least three occasions among the gonambonitoids, early strophomenoids, and orthotetidines. This is not surprising if such pseudopunctae represented spiral perpetuations of screw dislocations on sheeted secondary shell. However, pseudopunctae with taleolae also appear to be homoplastic, for even if the chonetidines and productidines inherited their taleolar shells from a plectambonitoid stem group, leptaenids and strophedontids are unlikely to have derived their taleolae from the same source.

This potential for microtextural homoplasy is endorsed by the extraordinary condition of the shell of orthotetidine schuchertelloids (Fig. 271.3–271.4), the fabric of which is crenulated by arrays of asymmetrical, conical deflections invariably pointing externally (THOMAS, 1958). In *Schuchertella* and *Streptorhynchus,* these externally directed deflections (extropunctae) (WILLIAMS & BRUNTON, 1993) are densely arranged more or less radially at about 150 per mm^2. On internal, exfoliated surfaces, mature extropunctae form shallow craters about 50 μm in diameter bounded by up to ten laminar sets arranged concentrically around elliptical cores (4 to 5 μm in maximum diameter) and usually with a medial slot. Exceptionally a single lamina lines part of the crater sides and merges with the core as a spirally twisted band with a medial slot. On exfoliated external surfaces extropunctae occur as low domes up to 30 μm across that consist of successions of curved laminae in rosettes surrounding cores of oblique or twisted plates, some with medial slots.

The laminar cores of extropunctae preclude any homology with punctae like those

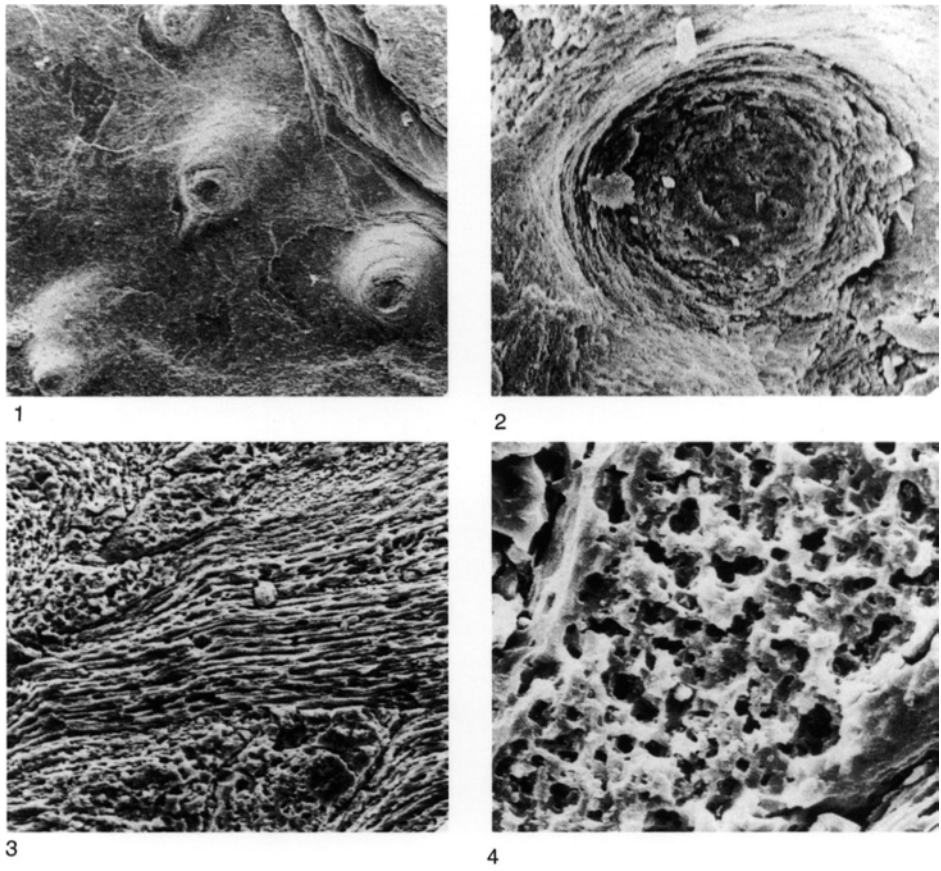

FIG. 270. Pseudopunctation in the leptaenid *Leptagonia caledonica* BRAND; *1,* general view of tubercles with taleolar cores on internal surface of ventral valve, ×85; *2,* external view of transverse fracture section of pseudopuncta with roughened, pock-marked surface to taleolar core, ×400; *3,* general view and *4,* detail of section of a ventral valve showing disposition of laminae around taleolae (exterior toward the top), fully developed taleolar base secreted unconformably on horizontal laminae (bottom right-hand corner of *3*), ×350, and canal system within taleola of *4,* ×1,450 (Williams & Brunton, 1993).

in the laminar-shelled craniids, but they are much the same as those of pseudopunctae lacking taleolae. Accordingly the reversed orientation of deflection of the rosettes could be attributed to different rates of secretion of the organic components of the cores. More slowly growing so-called keratin filaments may have been the dominant constituent in extropunctae compared with rapidly secreted strands of proteinaceous membranes in pseudopunctae.

The function of pseudopunctae (with or without taleolae) and extropunctae is contentious. Internal tubercles or indentations associated with all three kinds of conical deflections of shell fabric can be partly or entirely capped by laminae (or fibers) that signalled a termination of the growth of these structures. Pseudopunctae and extropunctae, however, can normally be traced through a shell and show little or no branching. This and the prospect that taleolae had an organocalcitic composition comparable with that of muscle scar bases affirm the view that the main function of both kinds of pseudopunctae and extropunctae was to pro-

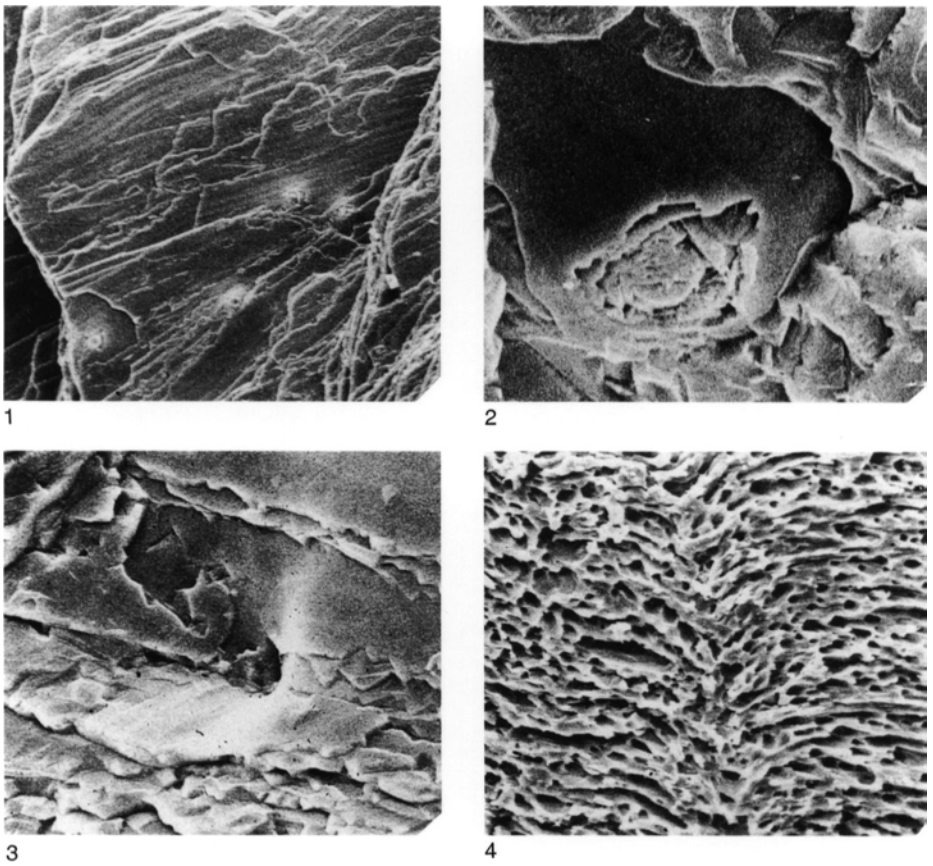

FIG. 271. Extropunctation in the orthotetidine *Schuchertella lens* (WHITE); *1,* external surface of fragment of laminar secondary shell in general view, ×230, and *2,* in detail to show an extropuncta, ×2,100; *3,* internal surface of laminar secondary shell showing the conical depression of an extropuncta delineated by spirally disposed laminae, ×980; *4,* etched section of a dorsal valve with conical deflections of an extropuncta directed toward the exterior below the lower edge of the micrograph, ×470 (Williams & Brunton, 1993).

vide holdfasts (Fig. 272) for mantle filaments (WILLIAMS, 1956) with rosettes, irrespective of the direction of deflection, additionally acting as rivets joining finely sheeted successions as friable as those of the strophe odontid *Pholidostrophia* (WILLIAMS, 1953). It has also been suggested that tubercles, especially those with taleolar cores, were the bases of transmantle muscle fibers operating fimbriae that sieved and conducted the flow of water in the mantle cavity (GRANT, 1968; MANANKOV, 1979). In view of the strongly ciliated nature of the inner epithelium lining the mantle cavities of all living brachiopods, fimbriae would seem to be superfluous to the hydrodynamic requirements of strophomenides. Indeed, the internal development of pseudopunctae in some stocks seems to confirm this conclusion.

Acceleration in the apical growth of pseudopunctae continually resulted in the prolongation of their tubercles into sharp cones or even spines (endospines) on the valve interiors. They are especially well developed in productidines and are commonly disposed in fringes along subperipheral rims where they could have functioned as straining or filtering systems (see Fig. 308).

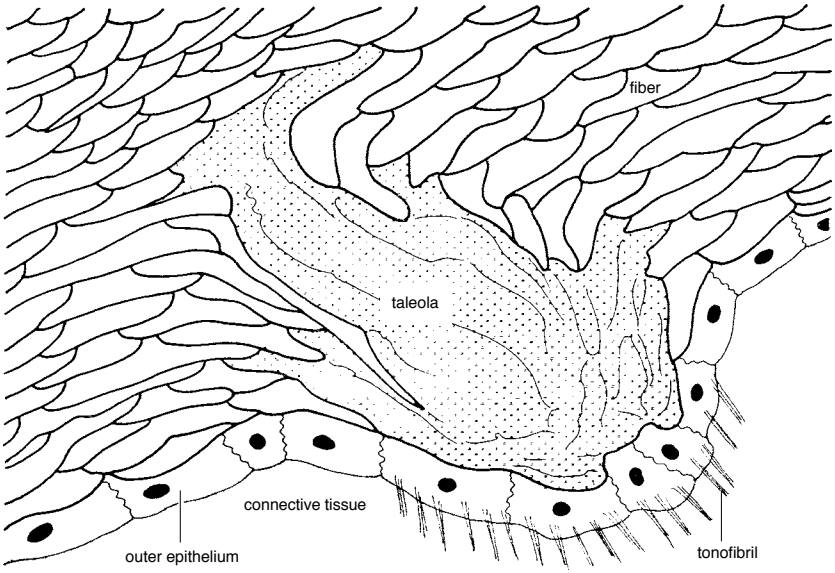

FIG. 272. Stylized oblique longitudinal section of a taleola deflecting the fiber of the secondary shell of the plectambonitoid *Sowerbyella* and showing its inferred relationship with secreting outer epithelium (Williams, 1968a).

The most extraordinary development of endospines, however, is found in productidine richthofenioids. In this group, the lidlike dorsal valve lies well within a subperipheral ring of endospines in the ventral valve, which grew centripetally. In many species these spines branched and amalgamated to form a complete net (coscinidium) over the opening of the ventral valve and may even have been elaborated into a regular honeycombed meshwork forming a high dome (*Sextropoma*). Such structures must have been enclosed in mantle (Fig. 273) so that a net would have been formed by the fusion of outer epithelium along zones of contiguity between converging struts. In this arrangement the inner epithelium would have been the outermost coat of the coscinidium and would, therefore, have been more exposed to the environment than it would have as a lining of the mantle cavity. However, judging from the mantle edge of such living brachiopods as *Terebratulina* and *Lingula,* the inner epithelium of a coscinidium was probably equipped with strongly developed cilia (which would have facilitated the circulation of sea water in the shell) and protected by a thick glycocalyx with a bounding pellicle.

INTERNAL TUBERCLES

Internal tubercles secreted within evaginations of the outer epithelium and serving as attachment sites for soft parts occur in other articulated brachiopods, notably the thecideidines and terebratulides. However, microscopic whorls of fibers are common features of the secondary layer of many species (Fig. 274.1) and are probably precursory to tubercles, like those found in the thecideidine *Bactrynium* (Fig. 274.2).

The infrastructure of thecideidine tubercles is much like that of pseudopunctae. In the Jurassic *Mimikonstantia,* which has a sheet of secondary shell, tubercles of the dorsal valve are composed of inwardly directed rosettes of fibers with cylindroid cores indistinguishable from the fabric of the primary layer, from which they arise more or less vertically (Fig. 274–275). Tubercles of the ventral valve, on the other hand, lie almost parallel with the internal surface and also have granular cores (Fig. 276; BAKER & ELSTON, 1984). In *Thecospira* no structural

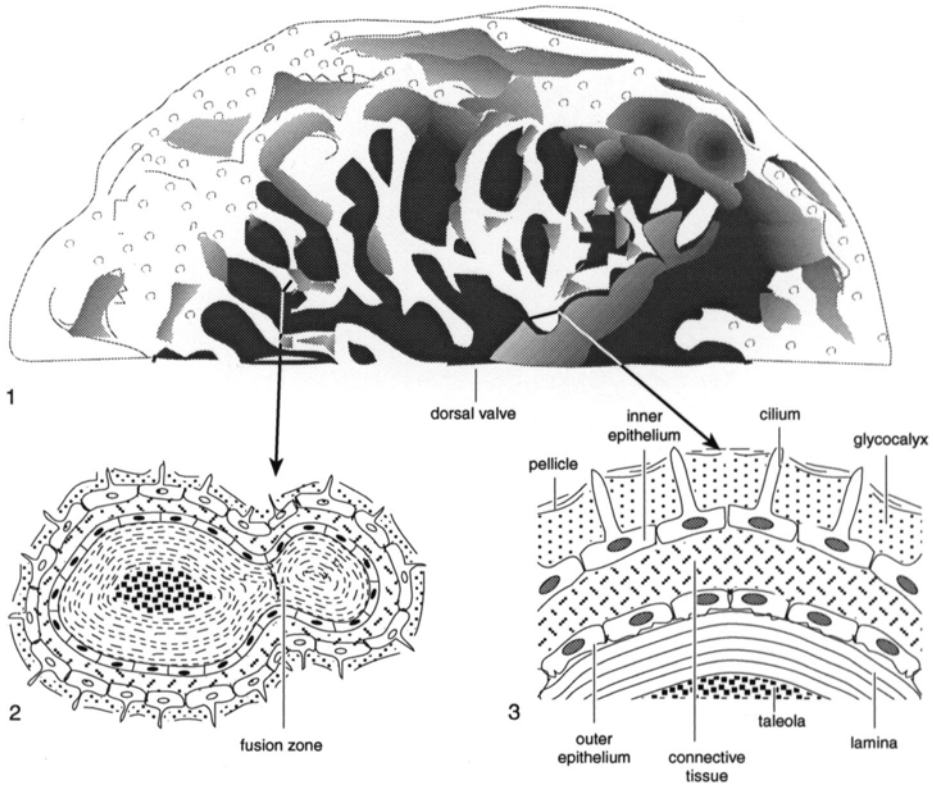

FIG. 273. Richthofenioid coscinidium; *1,* diagrammatic external view of part of a coscinidium of *Cyclacantharia* COOPER & GRANT, approximately ×4.6; *2,* inferred fusion of endospine (with taleolar core) and a lateral branch of an adjacent endospine; *3,* transverse section through the inferred mantle cover of a main strut (with taleolar core) (new).

differentiation of tubercles has been reported (BENIGNI & FERLIGA, 1988). All tubercles of both valves have well-developed cores (about 50 μm in diameter) enclosed by rosettes of fibers of the secondary shell, which are deflected inwardly. The cores are composed of irregular calcite crystals with no preferred orientation. They are continuous with a primary layer of the same fabric, which has probably been affected by recrystallization. Some parts of cores appear to incorporate bits of contiguous fibers and, in that respect, are unlike true taleolae.

Thecideidine tubercles are structurally and functionally different from strophomenide pseudopunctae in several respects. In particular, tubercles are not uniformly distributed over valve interiors but are mainly concentrated within subperipheral rims of valves where they support mantle margins. Accordingly, at those stages in shell growth entailing migration of the shell and mantle margins, mature tubercles undergo resorption (WILLIAMS, 1968a; BAKER, 1970a). Moreover the development of nonfibrous cores in tubercles is essentially an early stage in the neotenous shedding of a fibrous secondary shell. In living *Thecidellina,* with nothing more than vestiges of secondary shell, tubercles are composed almost entirely of splayed acicular crystallites of calcite (Fig. 275.2) and are only morphologically distinguishable from the rest of the primary shell, as any associated secondary fibers are restricted to small groups of 20 or so capping some tubercles (WILLIAMS, 1973).

The internal tubercles of terebratelloid kraussinids and megathyrids are homologous

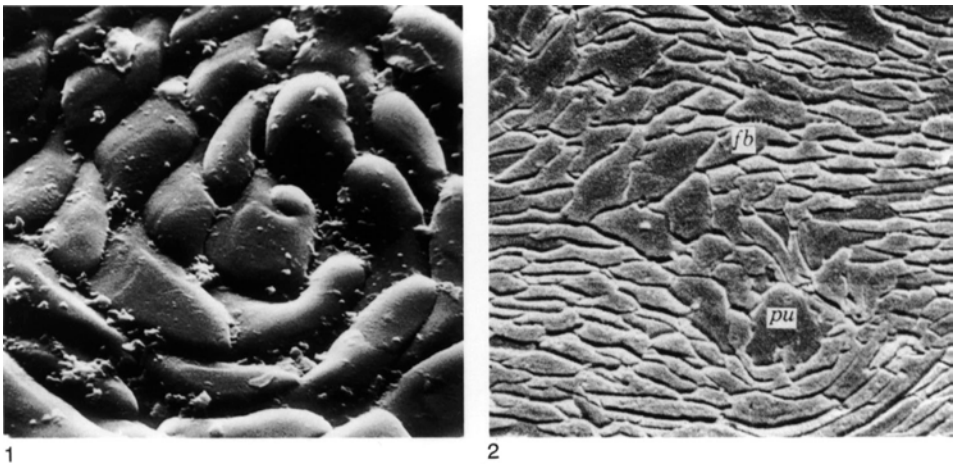

FIG. 274. Internal microstructures; *1,* whorl of fibers on the internal surface of the secondary shell of the rhynchonellide *Hemithiris psittacea* (GMELIN), ×1,200 (new); *2,* tubercle (*pu*) in the fibrous (*fb*) secondary shell of a ventral valve of the thecideidine *Bactrynium emmrichii* (GÜMBEL), ×1,100 (Williams, 1973).

with thecideidine thecospiroids. They consist of inwardly deflected rosettes of fibers that may exceed 100 μm in diameter. Fibers may become larger at the cores of tubercles and may even be replaced locally by a crystalline fabric (SMIRNOVA & POPIEL-BARCZYK, 1991). Like thecideidine tubercles, they are mainly concentrated as subperipheral rims and are also subject to resorption during the outward migration of the shell and mantle margins.

SHELL DAMAGE AND REPAIR

Apart from changes arising from the normal processes of secretion and growth, the brachiopod shell can also record permanent

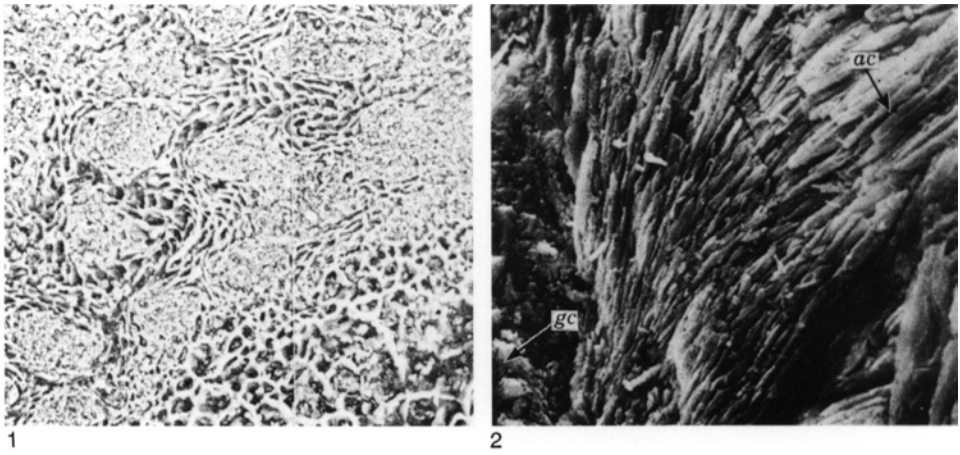

FIG. 275. Thecideidine tubercles; *1,* section of the subperipheral rim of *Mimikonstantia sculpta* BAKER & ELSTON showing transverse sections of tubercles of granular primary shell associated with secondary fibrous shell, ×250 (Baker & Elston, 1984); *2,* fractured edge of dorsal valve of *Thecidellina barretti* (DAVIDSON) showing acicular crystallites (*ac*) and granular calcite (*gc*) within a tubercle of primary shell, ×1,400 (Williams, 1973).

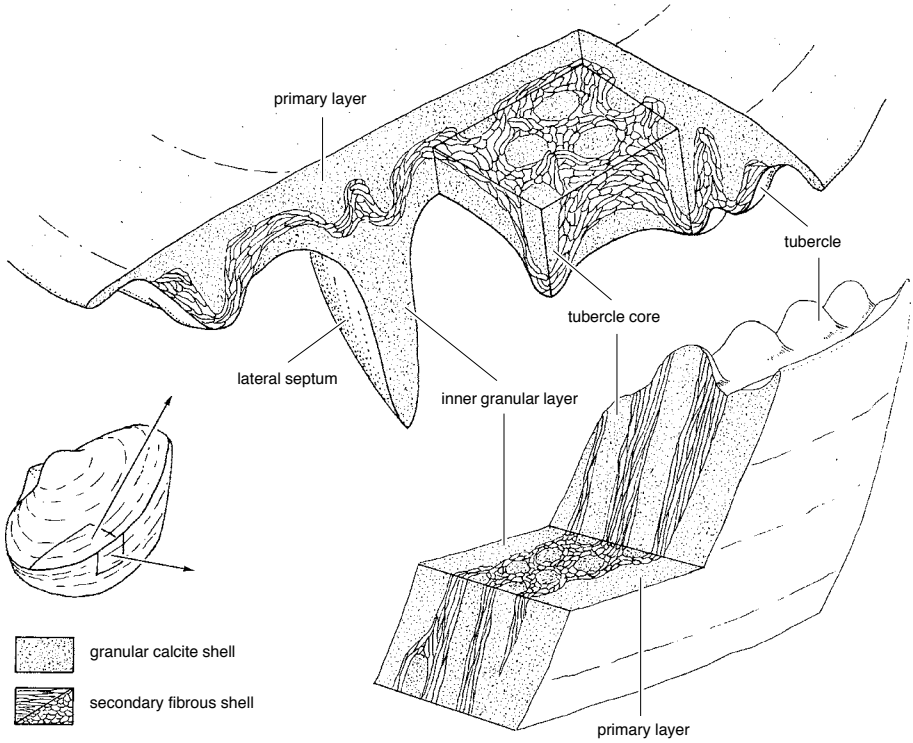

FIG. 276. Diagrammatic reconstruction of the shell microstructure of the thecideidine *Mimikonstantia sculpta* BAKER & ELSTON showing the disposition of tubercles in the dorsal valve (top) and in the ventral valve (bottom right) (Baker & Elston, 1984).

damage from an extraneous source such as fractures and other malformations on surfaces and within the fabrics of fossil and living shells. Repair involves reversions or accelerations in the secretory regimes of mantles, which themselves are usually undergoing regeneration. A higher organic content renders organophosphatic shells more plastic than the brittle calcitic shells, and this difference is evident even in damage by fracture. A repaired zone of damage extended for about 200 μm on the surface of a valve of the Cambrian acrotretoid *Prototreta.* Within this zone two sets of slitlike indentations disrupted ten fila. One set of gashes is feasibly interpreted as a fracture in the living shell, the other, an en echelon set, as tension gashes (Fig. 277). Both sets are consistent with having been formed in a lateral shear zone, parallel with the trace of tissue undergoing repair. Some of the tension gashes are associated with minute folds superimposed on fila. The folds are also consistent with the assumed stress fields but could not have been formed in brittle shells (WILLIAMS & HOLMER, 1992).

The sequence of repair of fractures in organophosphatic shells that are deep enough to expose the underlying outer epithelium has been described for living *Glottidia* (PAN & WATABE, 1989). Within the fracture zone, any shell debris is phagocytized by amoebocytes and partly released into a mantle canal(s). Concurrently the cuboidal epithelial cells at the fracture site become columnar and assume the characteristics of vesicular cells secreting periostracum at the outer mantle lobe. At the fracture site, the reverted cells secrete a sheetlike pellicle covering the exterior and then an inner layer that, in due course, differentiates into a normal

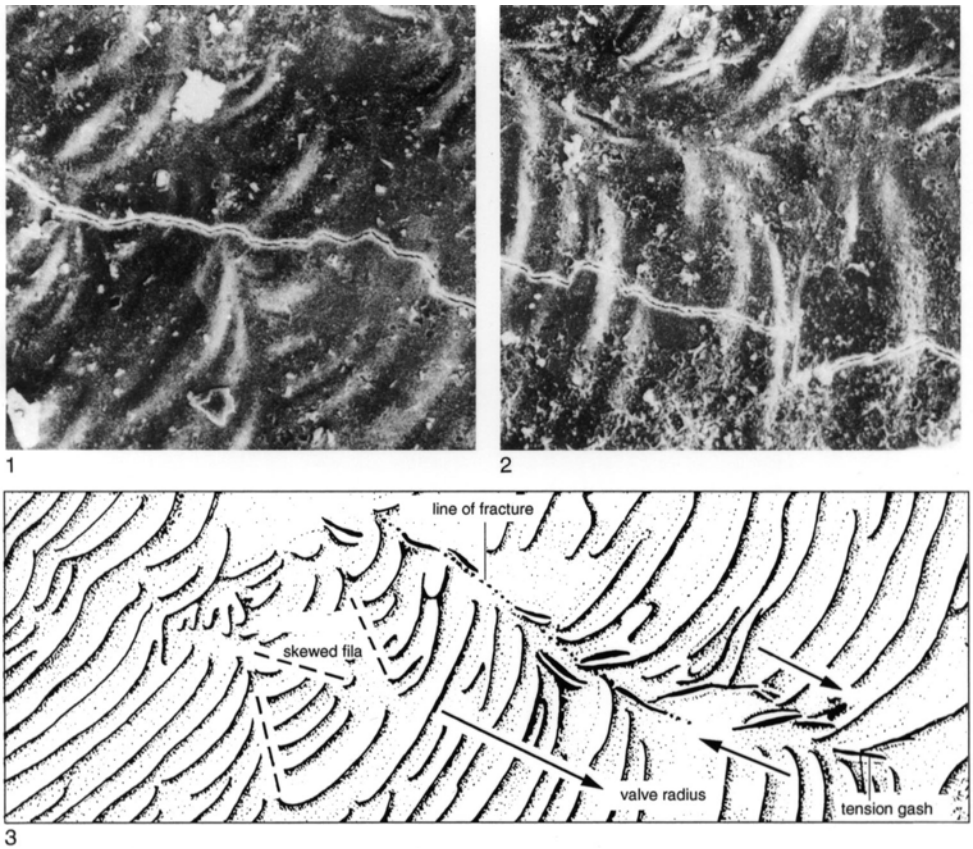

FIG. 277. Repaired shell of the acrotretoid *Prototreta* sp.; *1–2,* malformed drapes of fila on the exterior of a dorsal valve with tension gashes and associated minor folding, ×350 and approximately ×350; *3,* reconstruction of the line of fracture induced by the inferred stress couple, ×350 (Williams & Holmer, 1992).

periostracum. Within 90 days of fracture the cells revert once more to a cuboidal shape and start secreting a biomineralized primary layer followed by inner secondary shell.

The nature and repair of fractures at the surfaces of brittle calcitic shells are better understood in relation to disruptions of radial ornamentation in finely costellate shells like that of the strophomenid *Rafinesquina* (WILLIAMS & ROWELL, 1965b, p. 74). When injury to part of the mantle edge was severe enough to impede forward growth, the space anterior to the zone of damage became constricted and was ultimately sealed off by the encroachment and fusion of the flanking unaffected parts, which thereby restored a fully functional and continuous mantle edge. Such encroachment involved an abnormal proliferation of tissue toward the area of injury, as is shown by the increased number of costellae given off to converge in that direction. Concomitantly, the space immediately in front of the damaged part of the mantle edge became closed by outer epithelium, which originated behind the flanking parts of the mantle edge as they moved forward and was responsible for the deposition of unribbed shell, presumably beneath a newly secreted cover of periostracum in a sequence like that effecting repair of the *Glottidia* shell (Fig. 278).

The sequence of repair of damaged fabric of calcitic shells can be determined by studying the effects of mantle retraction, which may be periodic and genetically controlled or randomly induced by extraneous agencies.

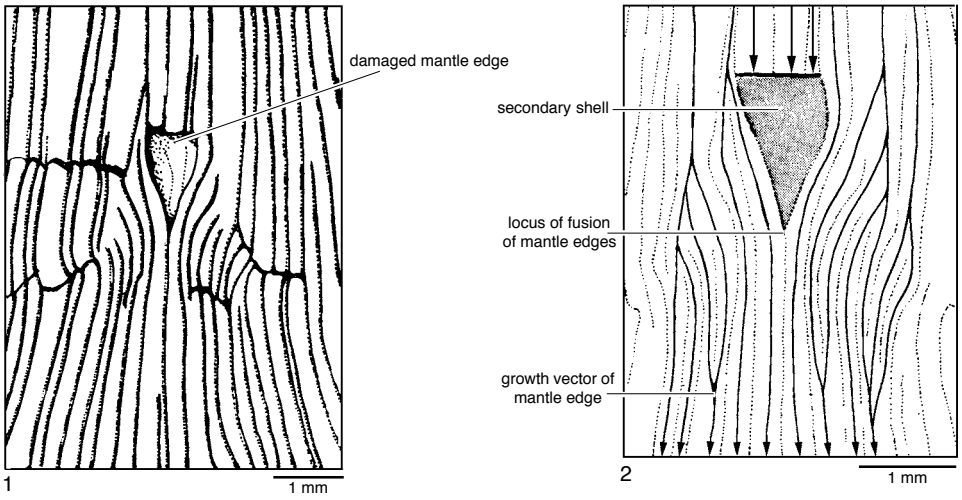

FIG. 278. Shell repair in the strophomenide *Rafinesquina nasuta* (CONRAD) showing *1,* inferred relationships of area of repair, with *2,* undamaged growing mantle edges (Williams & Rowell, 1965b).

The former are responsible for surface ornamentation and are not considered in this section. The latter can cause disruptions of the secondary shell, which trigger a distinctive sequence of secretory repair (WILLIAMS, 1971a).

In the living, impunctate rhynchonellide *Notosaria,* a violent retraction of the mantle causes an abrupt termination of all secretion within the affected part of the shell (Fig. 279–280). As soon as retreat (regression) has ended, selective deposition begins. Cells must readjust to resume secretion at new sites because those parts of apical plasmalemmas responsible for carbonate secretion start depositing calcitic pads in continuity

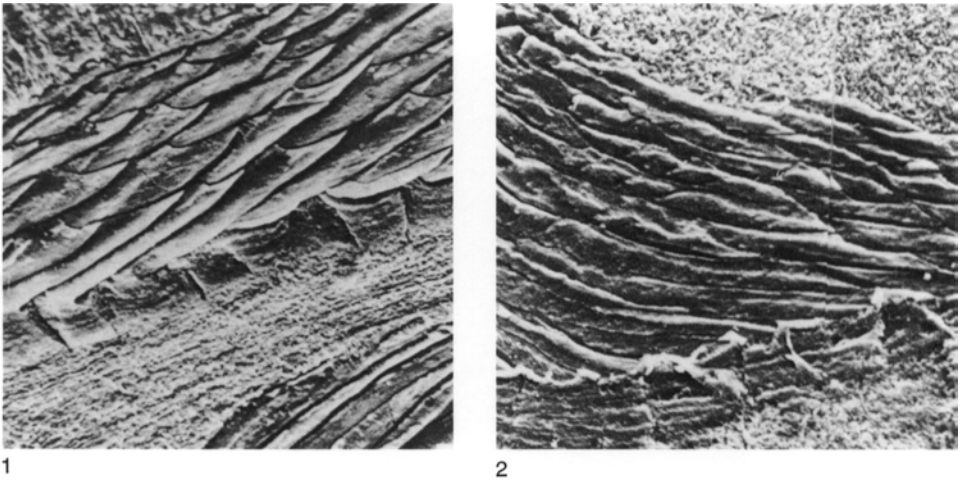

FIG. 279. Shell repair in fibrous-shelled brachiopods; *1–2,* general views of regressed successions of fibrous secondary shell, showing primary layer and calcitic pads underlying the normal succession (upper part of *1*), of primary and secondary shell in sections of *1,* the rhynchonellide *Notosaria nigricans* (SOWERBY), ×1,300 and of *2,* the terebratelloid *Magasella sanguinea* (LEACH) with a proteinaceous layer marking the regressive interface, ×1,100 (Williams, 1971a).

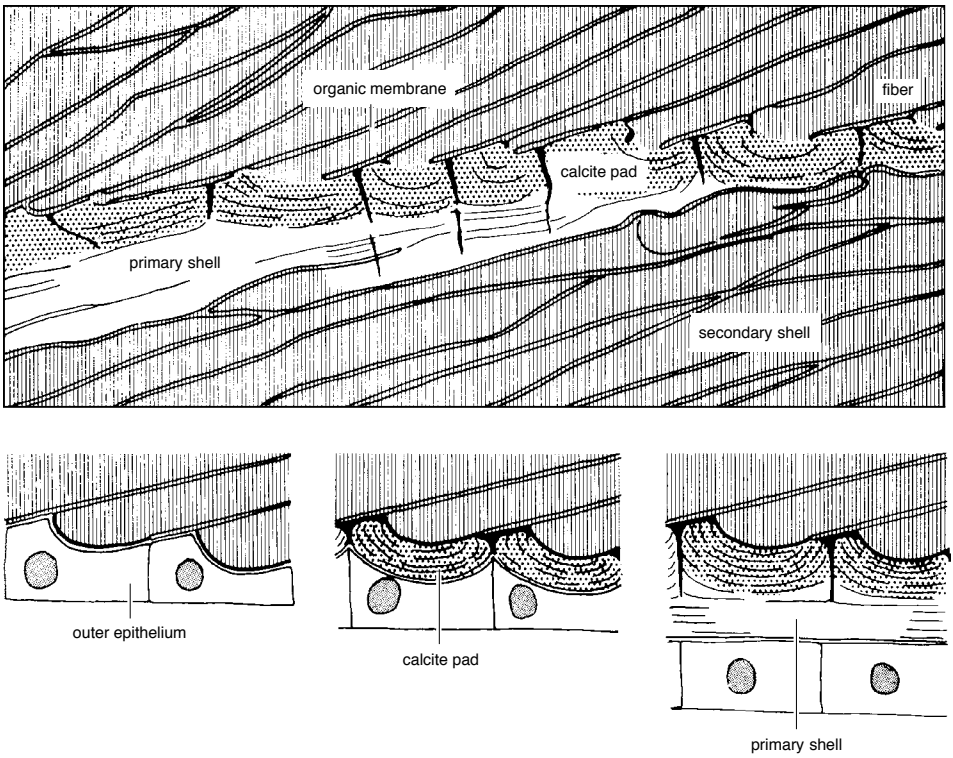

FIG. 280. Stylized tracing of shell succession of the rhynchonellide *Notosaria nigricans* (SOWERBY) shown in Figure 279.1 indicating the nature of a regression and the inferred relationships of retracted outer epithelium resuming secretion (Williams, 1971a).

with terminal faces of different fibers from those secreted by them before regression. Over a period of about two weeks, the pads form a continuous layer about 5 μm thick, interrupted by narrow, vertical slots corresponding to intercellular spaces.

This layer of pads is secreted by all outer epithelial cells that had been brought into juxtaposition with the secondary shell surface irrespective of the phase of the secretory regime they were in prior to retraction. Thus cells of the outer surface of the outer mantle lobe, which normally deposit primary shell, secete pads indistinguishable from those laid down by secondary outer epithelium. Once the pads have been deposited, however, cells revert to their respective secretory regimes at the point where they left off; and the normal processes of shell secretion and growth are brought back into play. In this way impersistent bands of secondary fiber (false mosaics of BRUNTON, 1969) become intercalated within shell successions (Fig. 281).

Retraction of the mantle in endopunctate shells differs from that of the impunctate *Notosaria* in only one respect. In *Magasella,* which can be heavily rutted with depositional breaks penetrating deep into the secondary layer, a proteinaceous membrane (Fig. 279.2) is secreted on the surface of re-

gression, which subsequently becomes the seeding sheet for the foundation layer of calcitic pads marking the first stage in recovery (transgression). This membrane cuts across punctae indicating that caeca are withdrawn during retraction. It would, therefore, not be surprising to find that caeca can get trapped along the regressive interface between the old surface and the newly formed shell and are eventually pinched out, so that punctal heads in the immediate vicinity of retraction surfaces within the living shell could be emptied of caeca by the processes of mantle transgression.

The frequency of damaged shells in fossil faunas varies among the main groups of articulated brachiopods. The proportions of shells with repaired breaks, represented in assemblages from Ordovician to Tertiary in age vary from 13 percent for strophomenides to just 1 percent for rhynchonellides (ALEXANDER, 1986). This discrepancy can be attributed to a number of factors. The likelihood, however, is that the laminar shells of strophomenides (especially those without taleolae) were more friable than the orthodoxly stacked fibrous ones of rhynchonellides. Yet it is also likely that, when crushed, fibrous shells would have cleaved more easily and lethally than those composed of cross-bladed laminae, which would have behaved like plywood. Consequently the proportions of lethally damaged shells among rhynchonellides could have been significantly greater than among the strophomenides. Even so, regeneration of the brachiopod shell seems to have been a more common feature of the organophosphatic and laminar calcitic brachiopods than of fibrous groups.

Koskinoid perforations of the shells of some extinct brachiopods are appropriately described in conclusion to this section as they are widely believed to have accommodated extensions of soft parts. The ventral valves of the atrypidine *Uncites* and of many orthotetidines are penetrated by microscopic tunnels (koskinoid perforations). The perforations tend to concentrate in the umbonal regions; and, since perforated species invariably lacked functional pedicle openings, they have been interpreted as byssuslike threads (JUX & STRAUCH, 1966), distal branches of internal pedicles (SCHUMANN, 1969; MARTINEZ-CHACON & GARCIA-ALCADE, 1978), or attachment fibrils secreted by papillae of outer epithelium, which first made the tunnels by shell resorption (GRANT, 1980).

FIG. 281. Fracture surface of the shell of the recent rhynchonellide *Hemithiris psittacea* (GMELIN) showing a layer of secondary fibers (false mosaic) intercalated between primary layer above and below, ×1,100 (Brunton, 1969).

The perforations are usually orthogonal to the shell and occur as close clusters of almost perfectly circular, transverse sections on laminar surfaces without any deflection or general disturbance of the laminae themselves in the manner characteristic of the fabric of shell growing around a persistent

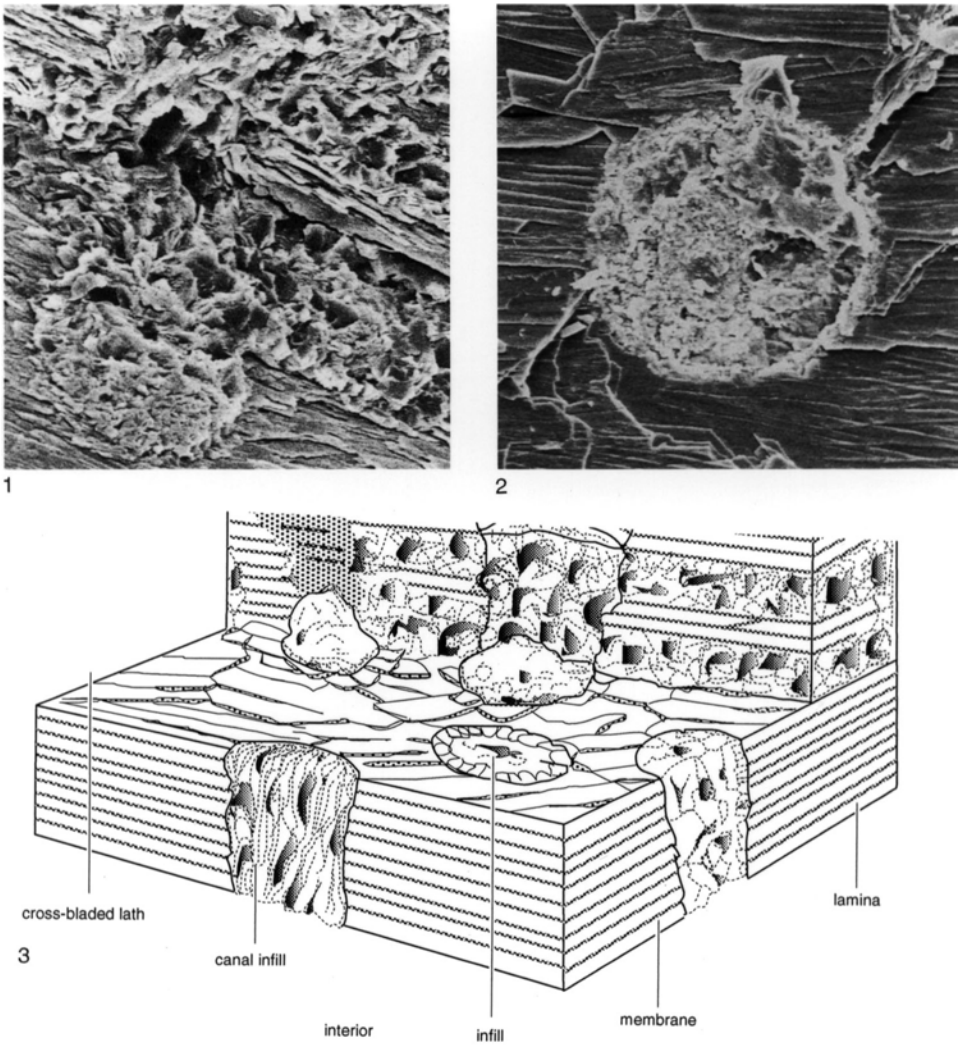

FIG. 282. Koskinoid perforations; *1,* fracture section of ventral valve of Carboniferous *Brochocarina trearnensis* MCINTOSH showing circular infill representing tunnel in bottom left-hand corner connecting with rubbly infill representing two lateral galleries separated by shelf of laminae that has been penetrated by a perforation in the top left-hand quarter, ×475 (Williams & Brunton, 1993); *2,* fracture surface of ventral valve of Permian *Streptorhynchus pelicanensis* FLETCHER showing a perforation tunnelled through the secondary laminae, which are undisturbed up to the rubbly periphery of the tunnel, ×300 (new); *3,* diagrammatic representation of koskinoid perforations based on those found in *B. trearnensis* (Williams & Brunton, 1993).

extension of the soft parts (Fig. 282). The tunnels vary in diameter from just over 10 μm to about 70 μm in some orthotetoids and schuchertelloids. Their walls are relatively smooth and sharply distinguishable from any infill and are rarely associated with horizontal galleries containing the same infill. There are no known means of having tunnels so neatly drilled and then occupied by extensions of the mantle (or rudimentary pedicle); and koskinoid perforations are more reasonably explained as having been made by burrowing parasites (THOMAS, 1958; WILLIAMS & BRUNTON, 1993).